Influence of glacial sediments on the chemical quality of surface water in the Ulta valley, Cordillera Blanca, Peru

Rúna Magnússon^{1,a} (corresponding author), Erik Cammeraat^a, Andreas Lücke^b, Boris Jansen^a, Anaïs Zimmer^c, Jorge Recharte^c

- a) Institute for Biodiversity and Ecosystem Dynamics, University of Amsterdam, Science Park 904, 1098XH Amsterdam, The Netherlands.
- b) Institute of Bio- and Geosciences, Agrosphere Institute (IBG-3), Forschungszentrum Jülich GmbH, D-52425 Jülich, Germany.
- c) Instituto de Montaña, Calle Vargas Machuca 408, Miraflores, Lima, Peru.
- © 2020. This manuscript version is made available under the CC-BY-NC-ND 4.0 license http://creativecommons.org/licenses/by-nc-nd/4.0/

¹⁾ Present address: Plant Ecology and Nature Conservation, Environmental Sciences

Group, Wageningen University, PO Box 47, 6700 AA Wageningen, The Netherlands.

runa.magnusson@wur.nl

Abstract

The Rio Santa and its tributaries are an essential source of drinking and irrigation water. Its discharge relies on glacial meltwater, which is diminishing due to rapid glacial retreat. As a secondary effect, water quality can be compromised (pH < 3 and high SO_4^{2-} and trace metal concentrations) due to exposure of pyrite rich Chicama bedrock upon glacial retreat. However, little is known about the composition of Quaternary glacial sediments and their effect on water quality. This research aims at elucidating this effect by relating observed changes in water quality in streams to presence and chemical composition of morainic ridges in the Ulta valley in the Rio Santa basin. Changes in water quality upon contact with a morainic ridge were assessed using carbonate alkalinity titration, ion analysis and elemental analysis. Relative contributions of glacial meltwater and precipitation were assessed qualitatively using stable water isotope analysis. We used a novel method to explain the provenance of contaminated glacial sediments using a reconstruction of their source area. The mineralogical composition of a morainic ridge was strongly related to the geology of the source area indicating that mineralogical composition of tills may be predicted using this technique. Effects of glacial sediments in morainic ridges on water quality were minimal but depended on till mineralogical composition. Tills with a high content of Chicama shales tended to increase solute loads of Mg and SO₄². Isotope signatures suggest that during the dry season, moraines may store precipitation-derived shallow groundwater. Clear trends in water quality were observed along an altitudinal gradient, potentially related to increased groundwater contribution downstream and shifts in dominant weathering mechanisms. Future research should focus on disentangling these various drivers of water quality in glacial catchments.

Keywords: Water Quality, Morainic Ridges, Glacial Sediment, Pyrite Weathering, Paleoglacier Reconstruction, Stable Isotope Analysis, Cordillera Blanca, Peru, Tropical Glaciers

1. Introduction

Due to mass loss of glaciers, glacier-fed freshwater supplies are expected to decline globally on the long term (Jiménez Cisneros et al., 2014). Although a worldwide phenomenon, mass loss of glaciers is especially pronounced in the Andes (Rabatel et al., 2013). Due to decreasing extent of glaciers, freshwater reservoirs in the Cordillera Blanca are diminishing in size (Kaser et al. 2003; Mark and Seltzer 2003; Mark et al., 2010; Baraer et al., 2012), while glacial meltwater is an important source of water within the Río Santa watershed and parts of the coast of Peru. With 600 km², the Cordillera Blanca is the largest glaciated area in the tropics, comprising a quarter of all tropical glaciers. Its waters mainly drain into the Río Santa watershed, where it is used to maintain intensively cultivated areas and generate hydropower (Kaser et al., 2003).

Water quality in the Río Santa watershed is affected negatively both by anthropogenic activity such as mining and by natural sources of contamination. The latter is most notably caused by sulphide weathering occurring in the pyrite-rich Jurassic "Chicama Formation" (Fortner et al., 2011; Burns et al., 2011; Gordon et al., 2015). A case study by Fortner et al. (2011) in the Río Quilcay, a tributary of the Río Santa originating from the Quilcayhuanca quebrada (glacial valley), indicated that several water quality parameters exceeded limits for human consumption issued by the World Health Organization and Peruvian drinking water standards. Surface water pH levels of 3 to 4 are common and as a result of the ensuing enhanced heavy metal solubility, concentration limits for irrigation and agriculture are exceeded locally (Fortner et al., 2011; Bury et al., 2013).

Within this context, this study focuses on the influence of till deposits in morainic ridges on water quality in a previously unstudied and pyrite-containing glacial valley in the Cordillera Blanca. It is still unclear how exactly natural contamination from mineral sources affects the chemical quality of surface water. While the presence of upstream Chicama Formation has been

identified as a source of natural contaminants due to rock weathering, a main point of debate is the effect of mineralogy of Quaternary fluvioglacial deposits on natural contamination (Fortner et al., 2011; Burns et al., 2011). Since these deposits have never been studied in detail in the Peruvian Andes, little is known about their mineralogical composition. Whereas the Chicama Formation is confined to the uppermost reaches of the Cordillera Blanca (*Figure 1*), redistribution of Chicama material in the form of fluvioglacial deposits could contribute to additional natural contamination of water further downstream in catchments. Attempts to relate the presence of fluvioglacial deposits to water quality in streams intersecting these deposits remain incidental. Moreover, hydrological behaviour of these deposits remains largely unknown (Gordon et al., 2015). This study contributes to filling this gap of knowledge through measurement of chemical water quality up- and downstream of Quaternary fluvioglacial deposits combined with chemical and hydrogeological characterization of these deposits. This approach may yield insights into the effect of glacial redistribution of potentially contaminating minerals on the chemical quality of surface water in glacial systems worldwide.

In the proglacial zone highly erodible material is present which is initially water-saturated and has a high water/rock contact area. This facilitates high weathering rates and solute loads (Anderson et al., 2000). In prior studies of weathering processes in the Cordillera Blanca, sulphide weathering (due to presence of pyrite) has been identified as the dominant weathering process (Fortner et al., 2011; Burns et al., 2011; Walsh, 2013). Sulphide and carbonate weathering are the dominant weathering processes in proglacial and subglacial zones worldwide (Anderson et al., 2000). Weathering of pyrite precipitates ferric oxyhydroxides and produces SO_4^{2-} and H^+ , which rapidly decreases the pH of surface waters and may cause other compounds to dissolve (Åström & Åström, 1997; Munk et al., 2002). Buffering of acidification by CO_3^{2-} or HCO_3^{-} has been shown

to occur in highly acidic streams (Munk et al, 2002; Fortner et al., 2011). Upon depletion of sulphides and carbonates, the role of silicate weathering increases in the proglacial zone (Tranter et al., 2005; Anderson et al., 1997; Walsh, 2013).

Gordon et al. (2015) found that moraines in the Quebrada Quilcayhuanca were in many cases connected to groundwater-bearing subsurface talus deposits, which are important aquifers in the Cordillera Blanca (Baraer et al., 2015; Glas et al., 2017). Baraer et al. (2015) found that during the dry season such talus deposits may be significant sources of groundwater, derived from preceding wet-season precipitation. This may result in addition of precipitation-derived groundwater to the outflow of the morainic complex and cause water to be less representative of pyrite weathering. The relative contribution of glacial meltwater and groundwater to the total outflow of such a deposit is difficult to infer from field assessments. However, previous studies have used endmember mixing models to derive isotope and chemical signatures of precipitation-derived groundwater and glacial meltwater in the dry season (Mark & Seltzer, 2003; Mark et al., 2005; Baraer et al., 2009; Burns et al., 2011; Baraer et al., 2015; Gordon et al., 2015). In the Andes, differences in enrichment of heavy isotopes in precipitation are dominated by the altitude effect. Due to orographic uplift, progressive condensation of moisture from air leads to increasing depletion of heavy isotopes in rainfall with elevation (Rozanski & Araguás-Araguás, 1995). Additionally, isotope ratios in surface water may be affected by the contribution of glacial melt to total stream discharge, since glacial meltwater is depleted in heavy isotopes compared to groundwater (Baraer et al., 2015; Gordon et al., 2015; Mark & McKenzie, 2007). As such, isotopes of oxygen and hydrogen may be used to distinguish between various sources of water based on source area elevation (Burns et al., 2011; Baraer et al., 2015; Gordon et al., 2015).

Morainic ridges largely consist of subglacially eroded material but may include englacial and supraglacial material and outwash sediments deposited at the glacier margin (Boulton, 1986). Subglacial erosion rates vary throughout a glacier and depend on a multitude of factors related to glacial flow rates such as subglacial terrain. Historically, glacial flow and mass balance equations have been used to reconstruct former glacier extents and monitor glaciers over time (Rodbell, 1992; Kaser & Georges, 1997; Mark & Seltzer, 2005; Racoviteanu et al., 2008; Benn & Evans, 2010). Theoretically, the composition of a morainic ridge should correspond to the geology of its source area, especially in areas of maximum glacial flow rate. Therefore, this study adopts a novel application of glacial mass balance equations in order to predict mineralogical composition of moraines based on the lithology of the former glacier extent. Such an approach may prove useful in the prediction of the provenance of contaminated sediments in various glacial environments. Additionally, subglacial lithology could be predicted based on the composition of currently developing morainic deposits, which may prove useful in the context of glacial retreat worldwide.

The aim of this study is to assess the influence of Quaternary glacial sediments, present in the proglacial zone as morainic ridges, on chemical surface water quality in the Quebrada Ulta. The objectives are to:

- (1) assess predictability of till composition based on a morainic ridge's position in the landscape by reconstruction of the source area of moraine complexes,
- (2) assess the influence of chemical composition of morainic ridges on the chemical quality of surface water through measurement of chemical composition of sediments and water,
- (3) assess the influence of texture and saturated hydraulic conductivity of sediments on the chemical quality of surface water

(4) relate changes in water quality upon contact with a morainic ridge to changes in relative contribution of glacial meltwater and precipitation-derived groundwater as derived from qualitative assessment of isotope ratios of water

We expect that the composition of morainic ridges will be correlated to the subglacial geology of the extent of glaciation at the time of deposit, most notably that of the most erosive zone around the ELA (Equilibrium Line Altitude) (Benn & Evans, 2010; Dahl & Nesje, 1992). In turn we expect that changes in water quality upon contact with a morainic ridge will be related to the presence of specific minerals and compounds in the morainic ridge. This may also be expressed through differences in texture and saturated hydraulic conductivity of tills. We expect to find less deterioration of water quality in cases where the morainic ridge is connected to subsurface precipitation-derived groundwater flows. Within the context of a ubiquitous trend of glacial mass loss and adverse impacts of global warming on freshwater supplies, this study is of global relevance.

2. Methods

2.1 Research Area

The Quebrada Ulta is the catchment of the Río Buín tributary to the Río Santa, situated close to the town of Carhuaz in the province of Ancash, Peru. To our knowledge no publications exist that describe the geohydrology or water quality within this catchment, while several do exist for nearby valleys such as the Quebrada Quilcayhuanca (Gordon et al., 2015; Fortner et al., 2011; Baraer et al., 2012; Burns et al., 2011, Glas et al., 2017), Yanamarey (Bury et al., 2013; Baraer et

al., 2012; López-Moreno et al., 2017), Llanguanuco, Querococha and Pumapampa (Baraer et al., 2012).

The Quebrada Ulta ranges from approximately 3500 to 6750 meters in altitude and is flanked by several glaciated mountaintops, among which the Nevado Huascarán, which is the highest peak of the Cordillera Blanca. The geology of the Quebrada Ulta is dominated by granodiorite and tonalite intrusives, with some outcrops of the meta-sedimentary Jurassic Chicama formation in the higher regions of the quebrada (*Figure 1*). The catchment area of the Río Buín contains various fluvioglacial, colluvial and glacial deposits (IGMM, 2011) and several glacial lakes and paleo-lakes that formed upon the retreat of glaciers. Such glacial lakes may be dammed by ice, bedrock or morainic ridges. Often several levels of morainic ridges are present within a quebrada, related to different episodes of glacial advance. This creates a staircase-like landscape with glacial lakes (or paleo-lakes) dammed by morainic ridges at different altitudes (Iturrizaga, 2014).

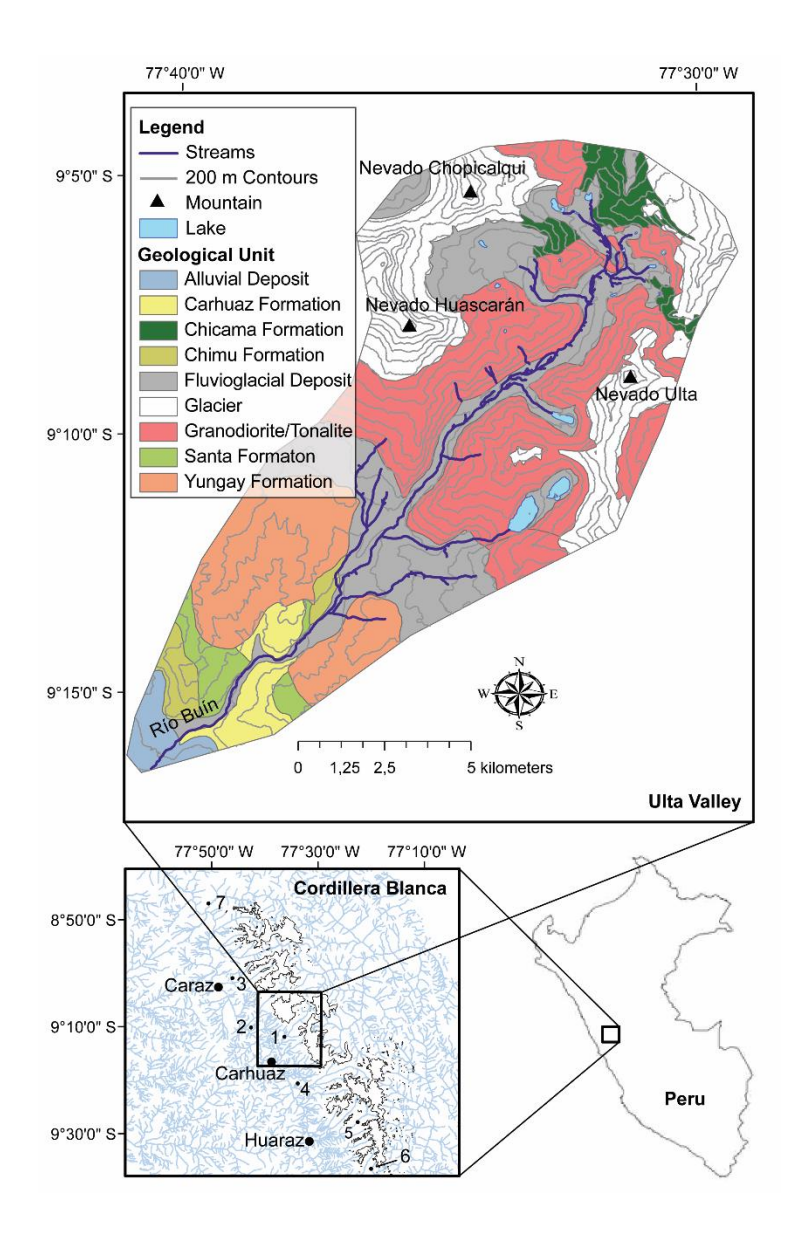


Figure 1) Location of the Study Area, with WGS 1984 coordinates. Geology adapted from IGMM (2011). Numbers 1 – 7 indicate locations of previous studies mentioned throughout this study. 1) Río Buín (this study), 2) Río Mancos, 3) Río Llullan, 4) Marcara, 5) Río Quilcay / Quilcayhuana, 6) Río Negro / Olleros, 7) Quitarasca.

The local climate is characterized by relatively large daily and small seasonal temperature variations and a distinct dry (May-September) and wet season (October-April) due to oscillation

of the cloud belt of the Intertropical Convergence Zone. As a result, monthly mean temperatures remain between 5 and 10 °C throughout the year, but precipitation differs from below 50 mm per month during the dry season up to 150 mm per month during the wet season (Kaser et al., 1990). In the Quebrada Ulta, glacial cover of the Huascarán-Chopicalqui massif decreased by 18.67 % between 1970 and 2003 (Racoviteanu et al., 2008). Based on previous studies in other quebradas of the Cordillera Blanca it can be expected that a decrease of glacial extent leads to reduced availability of meltwater as a source of freshwater runoff in the area (Kaser et al. 2003; Mark and Seltzer 2003; Mark et al., 2010; Baraer et al., 2012). As a consequence of local climate, mass accumulation from precipitation is mostly confined to the wet season in the highest part of the glacier (Kaser & Georges, 1997), whereas precipitation in the form of snow on the tongues of the glaciers of the Cordillera Blanca tends to melt within days (Kaser et al., 1990). This causes steep vertical gradients (Kaser & Georges, 1997).

2.2 Paleoglacier reconstruction

We test a novel method to explain the mineralogical composition of morainic ridges based on their source area, in this case the area occupied by the former glacier that created the morainic ridge ("paleoglacier"). Based on field observations and interpretation of a Digital Terrain Model (DTM) (ASTER GDEM v2, retrieved from https://lpdaac.usgs.gov, April 2016 and Sentinel MSI aerial photography (European Space Agency, 2016), we mapped morainic ridges. Additionally, glacial geomorphological features such as glacial trimlines were mapped using the Sentinel data and field observations. Trimlines are the demarcation lines visible between glacially eroded and non-eroded terrain, often presumed to represent the limit of a glacier's erosive zone (Benn & Evans, 2010). Geological data (IGMM, 2011), the DTM and glacial geomorphological features

were used to infer paleoglacier extents and subglacial lithology. Field-mapped morainic ridges were combined into polygons representing the original moraine deposits by connecting lateral and terminal moraines. For each of these polygons a watershed was generated using ArcMap 10.4 and the AcrHydro Tools toolbox (ESRI, 2011). Watersheds were adapted manually based on a set of criteria:

- (1) the paleoglacier is confined by trimlines and lateral moraines. Trimlines indicate the ice height and thus paleoglacier extent at some point of glacial equilibrium in the past (Ballantyne, 2002).
- (2) In the upper reaches of the paleoglacier watershed, any area with a slope in excess of 60° is interpreted as circue headwall (Meierding, 1982).
 - (3) Ice height was assumed to be the same on either side of a glacier tongue.

Adapted watersheds represent a reconstructed paleoglacier extent corresponding to a specific moraine deposit. To infer the ELA, we used the widely accepted Accumulation Area Ratio (AAR) method, which requires as input the total area of the former glacial extent and a DTM, of which a fraction (typically 0.65) is assumed to represent the paleoglacier's accumulation area (Rodbell, 1992; Kaser & Georges, 1997; Mark & Seltzer, 2005; Racoviteanu et al., 2008). However, as the mass balance of tropical glaciers is steeper, we used an AAR of 0.75 as proposed by Georges and Kaser (1997). The paleoglacier polygons were used to calculate the 75 % height percentile of all DTM cells within the polygons as the ELA. This was achieved by clipping the contour line of the 75 % percentile height to the extent of the paleoglacier. A 500 m buffer zone was generated around the reconstructed ELA as an "ELA zone", to represent the most erosive zone of the paleoglacier. The maximum altitude at which lateral moraines occur was used as a validation

for the minimum height of the ELA (Dahl & Nesje, 1992). Both from the entire paleoglacier extent and from the ELA zone, subglacial lithology was inferred by recording the percentage occurrence of specific geological units within those polygons. This generated a dataset of 15 morainic ridge complexes with a paleoglacier extent, ELA, paleoglacier lithology and ELA zone lithology. A full procedure can be found in *Appendix D.1*.

Morainic ridges were dated based on relations between the altitude and the age of moraine complexes in the Cordillera Blanca from literature (*Table 1*). Throughout the Cordillera Blanca, various episodes of glacier advance in the past have left distinct complexes of lateral and terminal moraines throughout different quebradas. Attempts to inventory and date these have been made by various authors based on relative positioning, lichenometry, ¹⁰Be and radiocarbon dating (Rodbell, 1993; Rodbell & Seltzer, 2000; Farber et al., 2005; Solomina et al., 2007; Rodbell, 2008).

Table 1) Overview of major groups of morainic ridges

Moraine group name ¹	Estimated age (yrs BP)	Typical altitude [m]	Comments
Pre-Holocene:			
Cojup	29 ka – 4.3 myr ^a	?	
Rurec	34-21 ka ^b	3400-3800 ^a	
Laguna Baja	16 ka ^b	3800-4000 ^a	
Manachaque	11 ka ^b	4000-4300 ^{a,c}	Possibly including Younger Dryas ^c
Holocene			
Various groups	7 – 0.1 ka ^d	> 4300 ^d	Including Little Ice Aged

al) Rodbell (1993), b) Farber et al. (2005), c) Rodbell & Seltzer (2000), d) Solomina et al. (2007)

2.3 Sampling

To assess the influence of the composition of morainic ridges on the chemical quality of surface water, a sampling scheme was set up in which water samples were collected at contact

areas of streams with proglacial tills in morainic ridges. Sampling was carried out during the dry season (between late June and mid-July 2016) to limit potential sources of surface water to glacial melt and groundwater. Water was sampled upstream and downstream of a contact zone, and proglacial till was sampled along the contact zone with the stream (distance from stream < 50 m). In case of larger moraine complexes, several till samples were collected from both lateral moraines. This sampling scheme was based on the premise that water bodies receive either direct runoff or groundwater from permeable deposits such as morainic ridges. Using rain gauges, no precipitation was recorded during the sampling period. In case springs were observed to discharge from a morainic ridge, a sample was taken of the spring water as well as two samples up- and downstream of the confluence point of the spring with a receiving stream. Since sampling was carried out in the dry season, we assume that these springs are perennial. To allow for mixing of the two water bodies, samples downstream from the confluence point were taken at a distance of at least ten times the width of the stream, but upstream of any other tributaries. In these cases, till samples were taken from as close to the spring as feasible (< 20 m). This was done in locations on various geological subunits and altitudes in the Quebrada Ulta. This way, changes in water quality upon contact with a morainic ridge could be related to the composition of the morainic ridge, while minimizing influence of other processes as much as possible. The sampling scheme is depicted in Figure 2.

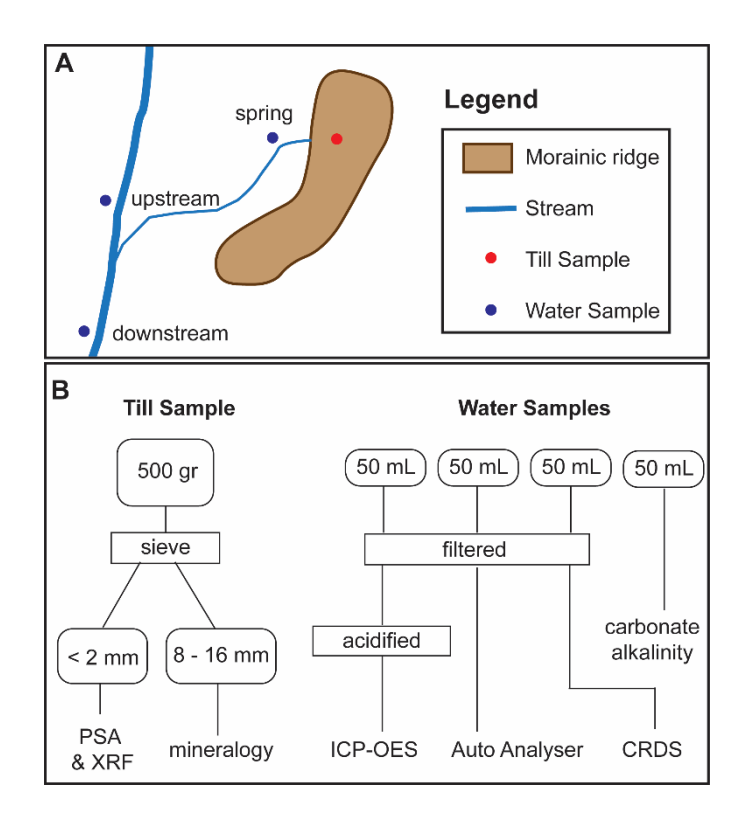


Figure 2) Spatial overview of the sampling procedure (a) and workflow for analysis of till and water samples (b). CRDS = Cavity Ring-down Spectroscopy, PSA = Particle Size Analysis, XRF = X-ray Diffraction. ICP-OES = Inductively Coupled Plasma Optical Emissions Spectroscopy.

2.4 Parent Material analysis

Proglacial till was sampled from parent materials by collecting approximately 500 g of material from below the A and B horizons in a zip lock bag. Material was sieved over a 16 mm, 8 mm and 2 mm sieve tower and all fractions were weighed.

A Niton XL3 series handheld X-Ray Fluorescence (XRF) analyser was used on milled and sieved (< 2 mm) material to quantify Ba, Mo, Nb, Zr, Sr, Rb, As, Pb, Zn, Cu, Fe, Mn, Cr, Ti, K, Ca, Al, P, Si, S and Mg concentration in tills. NIST 2709a, NIST 180-661 (National Institute of Standards and Technology) and SDAR-m2 (USGS) standard reference materials were measured to correct for measurement errors (see protocol in *Appendix D.2.3*). Other elements of interest such

as Na, S and Mg were not suitable for analysis with the used XRF analyser and were analysed in duplicate using microwave extraction in Aqua Regia and Inductively Coupled Plasma Optical Emission Spectroscopy (ICP-OES) (Optima 8300, Perkin Elmer, USA).

Particle Size Analysis (PSA) was performed on 20 g of unmilled, sieved (< 2 mm) material. Pre-treatment (removal of organic matter and iron oxides) followed Mehra & Jackson (1960) and Gee & Or (2002). After pre-treatment, soils were separated into a fraction > 63 μm and a fraction < 63 μm by wet-sieving. The fraction < 63 μm was freeze-dried and analysed with sedigraph analysis using X-ray attenuation (Sedigraph III Plus, Mircomeritics, USA). The fraction > 63 μm was analysed for particle size using a sieve tower and scale with 0.01 g precision. The GRADISTAT software designed by and described in Blott & Pye (2001) was used to calculate sand-, silt- and clay fractions of the soil material of < 2 mm from the sieve tower and sedigraph data. A protocol is available in *Appendix D.2.2.1*. Based on sand, silt and clay fractions, gravel content and OM content, saturated hydraulic conductivity (KSat) was determined using the SPAW Soil Water Characteristics Calculator (Saxton & Willey, 2005; Saxton & Rawls, 2006; Saxton, 2007). The equations used in SPAW can be found in Saxton & Rawls (2006).

To assess till Chicama content, the 8-16 mm fractions were mineralogically classified using a jeweller's loupe and Streckeisen's (1974) QAPF diagram after removal of clay coatings and iron oxides (see *Appendix D.2.2.5*).

2.5 Water analysis

For each water sampling location, temperature corrected pH and Electrical Conductivity (EC) were measured using a pH90 pH-meter and LF96 micro-conductivity meter (WTW, Germany). EC in meltwater streams in this region shows a diurnal trend due to temperature-dependent glacial melt contribution (Burns et al., 2011). Therefore, these data were detrended

using a time series of logged EC data with a 15-minute interval from a meltwater stream spanning 4 days. This series was used to fit sine functions to describe diurnal variation in EC measurement. The amplitude and phase of the sine function were related with distance to glacier (*fig. D2*, *Appendix D3.1*). An empirical relation was set up of distance to glacier and phase and amplitude of the diurnal sine functions, so that EC data of meltwater streams could be detrended based on their distance from an active glacier (see *Appendix D.3.1*). Specific compound or element concentrations and isotope ratios were not detrended for diurnal variation, since compound-specific discharge relations may depend on compound-specific geochemical processes (Nimick et al., 2003). Throughout the manuscript, detrended EC values are used for meltwater streams.

Water samples were taken in quadruplicate, using 50 mL high-density polyethylene bottles pre-rinsed with sample water. 3 out of 4 replicates were filtered using a rinsed syringe and 0.45 µm filter. 1 out of 3 filtered samples was acidified using 2 drops of 70 % nitric acid.

Alkalinity titrations were conducted in the field with a field titration set. Time between sampling and titration varied from 1 to 7 days. Titration of 10 mL unfiltered, unacidified sample was conducted using HCl [0.067 M] under continuous measurement of pH. We used the USGS Alkalinity Calculator tool (USGS, 2013) to calculate total alkalinity in CaCO₃ equivalents, HCO₃ and CO₃²⁻ concentrations applying Gran function plots as first choice (Andersen, 2002; Gran, 1950; USGS, 2013). The inflection point method was used instead in case insufficient data was available to construct a Gran function. The detection limit (LOD) was set to 1.7 μmol based on the minimum drop size and titrant concentration.

The acidified aliquot was used for ICP-OES (Optima 8300, Perkin Elmer, USA) to measure total element concentrations of major cations and trace elements (Al, Fe, Na, Ca, K, Mg, Cu, Ni, S, As, Cd, Co, Li, B, Ba, Mn, In, Sr, Ti, Be, Cr, Mo, Sb, Ga and Si). 8 mL of non-acidified sample

was used to measure NO_x, PO₄³⁻, SO₄²⁻, Cl⁻ and NH₄⁺ concentrations using an Auto Analyser (San++, Skalar, Netherlands). LODs per compound are in table C.6. Samples below LOD were set to LOD / 2. Total dissolved C (organic and inorganic) and N (nitrogen) were measured using a TOC WVP (Shimadzu Corporation, Japan) on 15 mL of sample using 700°C combustion catalytic oxidation. From the difference between total C and inorganic C the total amount of dissolved organic C (DOC) was calculated. The negative charge of DOC was calculated according to Oliver et al. (1983). The ion balance was calculated as the percentage difference between the total charge of anions and total charge of cations (using the elemental concentrations of the major cations) divided by the sum of positive and negative charges (*Appendix D.3.2*). Samples with an error in ion balance of over 15 % were omitted from further analysis.

Stable oxygen and hydrogen isotope analyses of water samples were performed by cavity ring-down spectroscopy (CRDS) (L2130-I, Picarro Inc., USA). About $0.8 \,\mu l$ of unacidified sample water was injected into the vaporizer, converted to water vapour and transported into the cavity with synthetic air as carrier gas. Water samples were measured in replicate together with internal laboratory standards calibrated against international isotopic reference materials (Brand et al., 2014). The isotopic compositions are expressed as δ -values in per mil (‰) as follows in eq. 1:

$$\delta = (R_{sample}/R_{standard} - 1) * 1000$$
 eq. 1

with R_{sample} and $R_{standard}$ as isotope ratios ($^{18}\text{O}/^{16}\text{O}$, $^{2}\text{H}/^{1}\text{H}$) of sample and standard, respectively. Isotope values of oxygen and hydrogen were normalized to VSMOW/VSLAP. Analytical precision as determined from internal standards was better than \pm 0.05 % for $\delta^{18}\text{O}$ and 0.1 % for $\delta^{2}\text{H}$. No precipitation could be sampled during the fieldwork period due to complete absence of precipitation. As an alternative, isotopic signatures were compared to known Meteoric Water Lines from literature to facilitate a qualitative interpretation.

2.6 Data Analysis

To assess the influence of morainic ridges on the chemical quality of surface water, a pairwise comparison was made between water chemical data up- and downstream of a morainic ridge. The extent to which these differences were related to till composition was assessed by correlating downstream – upstream differences to till physical and chemical data. To assess the role of the pyrite-rich Chicama formation in tills, locations were subdivided into high-Chicama tills (> 30 % Chicama) and low-Chicama tills (< 30 % Chicama). A comparison was made between the changes in water quality parameters between up- and downstream samples for the low-Chicama group and high-Chicama group using a two-sample test of difference of means. Afterwards, the same procedure was conducted for differences in water quality parameters in spring water among the high-Chicama and low-Chicama group. All water data (EC, pH, stable isotope ratios and compound concentrations) were tested for correlation with elevation. To assess the extent to which moraine deposits act as reservoirs for local precipitation, trends of stable isotope ratios with elevation were assessed for moraine-fed springs and meltwater streams separately and compared to known isotope ratio elevation trends in precipitation and surface water in the Cordillera Blanca (Rozanski & Araguás-Araguás, 1995; Windhorst et al., 2013; Baraer et al., 2015).

To assess relations between paleoglacier or ELA lithology and till composition, the percentage of areal cover of Chicama formation of a paleoglacier area or ELA zone was correlated to physical and chemical data of till from the corresponding morainic ridge. Additionally, correlation among individual compounds in tills was analysed and compared to till Chicama content to facilitate the identification of specific minerals in the Chicama formation responsible for observed effects on the chemical quality of surface water.

For all correlation analyses, Pearson's product-moment correlation was used for normally distributed data, Spearman's rank correlation was used in all other cases. A Student's t-test was used if the difference in water quality parameters was normally distributed and a Wilcoxon signed-rank test was used in all other cases. For paired differences, a two-sample t-test was used to test significant difference of means, or a Wilcoxon rank sum test for non-normally distributed differences. 0.05 was used as significance criterium, and p values of up to 0.1 were reported as tendencies. Bonferroni-Holm correction (Holm, 1979) was used on all separate analyses to correct for multiple testing. Data analysis was carried out in MATLAB R2014b.

3. Results

3.1 Paleoglacier reconstruction

Morainic ridges of various age are present in the Ulta valley (*Figure A.2*), ranging from large, vegetated moraines (southwest) to younger unvegetated moraines (northeast). Trimlines are almost exclusively found along the central valley (*Figure A.4*). *Figure 3a* - d shows the reconstructed paleoglacier extents and corresponding ELAs for 15 selected moraines grouped by age (full data in *Table C.1*). Minor adaptations to the existing geological map (IGMM, 2011) are made based on observations during the field campaign (*Figure A.3*).

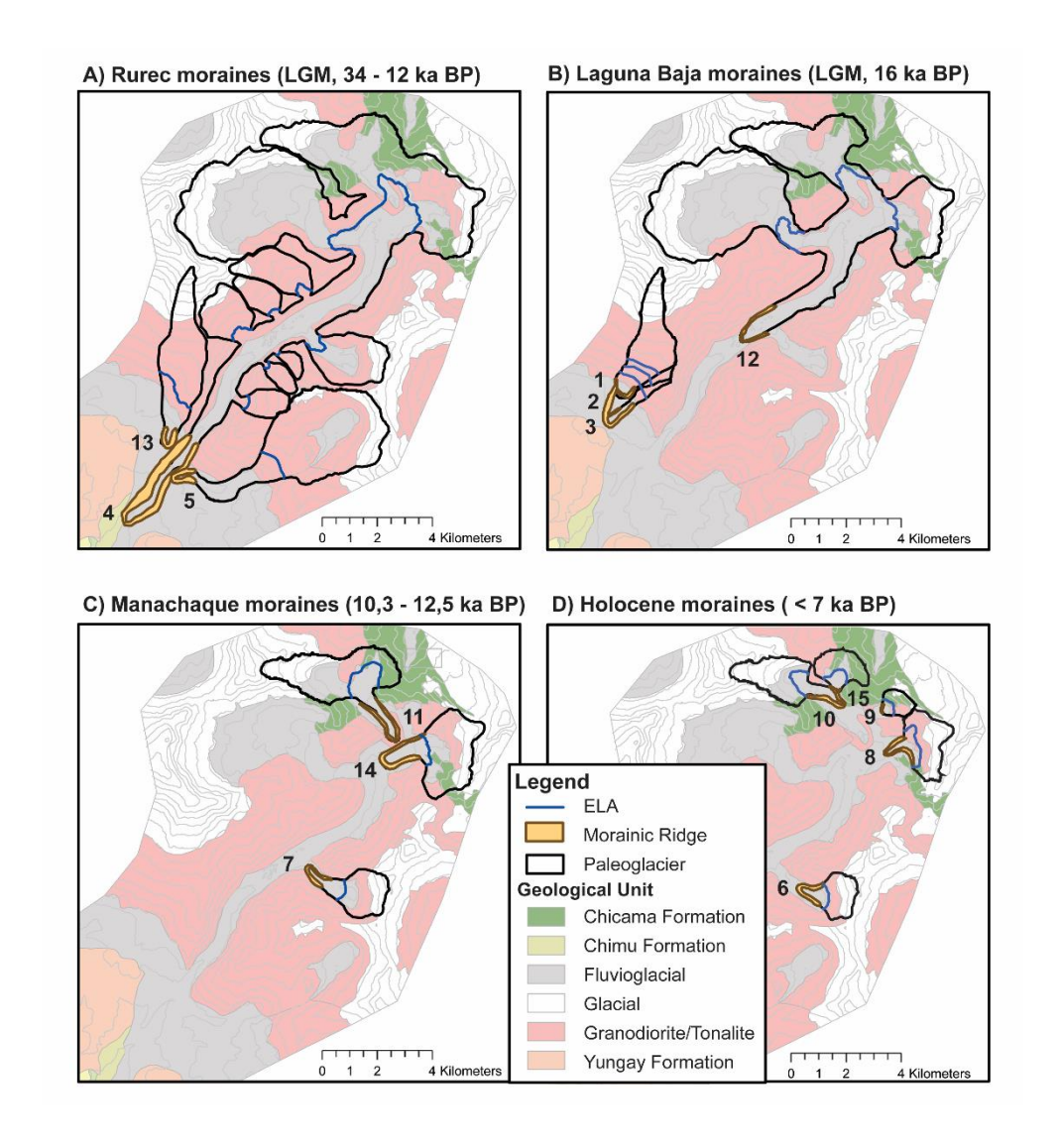


Figure 3) Map of morainic ridges, paleoglacier extents and ELAs reconstructed using watershed analysis. It is possible that paleoglaciers in figure 3A (glaciers 13, 4 and 5) were connected during this stadium.

3.2 Till composition

Tills mostly contain less than 20 % Chicama material, although higher concentrations are found with increasing elevation (*Figure 4*). Most tills are of a very poorly sorted texture with varying saturated hydraulic conductivity (0.8 – 4.1 cm/hr). Apart from Si, tills contain approximately 6-14 % Al, 0.8-9 % Fe, 1-3 % K, 1-2% Ca, 0.05-3.00 % C, 0-1.4 % S, 0-1.2 % Mg

and 0.02-0.27 % N and small amounts of other elements. The contents of S, Mg, Fe and As in tills are positively correlated, as are Si and K (*Figure 5*). Mo, Pb, Cu and Cr are mostly below detection limits and omitted from further analysis. The supplementary material contains all till properties (*Table C.3*), detection limits and relative errors of measurement (*Table C.2*). Since errors were high for As, Mn and S, values should be interpreted with caution.

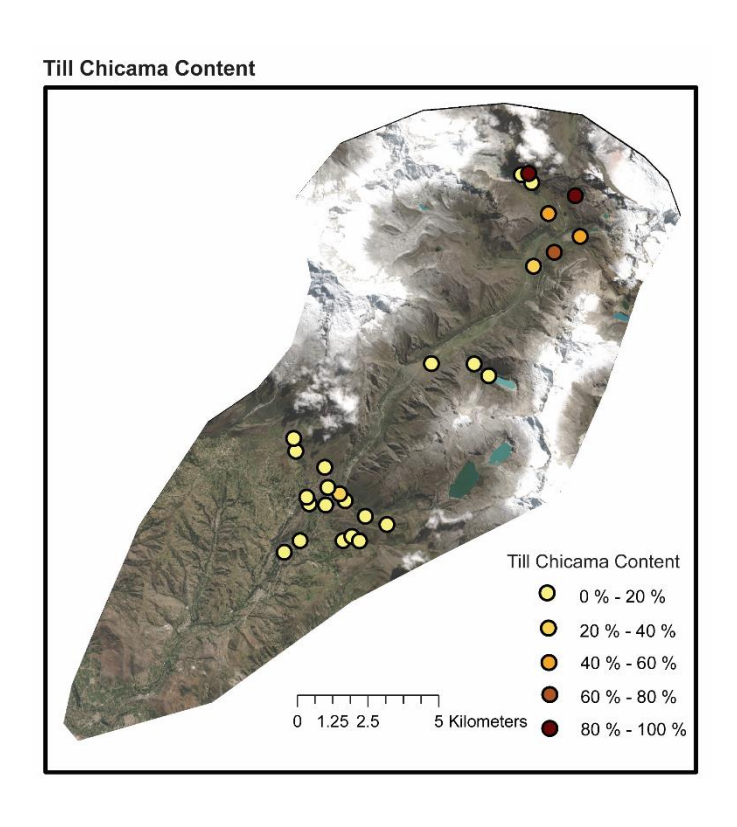


Figure 4) Soil sampling locations coloured by percentage of Chicama shales in till, reported as % of rocks in 8-16mm texture class. Sentinel MSI aerial photography (European Space Agency, 2016) is used as basemap.

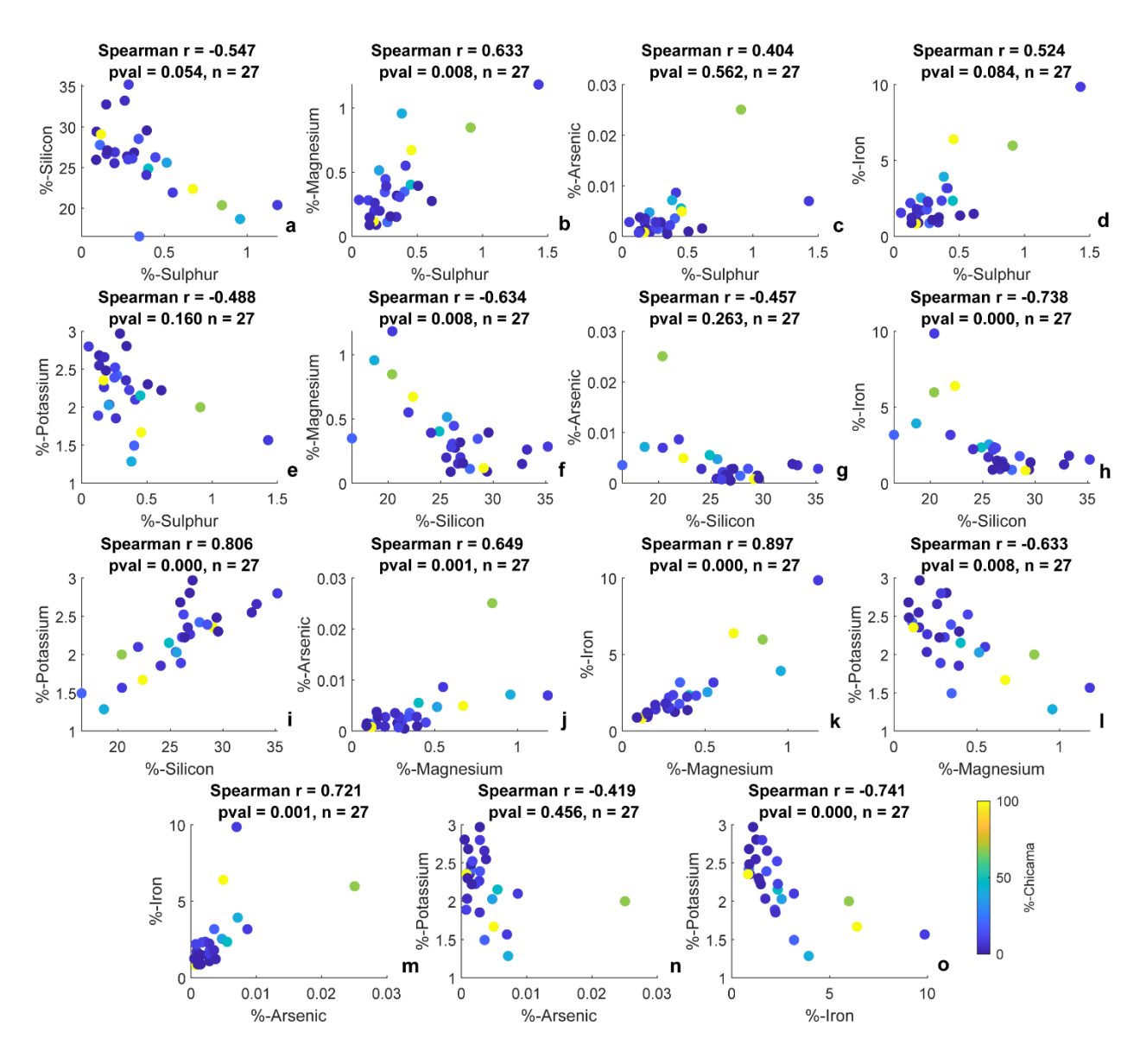


Figure 5) Correlations between element concentrations in till samples (all in mass-%), coloured by percentage of Chicama shale in till (as % of rocks in 8-16mm class). P-values are corrected p-values.

Table 2) Correlation (Spearman's R) matrix of till properties and paleoglacier lithology. P values are corrected p values.

	Till-Chicama [%]	Till-Ksat [cm/hr]	Till-S [%]	Till-Fe [%]	Till-As [%]	Till-Al [%]	Till-Mn [%]	Till-Si [%]	Till-K [%]	Till-Ca [%]	Till-Na [%]	Till-Mg [%]
ELA-	0.799	-0.439	0.185	0.509	0.570	0.199	0.098	-0.261	-0.542	0.059	0.645	0.509
Chicama	0.008 ***	1 NS	1 NS	0.817 NS	0.431 NS	1 NS	1 NS	1 NS	0.588 NS	1 NS	0.165 NS	0.818 NS
[%]		110	115	1.0	115	1.0	1.0	110	110	115	110	110
N = 14												
Glacier-	0.744	-0.458	0.069	0.448	0.485	0.130	-0.098	-0.011	-0.474	0.281 1	0.709	0.455
Chicama	0.029 **	1 NS	1 NS	1 NS	1 NS	1 NS	1 NS	1 NS	1 NS	NS	0.059 +	1 NS
[%]		NS	143	143	NS	143	143	No	143		т	IND
N = 14												
Till-		-0.249	0.200	0.537	0.446	0.130	0.329	-0.434	-0.569	0.071	0.537	0.503
Chicama		NS	1	0.051	0.256	1	1	0.307	0.026 *	1	0.051	0.098
[%] N = 27			NS	+	NS	NS	NS	NS	*	NS	+	+

 $= p \ value < 0.05, \ ^{**} = p \ value < 0.01, \ ^{***} = p \ value < 0.001, \ ^{+} = p \ value < 0.1, \ ^{NS} = not$ significant

Morainic ridges consisting of Chicama-richer till were deposited by paleoglaciers from source areas and ELA zones with a higher share of Chicama material. Higher Chicama content was associated with higher content of Fe, Mg and Na and decreased content of K (*Table 2*). A comparison of three till samples of both the left and right lateral moraine of the largest morainic ridge complex in the study area yielded distinctly different Chicama shale contents (1-3 % vs. 8-20 %).

3.2 Hydrochemistry

The most abundant anion is HCO_3^- with an average concentration of 344 μ mol/L, followed by SO_4^{2-} (avg. 156 μ mol/L) and Cl^- (avg. 133 μ mol/L). The most abundant cation is Ca^{2+} (total Ca avg. 324 μ mol/L), followed by Na^+ (total Na avg. 144 μ mol/L) and total Si was 160 μ mol/L on

average. Concentrations of Cr, Ga, In, Mo, Pb, Sb, As, Be, Cd, Co and Ni are generally below LOD (*table C.6*) and not used for further analysis.

EC is generally below 150, with a maximum of 290 μ S/cm (*Figure 6a*). pH is above 5.20 in all locations (*Figure 6b*). Alkalinity (3.2-2401 μ mol/L, LOD = 1.7 μ mol/L, Figure 6c) and SO₄²⁻ concentrations (< LOD – 762 μ mol/L, LOD = 15 μ mol/L Figure 6d) are highly variable. Health limits are exceeded only in few locations (*Figure 6e-6f*). The supplementary material contains all concentrations and detection limits (*Table C.6*), used health limits (*Table B.1*) and maps per compound (*Figures B.1 – B.19*).

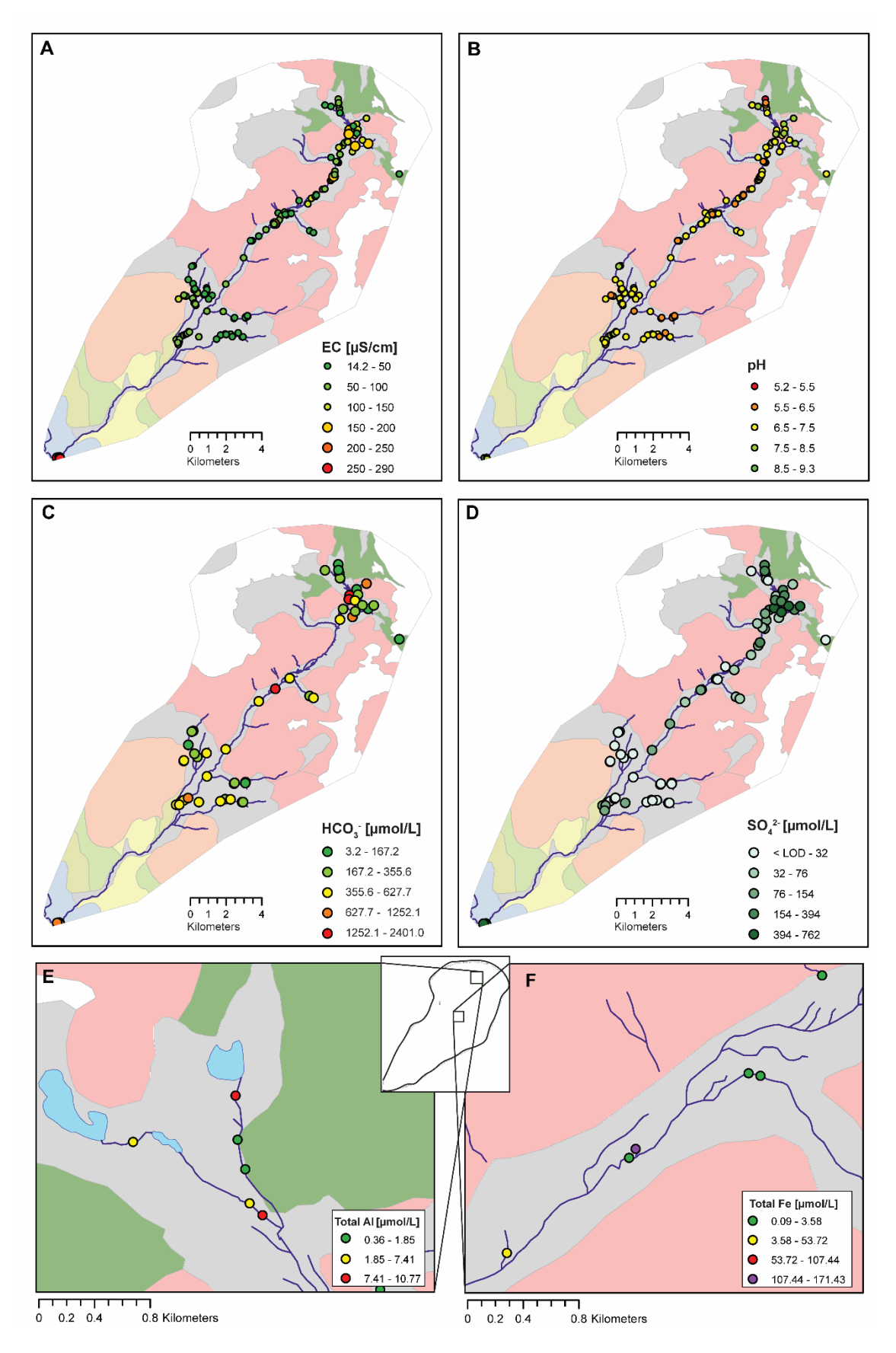


Figure 6) Spatial patterns in surface water EC (a), pH (b), concentration of bicarbonate (c) and sulphate (d). Hazardous concentrations of aluminum (e) and iron (f) were found in specific areas. Supplementary Figures B.2 – B.20 contain similar maps for every analysed compound. Legend for the geological basemap is in figure 1.

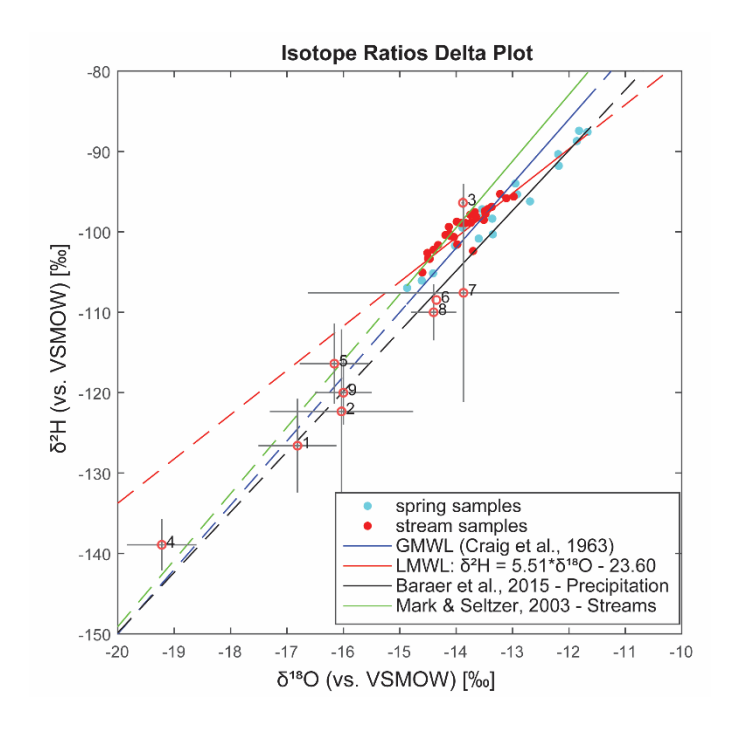


Figure 7) Stable isotope ratios of oxygen and hydrogen, reported on the VSMOW scale. Scatterplot dots are coloured by water type. GMWL indicates the Global Meteoric Water Line established by Craig et al. (1963). Reference data are mixing lines established for stream samples by Mark & Seltzer (2003), and a Local Meteoric Water Line for precipitation samples (2006-2007) in the Cordillera Blanca from Baraer et al. (2015). LML indicates a local mixing line established by fitting a linear trend line through meltwater stream (red) and spring (light blue) samples from this study. Statistics describe correlation between $\delta^{18}O$ and δ^2H for this study only. Dots with error bars represent findings from other studies cited below:

- 1) Glacial Meltwater, July 2009, Quilcayhuanca (Burns et al., 2011)
- 2) Groundwater (taken from springs), July 2009, Quilcayhuanca (Burns et al., 2011)

- 3) Glacial Meltwater, August 2010, La Paz (Guido et al., 2016)
- 4) Glacial Meltwater, March 2011, La Paz (Guido et al., 2016)
- 5) Glacial Meltwater, August 2012, La Paz (Guido et al., 2016)
- 6) High Elevation Streams, March 2011, La Paz (Guido et al., 2016)
- 7) Shallow Groundwater, August 2012, La Paz (Guido et al., 2016)
- 8) Shallow Groundwater, 2008, Cordillera Blanca (Baraer et al., 2015)
 - 9) Streams, 2008, Cordillera Blanca (Baraer et al., 2015)

A delta plot of isotope values found in the Ulta valley shows correspondence with known delta plots for precipitation and surface water in the Cordillera Blanca. However, our samples show a lower slope value (*Figure 7*), especially evident in meltwater streams ($\delta^2 H = -27.0 + 5.2\delta^{18}O$) and less in springs ($\delta^2 H = -16.4 + 6.1\delta^{18}O$). Compared to data from previous studies of isotope ratios in glacial meltwater and shallow groundwater (Guido et al., 2016; Burns et al., 2011) our isotope values are relatively enriched and highly variable among individual tributaries (*Figure B.17-B.18*).

3.3 Effect of till composition on water quality

No generic change in compound or element concentration is found combining all downstream and upstream measurements. Changes in the chemical quality of surface do however depend on the mineralogical composition of tills in the morainic ridge. Relations between till composition and water quality parameters are presented as correlations between till properties and observed changes in water quality parameters (calculated as downstream sample – upstream sample) (*Figure 8*). For 23 locations both up- and downstream water measurements and a till sample are available. Only 13 locations have alkalinity and isotope data. For 11 locations a direct measurement of a moraine-fed spring was available.

Changes in Mg concentration correlate significantly with Chicama content of tills (Figure 8a,), and change in SO_4^{2-} concentration (Figure 8b) shows a tendency (Table C.5). Tills with a lower KSat are associated with increases in SO_4^{2-} , Fe and Mg, although only the correlation with Mg is significant and SO_4^{2-} shows a tendency (Figure 8d-e). The hypothesized correlation between KSat and EC is insignificant (Spearman's r = -0.12, p = 1, n = 23). In some cases, presence of a specific compound in tills is associated with an increase of concentration of that compound in water after contact with a morainic ridge (e.g. for SO_4^{2-} , Figure 8c), although never to a significant extent. All other relations not depicted in figure 8 are insignificant (Table C.5).

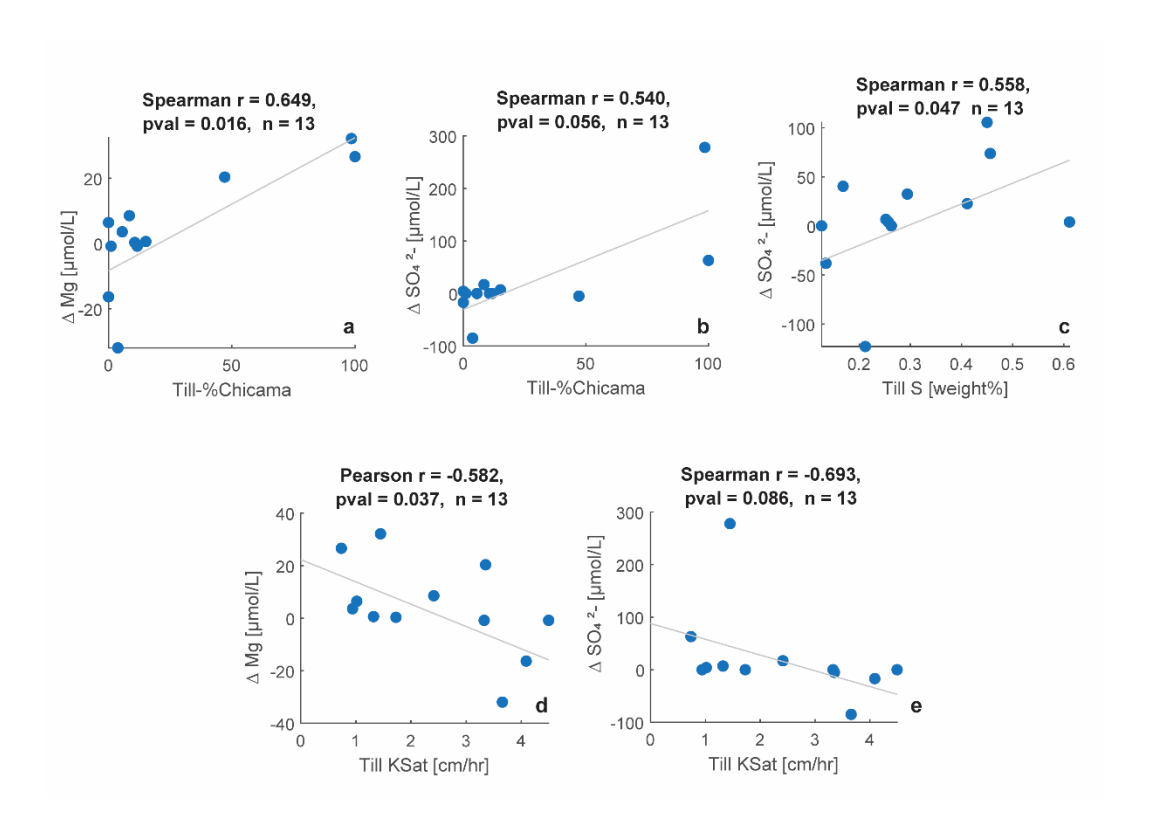


Figure 8) Correlations between till physical and chemical properties and observed changes in water quality calculated as Δ = concentration downstream of till – concentration upstream of till. KSat = Saturated Hydraulic Conductivity. P-values are corrected p-values.

Higher Chicama content in tills is associated with increases in Mg and Fe and decreases in Al and heavy isotope enrichment downstream of the till deposit (*Figure 9a-9e*). Only the change in Mg differs significantly among low-Chicama and high-Chicama tills. Spring water originating from till with high Chicama content shows increased concentration of SO_4^{2-} , Ca, K and Mg relative to springs originating from tills with low Chicama content (*Figure 9f-9i*), although none of these differences are significant. All other differences not depicted in *Figure 9* are insignificant (*Table C.4*).

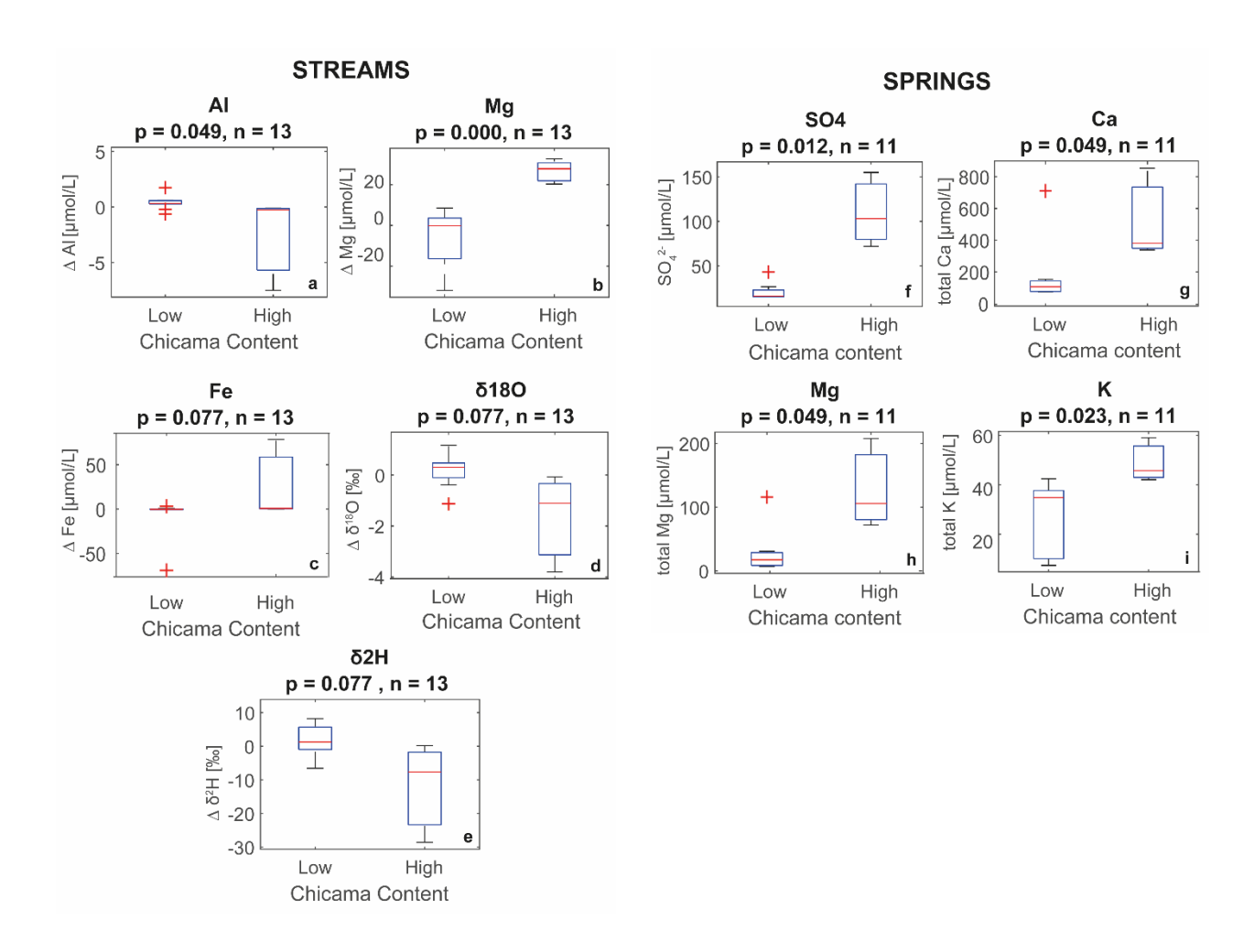


Figure 9 a-g) Changes in water quality parameter observed upon contact with moraines with high and low content of Chicama shales. Changes in water quality were calculated as △ = concentration downstream of till − concentration upstream of till. h-l) Difference between water quality parameters of

springs between springs originating from moraines with high and low content of Chicama shales. "+"signs indicate outliers. P-values are corrected p-values.

3.4 Altitudinal trends in water quality

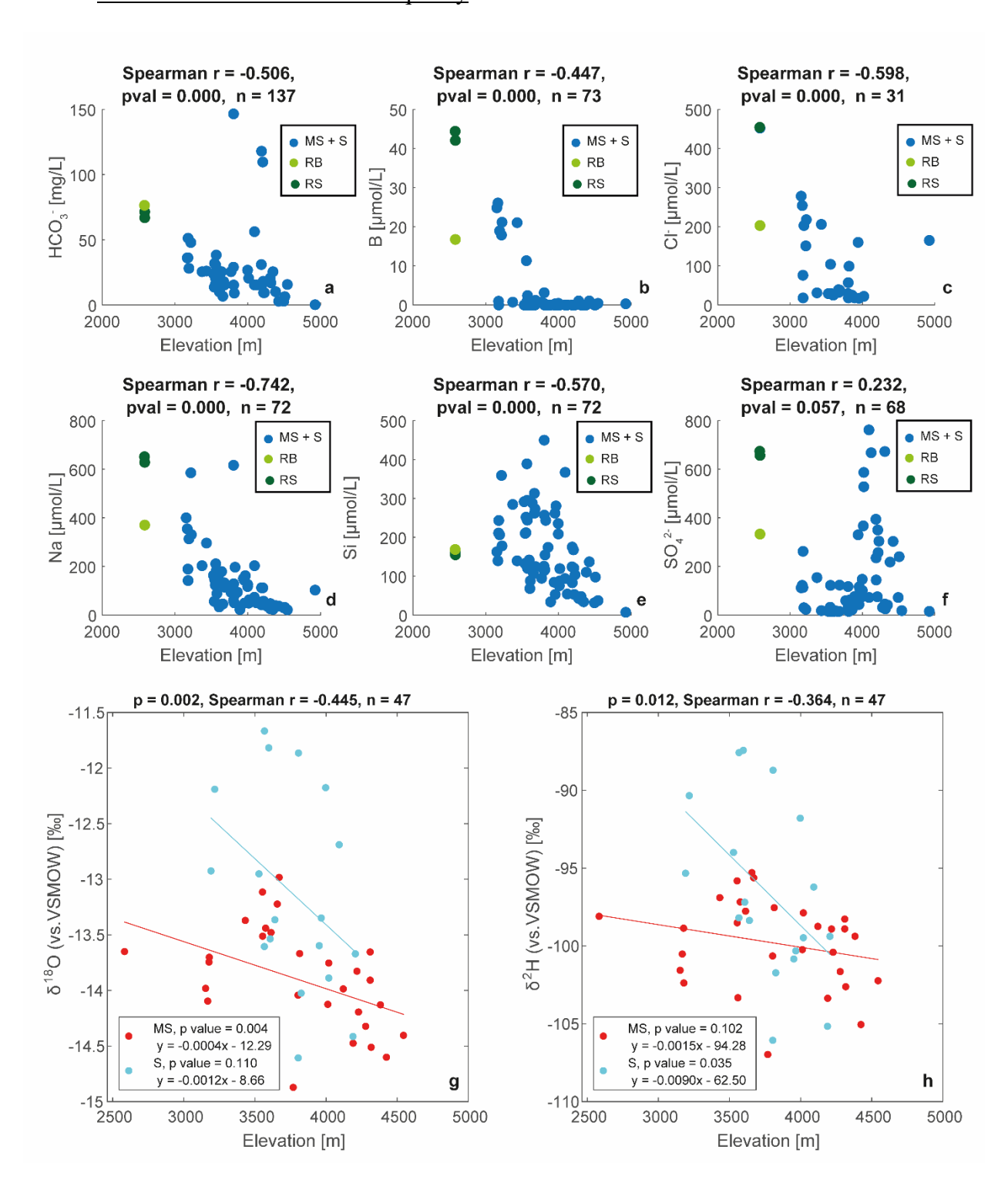


Figure 10) Correlations between water quality parameters and elevation of water sample location. a-f)

Trends in solute concentrations of meltwater streams and springs (MS + S) over elevation, Rio Santa (RS) in dark green, Rio Buin (RB) in light green. P values are corrected p-values. g-h) Correlation between elevation and isotope ratios of oxygen (g) and hydrogen (h). Red dots indicate meltwater stream (MS) samples, light blue dots indicate spring (S) samples. The reported correlation statistics in the figure titles are for both water types combined.

EC and pH do not correlate with elevation (p = 0.62 & 0.18, respectively), but carbonate alkalinity decreases significantly with elevation. Furthermore, concentrations of B, Na, Cl and Si decrease significantly with elevation, whereas SO_4^{2-} shows a tendency of increase with elevation (*Figure 10a-10f*). Other compounds show no significant correlation with elevation. Both $\delta^{18}O$ and δ^2H show a significant negative correlation with elevation (*Figure 10g - 10h*). Overall, $\delta^{18}O$ is given by -11.26 -0.0006*Z and δ^2H is given by -86.82 – 0.0031*Z, where Z is elevation in meters. Steeper declines in heavy isotope enrichment are found for spring samples than for meltwater stream samples, although only significant for δ^2H (*Figure 10g - 10h*).

4. Discussion

4.1 Comparison with other glacial valleys in the Río Santa Basin

In general, waters of the Río Buín catchment contain far lower levels of polluting solutes compared to results from previous studies in nearby tributaries of the Río Santa (Fortner et al., 2011; Burns et al., 2011). Most pH values are in the range of the global mean (7-10) for meltwater (Tranter, 2003). Trace metal contents are generally below the WHO limits, contrasting the results from Fortner et al. (2011) in the Río Quilcay catchment. Locations with low pH and high concentrations of Al, SO_4^{2-} and Fe are only observed in specific places in the northernmost

tributary in the study area originating from a wetland overlying Chicama Formation containing tills and to some extent in the easternmost tributaries (*Figure 6*). Moreover, Fortner et al. (2011) and Burns et al. (2011) report a very low alkalinity in the Quebrada Quilcayhuanca, whereas in this study HCO₃⁻ generally contributes more to total anions than SO₄²- and other anions (*Table C.6*). These differences are consistent with findings of Mark et al. (2005) and Walsh (2013). Mark et al. (2005) found that the Río Buín had the second highest alkalinity (56.5 mg/L of HCO₃⁻) of all tributaries to the Río Santa. *Figure 11* presents measurements of tributaries of the Río Santa from Walsh (2013) complemented with a measurement of the Río Buin (close to the confluence with the Río Santa) from this study. The negative correlation between Chicama cover and HCO₃⁻ (*Figure 11b*) is significant, suggesting that Chicama cover is indeed related to acidification. However, previous studies have not explicitly measured CO₃²⁻ / HCO₃⁻ ions but assumed that the sum of both is given by the difference in charge between measured anions and cations (Tranter et al., 2005; Fortner et al., 2011; Burns et al., 2011; Walsh, 2013).

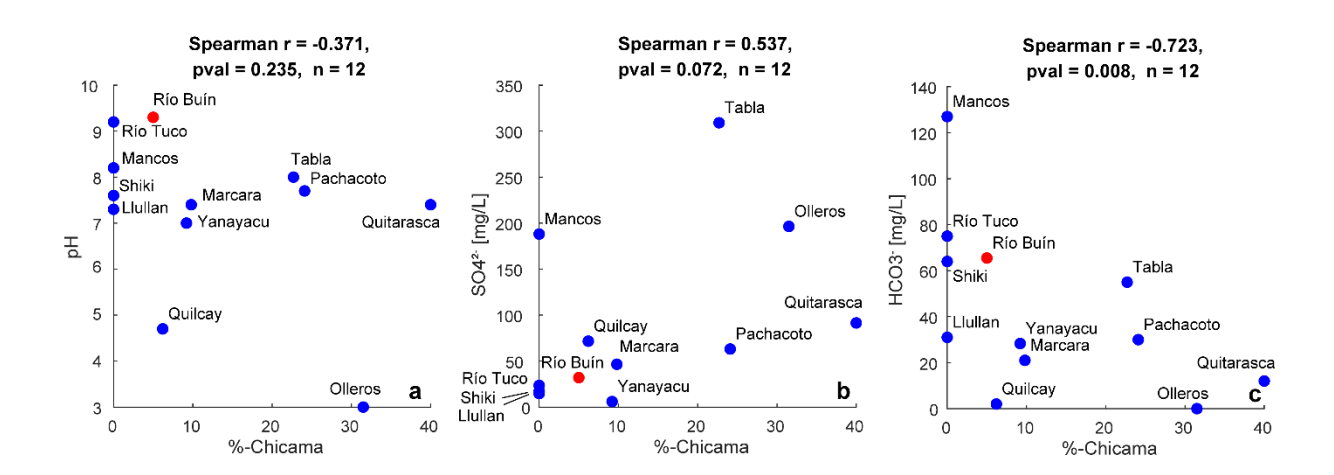


Figure 11) % areal cover of Chicama formation plotted against several important hydrochemical parameters. a) Chicama formation & pH, b) Chicama formation and sulphate, c) Chicama and bicarbonate. Data from Walsh (2013). Río Buín, with data from this study, is indicated in red. Locations of other catchments used for comparison can be found in Figure 1.

Correlations between Chicama cover and both pH and SO₄²-concentrations are not significant (*Figure 11a & 11c*). It seems counter-intuitive that no clear relations exist for Chicama Formation cover and H⁺ and SO₄²- concentration. This can be partly explained by a case-study by Walsh (2013) using data from Mark & Seltzer (2003), which indicates that subglacial weathering of pyrite has a more profound effect on water quality than aerial exposure of pyrite-rich material in the Quebrada Quilcayhuanca. Contrary to the Río Buín catchment, in Mancos, Tabla and Olleros hot springs are present which constitute an additional input of sulphides (Walsh, 2013). Another potential explanation is local variability in pyrite content of the Chicama formation (*Paragraph 4.3*).

Water samples are within the -15 ‰ to -11.5 ‰ range for δ^{18} O and -110 ‰ to -85 ‰ range for δ^{2} H and similar to ratios found by Mark & McKenzie (2007) in the Río Buín in 2004 – 2006. These findings are comparable to results from other studies in the Cordillera Blanca (Burns et al., 2011) and the Bolivian Andes (Guido et al., 2016), although differences may exist based on valley-to-valley variation, seasonal variation (Mark & McKenzie, 2007) and year-to-year variation (Gonfiantini et al., 2001). Our minimum δ^{18} O value of -14.87 ‰ is comparable to the value found for the topmost snow layer of the Huascaran glacier (Thompson et al., 1995). Burns et al. (2011) found a difference in isotopic composition between streams and springs, the latter having a slightly less negative average δ^{18} O composition. Similarly, we find that δ^{18} O is higher on average in springs than in meltwater streams (p < 0.005, n = 71).

Interestingly, we find a mixing line of δ^2H and $\delta^{18}O$ with a lower slope value and higher intercept than earlier mixing lines established for both surface water and precipitation for the Cordillera Blanca (Mark & Seltzer, 2003; Baraer et al., 2015). This is particularly pronounced in meltwater streams and less in springs (*Figure 7*). A lower slope value and higher intercept

(deuterium excess) for surface water may be an indication of post-precipitation fractionation processes such as evaporation (Dansgaard, 1964). This could indicate that meltwater streams undergo evaporation along their trajectory in this catchment, whereas shallow groundwater from moraine-fed springs does not, or to a lesser extent. In contrast, previous isotopic studies of surface water in the Cordillera Blanca did not find significant effects of post-precipitation fractionation (Baraer et al., 2015; Mark & Seltzer, 2003). In general, spring water samples in the Ulta Valley are more comparable to the multi-year local meteoric water line of precipitation for the Cordillera Blanca area from Baraer et al. (2015) than water from meltwater streams (*Figure 7*), indicating that morainic ridges may act as reservoirs for infiltrated precipitation.

Few studies incorporate detrending (*paragraph 2.5*) for temporal variations of chemical quality of water and most do not mention detrending at all (Mark et al., 2005; Fortner et al., 2011; Burns et al., 2011; Baraer et al., 2015), although variation of EC due to diurnal variations in glacial melt has been demonstrated to exist (*Appendix D.3.1* and Burns et al., 2011). EC is inversely related to discharge in proglacial environments as glacial melt is usually more dilute than water from other sources (Burns et al., 2011). However, for pH, isotope ratios and specific compound concentrations, these relations may not be straightforward. Nimick et al. (2003) found widely different compound-specific relations with discharge, which could be explained to some extent by compound-specific sorption processes and geochemical alterations occurring within streams. Additionally, as glacial meltwater may differ in composition from other water sources, not all compounds are suspected to vary with meltwater discharge (Burns et al., 2011; Baraer et al., 2015). Spatial differences in diurnal variation in EC throughout glacial catchments may be an interesting indication for relative glacial melt contribution.

4.2 Spatial trends of water quality in the Ulta Valley

Increasing Si and HCO₃⁻ concentrations are observed downstream as opposed to decreasing SO_4^{2-} concentration (*Figure 10 & 12*). This is consistent with theories of sequential weathering of pyrite and carbonates followed by silicates in proglacial deposits of increasing age (Anderson et al., 2000; Tranter et al. 2005; Burns et al., 2011; Walsh, 2013). These changes may also reflect variations in local geology from Chicama Formation to intrusive rocks further downstream from the active glacier zone in the Quebrada Ulta (*Figure 12*). It may also indicate that streams receive increasing amounts of shallow groundwater derived from precipitation, which has been found to result in higher concentrations of Na and HCO₃⁻, lower SO_4^{2-} concentrations and higher $\delta^{18}O$ compared to glacial meltwater (Baraer et al., 2015; Burns et al., 2011). Lastly, increasing B concentrations (*Figure 10b*) could be related to the use of pesticides.

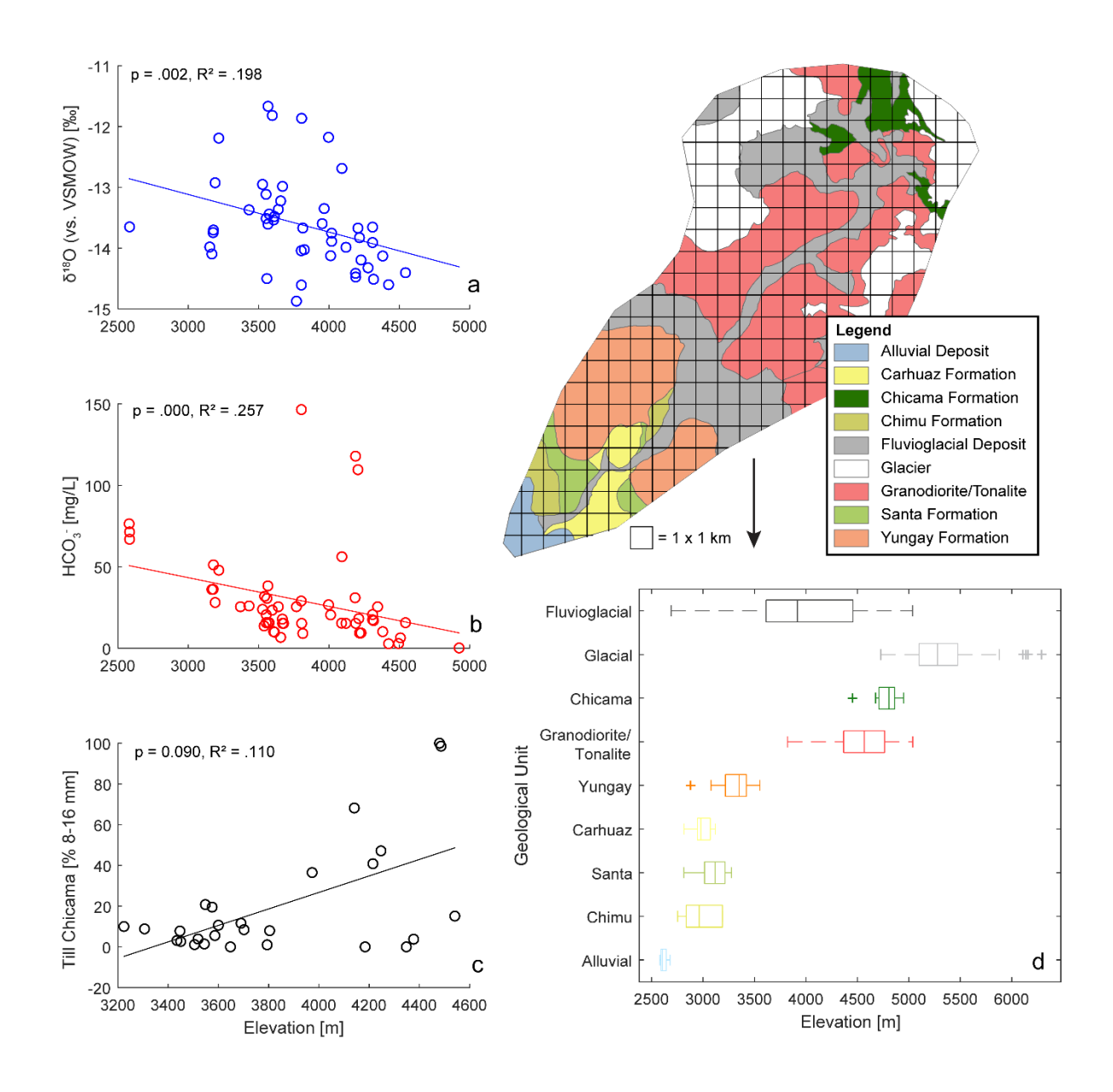


Figure 12) Summary of main trends potentially influencing observed altitudinal variation in water quality. a) $\delta^{18}O$ of spring and meltwater stream samples over elevation. b) bicarbonate concentration of all available water samples over elevation. c) Chicama shale content of till over elevation. d) dominant geology of 1 x 1 km fishnet cell over mean elevation of fishnet cell. "+"-signs indicate outliers.

We found differential trends over elevation for water isotopes in meltwater streams and springs (Figure 10g-h). A correlation between isotope signatures and elevation in precipitation and surface water is found throughout the Cordillera Blanca and may be attributed to (1) the elevation of source precipitation, known as the "rain-out effect" (Windhorst et al., 2013; Rozanski & Araguás-Araguás, 1995) and (2) a decrease in relative contribution of glacial meltwater (depleted in heavy isotopes) versus shallow groundwater (Baraer et al., 2015; Gordon et al., 2015; Burns et al., 2011; Mark & McKenzie, 2007). Especially in case of precipitation derived shallow groundwater, spring isotopic composition is expected to follow trends for δ^{18} O in precipitation against elevation, whereas (partly) meltwater derived streams may not, due to contribution of glacial melt from high source elevation (Mark & McKenzie, 2007). To test our hypothesis that moraines may act as reservoirs for precipitation derived shallow groundwater during the dry season, we compared isotope ratios and their trends against elevation in springs and streams with literature values for surface water and precipitation in Andean catchments. In Andean catchments, slope values for δ^{18} O in precipitation against elevation are typically between -0.24 and -0.17 \% per 100 m rise, and between -1.7 and -1.12 ‰ per 100 m rise for δ^2 H (Baraer et al., 2015; Windhorst et al., 2013; Rozanski & Araguás-Araguás, 1995). Results in Figure 10g-h indicate that overall, slope values for surface water in the Ulta Valley are much lower (-0.06% for δ^{18} O and -0.31% for δ^2 H). Slope values for regression lines of δ^{18} O and δ^2 H over altitude for spring water (-0.12‰ and -0.90‰) (Figure 10g-h) are more comparable to previously mentioned findings for precipitation, albeit still low. Especially at lower elevation, springs are demonstrated to be more enriched in heavy isotopes than meltwater streams (Figure 10g-h), also indicating that springs likely contain less meltwater than streams (Gordon et al., 2015). Apart from a significant relation with elevation, distinct spatial variability in isotope signatures is observed. Tributaries from subcatchments with a larger degree of glaciation have relatively low δ^{18} O and δ^{2} H levels (*Figure B.17* & B.18), which may indicate a larger fraction of glacial meltwater with a high source elevation. Several springs originating from moraines and talus slopes show particularly positive isotope ratios (Figure B17 - B.18) compared to stream samples from the same altitude. One lake sample shows an anomalously high enrichment of heavy isotopes, which is attributed to high evaporation of water. Altogether, samples from moraine-fed springs are more enriched in heavy isotopes, show larger similarity to the local meteoric water line (Baraer et al., 2015) and show larger similarity to known gradients of heavy isotope enrichment over source area elevation of precipitation. This suggests that moraines act as reservoirs of precipitation during the dry season. However, isotope ratios of spring water samples also show higher variability over elevation than meltwater streams (Figure 10g-h), which indicates a substantial degree of variation in source area or in postprecipitation fractionation. Shallow groundwater from moraine-fed springs may be derived from precipitation or infiltrated glacial meltwater from various source elevations, as a result of which individual springs may have distinct isotopic signatures (Baraer et al, 2015). Possibly, groundwater recharged at high elevation contributes to springs and/or baseflows at lower elevation via such subsurface aguifers. Tracer studies could be used to identify various pathways (Gordon et al., 2015).

4.3 Geochemistry of the Ulta Valley

Mineralogical classification of rock fragments yields clear spatial distinctions between presence of intrusives and Chicama rock fragments in tills (*Figure 4*), which in turn are strongly related to till source area (*Table 2, Figure 1*). According to Petford & Atherton (1996) intrusives in the Quebrada Ulta are generally metaluminous leucogranodiorite with high contents of sodic plagioclase, which is consistent with the findings of this study. Although the Chicama formation

is known to be a very heterogeneous deposit (sandstones, shales, argillites and pyrites) (Burns et al., 2011; Enay et al., 1996), the Chicama formation in the Cordillera Blanca consists mostly of dark shales with fine layers of sandstone (Smith, 1988). In the Ulta Valley, locally quartz-veins and sandstone fragments are found in till samples, although Chicama fragments are almost exclusively dark shales (*table C.2*), consistent with Smith's (1988) findings.

We found a tendency for a positive correlation between till Chicama content and till Fe content but no significant correlation between till Chicama content and till S content (Table 2). This is remarkable, as Fe and S are expected to occur as pyrite (FeS_2) in Chicama shales. Possibly, high initial rates of pyrite oxidation result in high leaching rates of SO₄² (Anderson et al., 2000; Tranter et al., 2005) whereas Fe precipitates locally as ferric oxyhydroxides (Åström & Åström, 1997; Munk et al., 2002). Indeed, a significant proportion of rock fragments analysed for this study contained ferric oxyhydroxide coating (Magnússon, pers. obs). Another potential explanation is local variability in pyrite content of Chicama shales within the Cordillera Blanca. Sampled Chicama shales could contain relatively little pyrite compared to those in other sites throughout the Cordillera Blanca, although element concentrations (Figure 5) suggest that it is present. Figure 5 demonstrates significant, positive associations between concentrations of S, As, Fe, and Cu indicating that arsenopyrite and chalcopyrite may also be present in the Ulta valley. The presence of these sulphides was already noted by Bodenlos & Ericksen (1955). Total Mg in tills also shows a tendency for a positive correlation with Chicama content (Table 2), and significant, positive correlations (almost 1:1) with till S content and till Fe content (Figure 5). This may be an indication that apart from pyrite, Chicama shales contain considerable amounts of Mg, possibly in the form of ferromagnesian minerals. Vikre (1998) found that due to hydrothermal alterations rocks close to contact zones may have atypical composition. The presence of Mg in the Chicama Formation or in contact zones is supported by the positive correlation between till Chicama content and observed difference in Mg concentration in water samples downstream and upstream of tills (*Figure* 8). To facilitate analysis of the effect of source rock composition on water quality throughout the Cordillera Blanca, local differences in the composition of Chicama shales (e.g. content of pyrite and ferromagnesian minerals) could be studied by X-ray Diffraction analysis (XRD).

4.4 Influence of Glacial Sediments

The lack of a clear generic effect downstream of morainic ridges compared to upstream indicates that the influence of morainic ridges on the chemical quality of surface water is likely very limited. However, pronounced differences in changes in ion and element concentrations are observable between waters that had been in contact with Chicama-rich and Chicama-poor tills (see figure 9). This indicates that the effect of tills on water quality depends on till composition (Chicama shale content in this case). Chicama-rich tills are associated with increased Mg concentrations, a compound that is also found in Chicama-rich tills (Figure 5). The hypothesized increase in concentration of SO₄²- in surface water after contact with a Chicama-rich moraine is visible (Figure 8 & 9), although effects are small and generally insignificant. Despite weaker correlations, the three samples with the highest HCO₃ content (> 1600 µmol/L) are all moraineor talus-fed springs, although due to low discharges little effect propagates downstream of such springs. Still, this may indicate that locally moraines (and potentially talus deposits) may be important sources of HCO₃. No significant increases in total Fe were observed upon contact with morainic ridges. The reason for low Fe concentrations is most likely its local precipitation as oxyhydroxide (Åström & Åström, 1997; Munk et al., 2002). Similarly, trace metals associated with acid rock drainage may be adsorbed onto mineral surfaces of the streambeds at circumneutral

pH (Munk et al., 2002; Schemel et al., 2007; Lee et al., 2002). Munk et al. (2002) found that 75 % of dissolved trace metals were removed from streams by sorption to precipitates in a confluence zone with pH 5 – 6.3 of a highly acidic and alkaline tributary, which is similar to pH in the Ulta Valley. This indicates that high alkalinity in the Ulta Valley likely buffers potential contamination. Lastly, the difference in observed effect between Chicama-rich and Chicama-poor moraines may be related to the relative contribution of coupled pyrite oxidation and CO₃²-dissolution typical of young proglacial deposits (Walsh, 2013; Tranter et al., 2005; Anderson et al., 2000). However, the occurrence of Chicama bedrock, the age of moraines and the relative importance of meltwater and precipitation-derived shallow groundwater seem to be subjected to the same altitudinal trend (*Figure 12*), making it difficult to attribute observed changes in water quality over altitude to any of these potential factors.

Interestingly, no significant impacts of Chicama material in tills on EC and pH are observed. In case of pH it is possible that the relatively high abundance of HCO₃⁻ within the Ulta valley buffers any addition of H⁺ resulting from natural weathering processes. Additionally, no significant effect of KSat on changes in EC is observed. This could also be explained by low contribution of moraine-fed springs to total water discharge.

5. Conclusion

The till mineralogy is strongly correlated to paleoglacier lithology. This correlation implies that it is possible to predict the subglacial lithology from recent moraine deposits. This may be a valuable tool in assessing the impact of deglaciation of catchments worldwide. In this respect it is noteworthy that most Chicama shales occur in the higher, still glaciated areas of the Quebrada Ulta. This may result in secondary negative effects of climate change on water safety in the Río Santa catchment through deglaciation.

Morainic ridges are found to have no significant generic effect on water quality in the Ulta Valley. Instead, the changes in the chemical water quality upon contact with a morainic ridge depend on the mineralogical composition (Chicama content) of the tills present in the ridge. Higher Chicama content is associated with increases in solute load of Mg and in some cases SO₄². Isotopic signatures of moraine-fed springs indicate that moraines are potential reservoirs for precipitation-derived shallow groundwater during the dry season. However, variable isotopic signatures among individual springs from morainic ridges independent of elevation suggest that relative storage of precipitation-derived and glacial meltwater varies among morainic ridges (and potentially also among talus cones and other permeable deposits) and represents an important factor in the influence of morainic ridges on water quality. Our results demonstrate that local changes in the chemical quality of surface water can be traced back to the mineralogy of specific glacial tills deposits and thereby to their source area geology. This may help to identify potential sources of natural contamination and to explain spatial patterns of chemical quality of surface water in glacial catchments.

Overall, water quality in the Río Buín catchment seems higher than in other areas in the Cordillera Blanca (most notably Quebrada Quilcayhuanca and the Río Negro catchment) when

compared to drinking water standards. Low provenance of Chicama Formation and high alkalinity help explain the relatively good water quality in the Río Buín catchment.

We found collinear trends in decreased presence of Chicama formation, occurrence of subglacial and proglacial weathering processes and relative quantities of meltwater and precipitation-derived shallow groundwater with decreasing elevation. Therefore, it remains a challenge to attribute trends in chemical water quality over elevation to any specific mechanism.

Acknowledgements

We would like to thank the SERNANPE and the Parque Nacional Huascaran for giving us access to the Quebrada Ulta and allowing for scientific research (license N° 011 -2016-SERNANP-PNH (05/07/2016)).

This work was supported in part by a group travelling scholarship of the AUF (Amsterdams Universiteits Fonds); The AUF had no role in the conceptualization, execution, analysis, interpretation or publishing of this research.

References

Andersen, C. B. (2002). Understanding carbonate equilibria by measuring alkalinity in experimental and natural systems. *Journal of Geoscience Education*, *50*, 389-403.

Anderson, S. P., Drever, J. I., & Humphrey, N. F. (1997). Chemical weathering in glacial environments. *Geology*, 25, 399-402.

- Anderson, S. P., Drever, J. I., Frost, C. D., & Holden, P. (2000). Chemical weathering in the foreland of a retreating glacier. *Geochimica et Cosmochimica Acta*, 64, 1173-1189.
- Åström, M., & Åström, J. (1997). Geochemistry of stream water in a catchment in Finland affected by sulphidic fine sediments. *Applied Geochemistry*, *12*, 593-605.
- Ballantyne, C.K. (2002), Paraglacial geomorphology. Quaternary Science Reviews 21, 1935-2017
- Baraer, M., McKenzie, J., Mark, B. G., Gordon, R., Bury, J., Condom, T. & Gomez, J., Knox, S. & Fortner, S. K. (2015). Contribution of groundwater to the outflow from ungauged glacierized catchments: a multi-site study in the tropical Cordillera Blanca, Peru. *Hydrological Processes*, 29, 2561-2581.
- Baraer, M., Mark, B., Wigmore, O., Fernandez-Rivera, A., McKenzie, J., & Walsh, E. (2012). From the Cordillera Blanca to the Pacific Ocean: Hydrological changes and consequences across the Río Santa watershed. *AGU Fall Meeting Abstracts*, 1, 07.
- Baraer, M., McKenzie, J. M., Mark, B. G., Bury, J., & Knox, S. (2009). Characterizing contributions of glacier melt and groundwater during the dry season in a poorly gauged catchment of the Cordillera Blanca (Peru). *Advances in Geosciences*, 22, pp. 41–49.
- Benn, D., & Evans, D. (2010). Glaciers and glaciation. 802 pp. Arnold, London.
- Blott, S. J., & Pye, K. (2001). GRADISTAT: a grain size distribution and statistics package for the analysis of unconsolidated sediments. *Earth surface processes and Landforms*, 26, 1237-1248.

- Bodenlos, A. J., & Ericksen, G. E. (1955). Lead-Zinc Deposits of Cordillera Blanca and Northern Cordillera Huayhuash, Peru, *United States Geological Survey Bulletin*, 1017, 166p.
- Boulton, G. (1986). Push-moraines and glacier-contact fans in marine and terrestrial environments. Sedimentology, 33, 677-698.
- Brand W.A., Coplen T.B., Vogl J., Rosner M., Prohaska T. (2014). Assessment of international reference materials for isotope-ratio analysis (IUPAC technical report). *Pure and Applied Chemistry*, 86, 425–467
- Burns, P., Mark, B., & McKenzie, J. (2011). A multi-parameter hydrochemical characterization of proglacial runoff, Cordillera Blanca, Peru. *The Cryosphere Discussions*, *5*, 2483-2521.
- Bury, J., Mark, B. G., Carey, M., Young, K. R., McKenzie, J. M., Baraer, M., French, A. & Polk,
 M. H. (2013). New geographies of water and climate change in Peru: Coupled natural and social transformations in the Santa River watershed. *Annals of the Association of American Geographers*, 103, 363-374.
- Craig, H., Gordon, L. I., & Horibe, Y. (1963). Isotopic exchange effects in the evaporation of water: 1. Low-temperature experimental results. *Journal of Geophysical Research*, 68, 5079-5087.
- Dahl, S. O., & Nesje, A. (1992). Paleoclimatic implications based on equilibrium-line altitude depressions of reconstructed Younger Dryas and Holocene cirque glaciers in inner Nordfjord, western Norway. *Palaeogeography, Palaeoclimatology, Palaeoecology*, 94, 87-97.
- Dansgaard, W. (1964). Stable isotopes in precipitation. *Tellus*, 16, 436-468.

- Enay, R., Barale, G., Jacay, J., & Jaillard, E. (1996). Upper Tithonian ammonites and floras from the Chicama basin, northern Peruvian Andes. *GeoResearch Forum*, 1, p. 2.
- ESRI (2011). Arc Hydro Tools v2.0 Tutorial.

 http://downloads.esri.com/archydro/archydro/Tutorial/Doc/Arc%20Hydro%20Tools%202.0

 %20-%20Tutorial.pdf
- European Space Agency (2016). Sentinel-2 MSI. Retrieved from http://geodata.science.uva.nl, on 10-06-2016.
- Farber, D. L., Hancock, G. S., Finkel, R. C., & Rodbell, D. T. (2005). The age and extent of tropical alpine glaciation in the Cordillera Blanca, Peru. *Journal of Quaternary Science*, 20, 759-776
- Fortner, S. K., Mark, B. G., McKenzie, J. M., Bury, J., Trierweiler, A., Baraer, M., Burns, P. J. & Munk, L. (2011). Elevated stream trace and minor element concentrations in the foreland of receding tropical glaciers. *Applied Geochemistry*, 26, 1792-1801.
- Gee, G. W., & Or, D. (2002). 2.4 Particle-size analysis. Methods of soil analysis. Part 4, 255-293.
- Glas, R. L., Lautz, L., McKenzie, J. M., Moucha, R., & Mark, B. G. (2017). Proglacial Hydrogeology of the Cordillera Blanca (Peru): Integrating Field Observations with Hydrogeophysical Inversions to Inform Groundwater Flow Simulations and Conceptual Models. *AGU Fall Meeting Abstracts*.
- Gonfiantini R., Roche M.-A., Olivry J.-C., Fontes J.-C. and Zuppi G. M. (2001). The altitude effect on the isotopic composition of tropical rains. *Chemical Geology 181*, 147-167.

- Gordon, R. P., Lautz, L. K., McKenzie, J. M., Mark, B. G., Chavez, D., & Baraer, M. (2015). Sources and pathways of stream generation in tropical proglacial valleys of the cordillera blanca, peru. *Journal of Hydrology*, 522, 628-644.
- Gran, G. (1950). Determination of the equivalence point in potentiometric titrations. *Acta Chemica Scandinavica*, *4*, 559-577.
- Guido, Z., McIntosh, J. C., Papuga, S. A., & Meixner, T. (2016). Seasonal glacial meltwater contributions to surface water in the Bolivian Andes: A case study using environmental tracers. *Journal of Hydrology: Regional Studies*, 8, 260-273.
- Holm, S. (1979) A simple sequentially rejective multiple test procedure. *Scandinavian Journal of Statistics*, 6, 65-70.
- Instituto Geológico, Minero y Metalúrgico. (2011). Serie A, Carta Geológica Nacional.
- Iturrizaga, L. (2014). Glacial and glacially conditioned L types in the cordillera blanca, peru. A spatiotemporal conceptual approach. *Progress in Physical Geography*, *38*, 602-636.
- Jiménez Cisneros, B.E., Oki, T., Arnell, N.W., Benito G., Cogley, J.G., Döll, P., Jiang, T. & Mwakalila, S.S. (2014). Freshwater resources. In: Climate Change 2014: Impacts, Adaptation, and Vulnerability. Part A: Global and Sectoral Aspects. Contribution of Working Group II to the Fifth Assessment Report of the Intergovernmental Panel on Climate Change [Field, C.B., Barros, V.R., Dokken, D.J., Mach, K.J., Mastrandrea, M.D., Bilir, T.E., Chatterjee, M., Ebi, K.L., Estrada, Y.O., Genova, R.C., Girma, B., Kissel, E.S., Levy, A.N.,

- MacCracken, S., Mastrandrea, P.R., & White, L.L. (eds.)]. Cambridge University Press, Cambridge, United Kingdom and New York, NY, USA, pp. 229-269.
- Kaser, G., Ames, A., & Zamora, M. (1990). Glacier fluctuations and climate in the Cordillera Blanca, Peru. *Annals of Glaciology*, *14*, 136-140.
- Kaser, G., & Georges, C. (1997). Changes of the equilibrium-line altitude in the tropical cordillera bianca, peru, 1930 50, and their spatial variations. *Annals of Glaciology*, *24*, 344-349.
- Kaser, G., Juen, I., Georges, C., Gómez, J., & Tamayo, W. (2003). The impact of glaciers on the runoff and the reconstruction of mass balance history from hydrological data in the tropical cordillera blanca, peru. *Journal of Hydrology*, 282, 130-144.
- Lee, G., Bigham, J. M., & Faure, G. (2002). Removal of trace metals by coprecipitation with Fe, Al and Mn from natural waters contaminated with acid mine drainage in the Ducktown Mining District, Tennessee. *Applied Geochemistry*, *17*, 569-581.
- López-Moreno, J. I., Valero-Garcés, B., Mark, B., Condom, T., Revuelto, J., Azorín-Molina, C., Bazo, J., Frugone, M. Vicente-Serrano, S. M. & Alejo-Cochachin, J. (2017). Hydrological and depositional processes associated with recent glacier recession in Yanamarey catchment, Cordillera Blanca (Peru). Science of The Total Environment, 579, 272-282.
- Mark, B. G., Bury, J., McKenzie, J. M., French, A., & Baraer, M. (2010). Climate change and tropical andean glacier recession: Evaluating hydrologic changes and livelihood vulnerability in the Cordillera blanca, peru. *Annals of the Association of American Geographers*, 100, 794-805.

- Mark, B. G., & McKenzie, J. M. (2007). Tracing increasing tropical Andean glacier melt with stable isotopes in water. *Environmental Science & technology*, 41, 6955-6960.
- Mark, B. G., McKenzie, J. M., & Gomez, J. (2005). Hydrochemical evaluation of changing glacier meltwater contribution to stream discharge: Callejon de Huaylas, Peru/Evaluation hydrochimique de la contribution évolutive de la fonte glaciaire à l'écoulement fluvial: Callejon de Huaylas, Pérou. *Hydrological Sciences Journal*, 50, 975-987.
- Mark, B. G., & Seltzer, G. O. (2003). Tropical glacier meltwater contribution to stream discharge: a case study in the Cordillera Blanca, Peru. *Journal of Glaciology*, 49, 271-281.
- Mark, B. G., & Seltzer, G. O. (2005). Evaluation of recent glacier recession in the Cordillera Blanca, Peru (AD 1962–1999): spatial distribution of mass loss and climatic forcing. *Quaternary Science Reviews*, 24, 2265-2280.
- Mehra, O.P., Jackson M.L. (1960). Fe Oxide removal from soil and clays by a dithionite-citrate system buffered with sodium carbonate. *Clays and Clay Minerals*, 7, 317-327.
- Meierding, T. C. (1982). Late Pleistocene glacial equilibrium-line altitudes in the Colorado Front Range: a comparison of methods. *Quaternary Research*, *18*, 289-310.
- Munk, L., Faure, G., Pride, D. E., & Bigham, J. M. (2002). Sorption of trace metals to an aluminum precipitate in a stream receiving acid rock-drainage; Snake River, Summit County, Colorado. *Applied Geochemistry*, 17, 421-430.

- Nimick, D. A., Gammons, C. H., Cleasby, T. E., Madison, J. P., Skaar, D., & Brick, C. M. (2003).

 Diel cycles in dissolved metal concentrations in streams: occurrence and possible causes.

 Water Resources Research, 39, 1247.
- Oliver, B. G., Thurman, E. M. & Malcolm, R. L. (1983). The contribution of humic substances to the acidity of colored natural waters. *Geochimica et Cosmochimica Acta*, 47, 2031–2035.
- Petford, N., & Atherton, M. (1996). Na-rich partial melts from newly underplated basaltic crust: The cordillera blanca batholith, peru. Journal of Petrology, 37, 1491-1521.
- Racoviteanu, A. E., Arnaud, Y., Williams, M. W., & Ordonez, J. (2008). Decadal changes in glacier parameters in the Cordillera Blanca, Peru, derived from remote sensing. *Journal of Glaciology*, 54, 499-510.
- Rabatel, A., Francou, B., Soruco, A., Gomez, J., Caceres, B., Ceballos, J.L., Basantes, R., Vuille, M., Sicart, J.-E., Huggel, C., Scheel, M., Lejeune, Y., Arnaud, Y., Collet, M., Condom, T., Consoli, G., Favier, V., Jomelli, V., Galarraga, R., Ginot, P., Maisincho, L., Mendoza, J., Menegoz, M., Ramirez, E., Ribstein, P., Suarez, W., Villacis, M. & Wagnon, P. (2013)
 Current state of glaciers in the tropical Andes: a multi-century perspective on glacier evolution and climate change. *Cryosphere*, 7, 81-102.
- Rodbell, D. T. (1992). Lichenometric and radiocarbon dating of holocene glaciation, cordillera blanca, peru. *The Holocene*, 2, 19-29.

- Rodbell, D. T. (1993). Subdivision of late pleistocene moraines in the cordillera blanca, peru, based on rock-weathering features, soils, and radiocarbon dates. *Quaternary Research*, *39*, 133-143.
- Rodbell, D. T., & Seltzer, G. O. (2000). Rapid ice margin fluctuations during the younger dryas in the tropical andes. *Quaternary Research*, *54*, 328-338.
- Rodbell, D. T., Seltzer, G. O., Mark, B. G., Smith, J. A., & Abbott, M. B. (2008). Clastic sediment flux to tropical Andean lakes: records of glaciation and soil erosion. *Quaternary Science Reviews*, 27, 1612-1626.
- Rozanski, K., & Araguás-Araguás, L. (1995). Spatial and temporal variability of stable isotope composition of precipitation over the South American continent. Bulletin de l'Institut Français d'études Andines, 24, 379-390.
- Saxton, K.E. (2007). SPAW (Soil-Plant-Air-Water) Field & Pond Hydrology v.6.02 [software]. Available: http://hrsl.ba.ars.usda.gov/SPAW/Index.htm [Accessed 11 December 2017].
- Saxton, K.E., and W.J. Rawls. (2006). Soil water characteristic estimates by texture and organic matter for hydrologic solutions. *Soil science society of America Journal*, 70, 1569–1578.
- Saxton, K., and P. Willey. (2005). The SPAW Model for Agricultural Field and Pond Hydrologic Simulation. InSingh, V., Frevent, D. (eds.), Mathematical Modeling of Watershed Hydrology. CRC Press LLC.

- Schemel, L. E., Kimball, B. A., Runkel, R. L., & Cox, M. H. (2007). Formation of mixed Al–Fe colloidal sorbent and dissolved-colloidal partitioning of Cu and Zn in the cement Creek–Animas River confluence, Silverton, Colorado. *Applied Geochemistry*, 22, 1467-1484.
- Solomina, O., Jomelli, V., Kaser, G., Ames, A., Berger, B., & Pouyaud, B. (2007). Lichenometry in the Cordillera Blanca, Peru: "Little Ice Age" moraine chronology. *Global and Planetary Change*, *59*, 225-235.
- Thompson, L. G., Mosley-Thompson, E., Davis, M. E., & Lin, P. N. (1995). Late glacial stage and Holocene tropical ice core records from Huascaran, Peru. *Science*, 269, 46.
- Tranter, M. 2003. Geochemical weathering in glacial and proglacial environments. *Treatise on Geochemistry*, 5, 189-205.
- Tranter, M., Skidmore, M., & Wadham, J. (2005). Hydrological controls on microbial communities in subglacial environments. *Hydrological Processes*, *19*, 995-998.
- United States Geological Survey (2013). The Alkalinity Calculator. Retrieved from: http://or.water.usgs.gov/alk/ on 13-06-2016
- Vikre, P. G. (1998). B110: Intrusion-related, polymetallic carbonate replacement deposits in the Eureka District, Eureka County, Nevada (Vol. 110). NV Bureau of Mines & Geology.
- Walsh, E. A. (2013). The Origin and Distribution of Trace Metals in the Río Santa Watershed, Peru. (Doctoral Dissertation, McGill University)

Windhorst, D., Waltz, T., Timbe, E., Frede, H. G., & Breuer, L. (2013). Impact of elevation and weather patterns on the isotopic composition of precipitation in a tropical montane rainforest. Hydrology and Earth System Sciences, 17, 409.

APPENDIX A MAGNUSSON ET AL. 2017 – FIELD MAPS

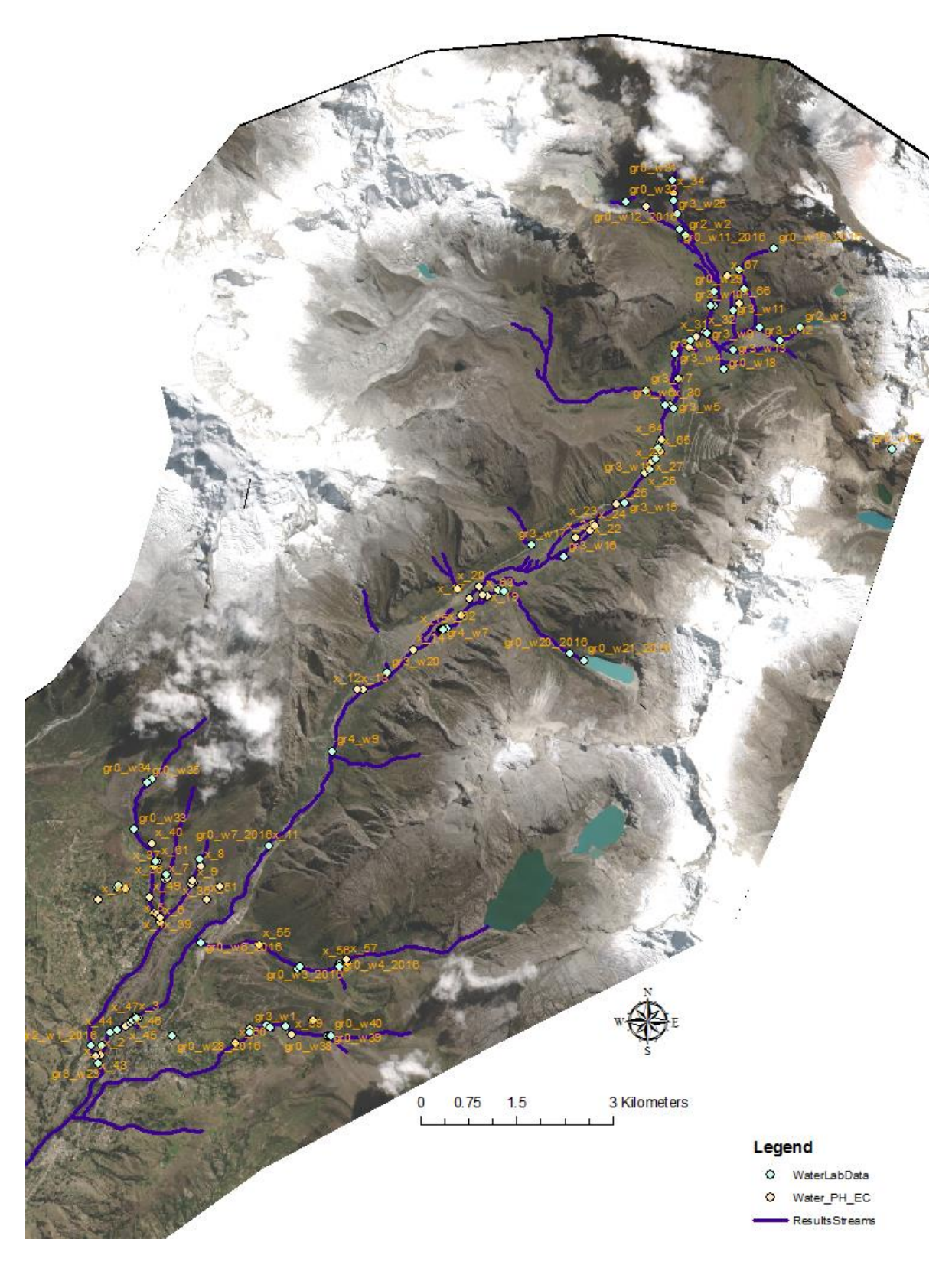


Figure A.1) Spatial Distribution of water sampling points.

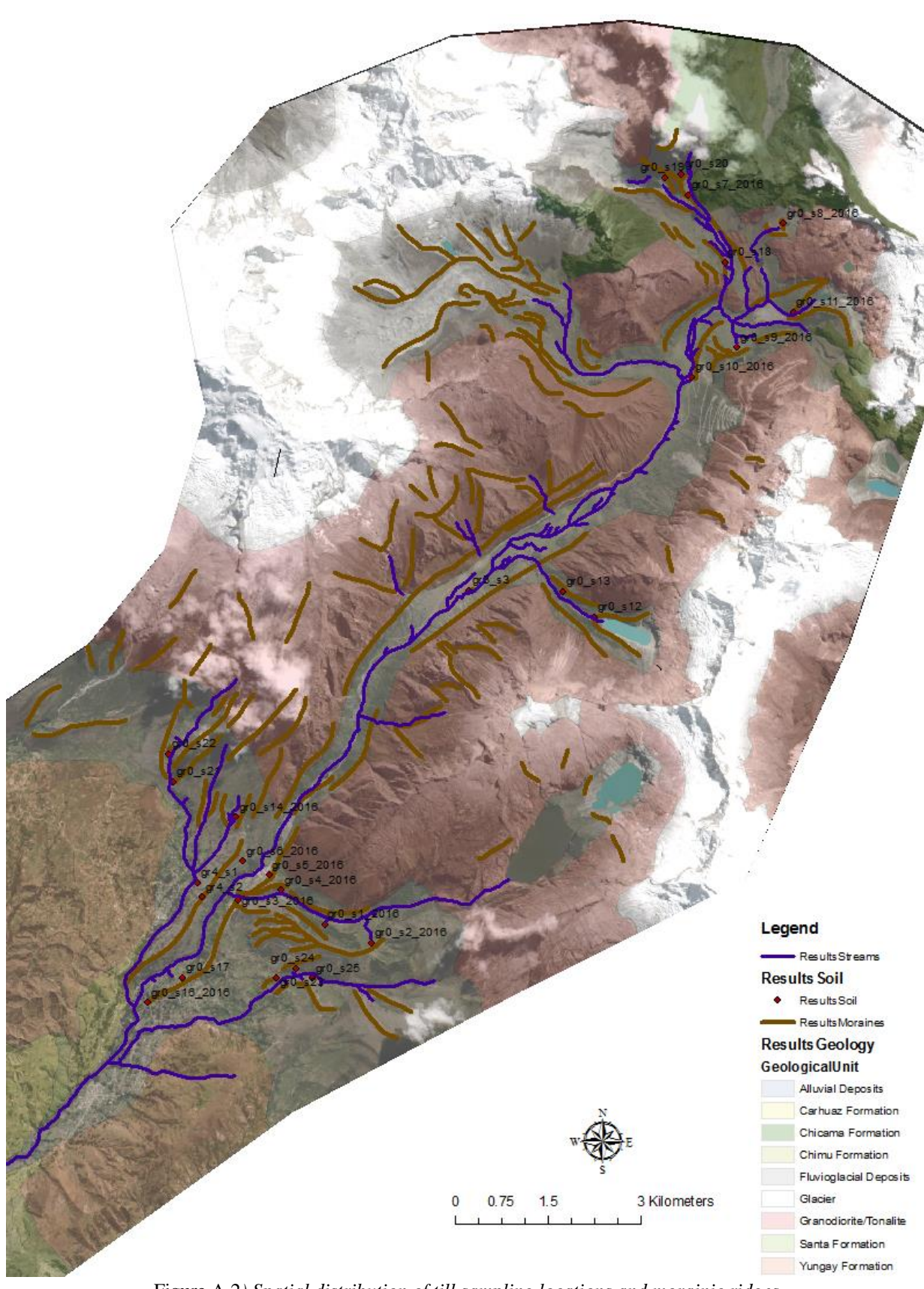


Figure A.2) Spatial distribution of till sampling locations and morainic ridges

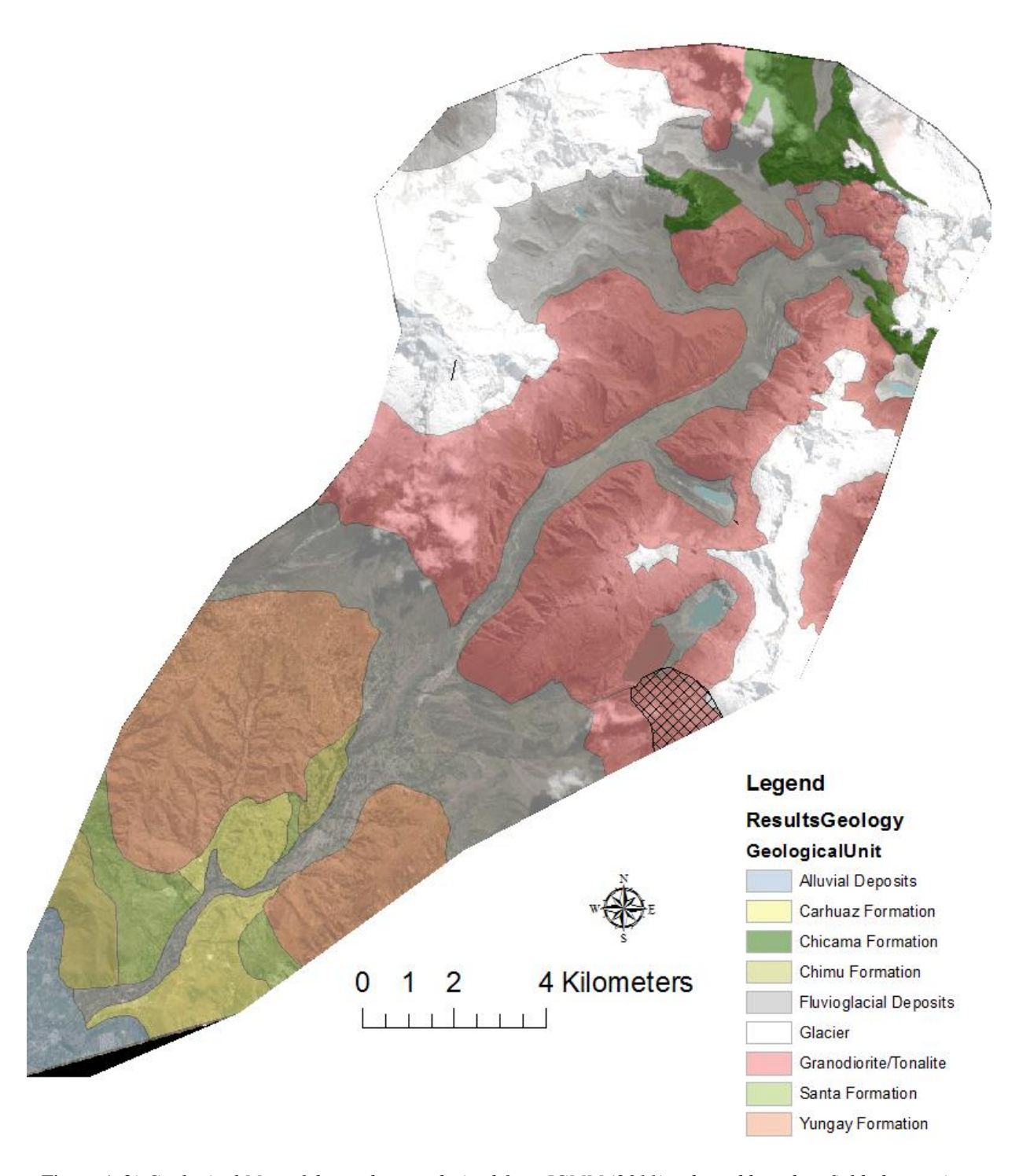
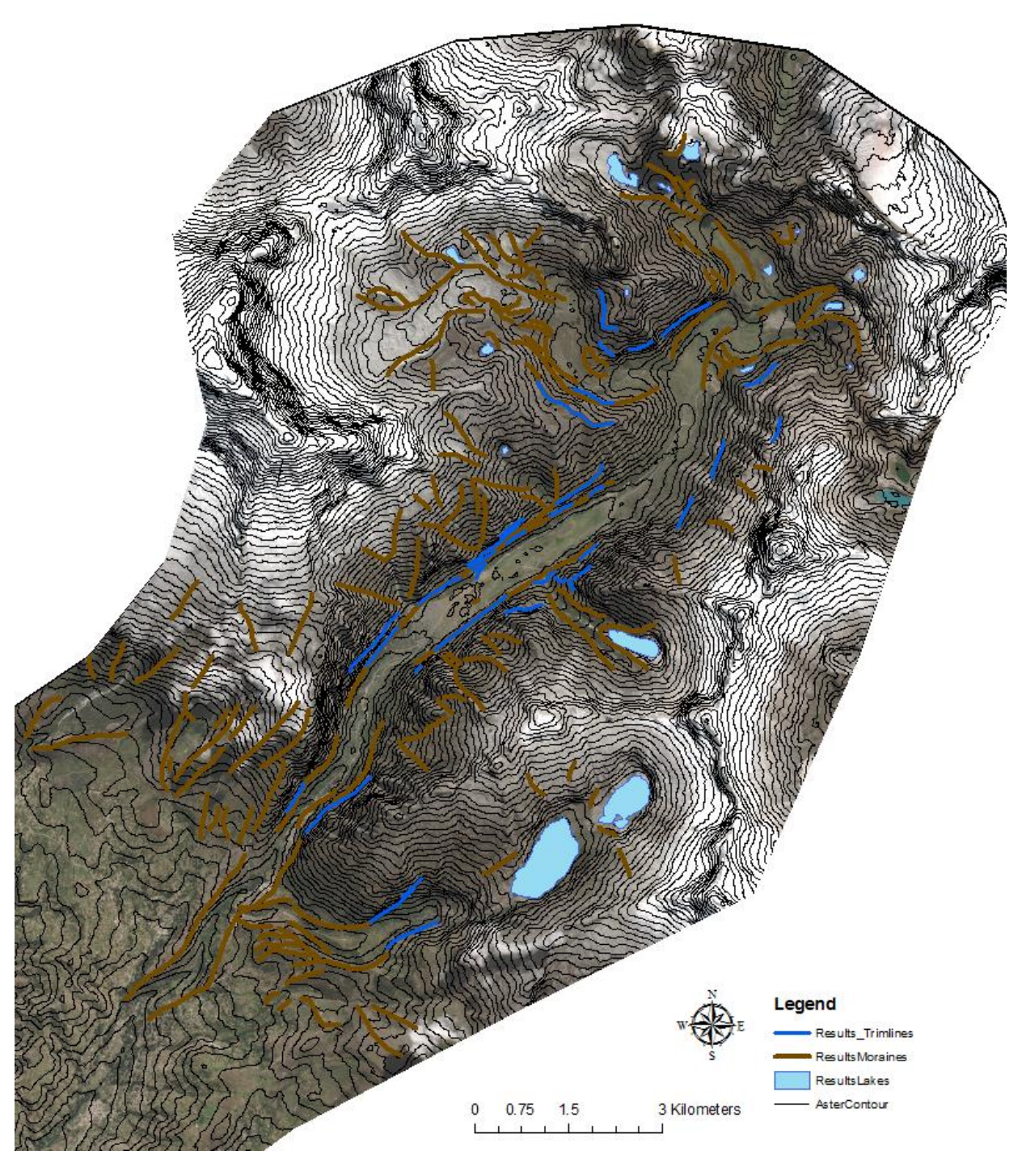


Figure A.3) Geological Map of the study area derived from IGMM (2011), adapted based on field observations



 $\underline{\text{Figure A.4}}) \ \textit{Glacial features (trimlines \& moraines) mapped based on field observations and Sentinel data (ESA, 2016).}$

APPENDIX B MAGNUSSON ET AL. 2017 – SOLUTE MAPS

Table B.1) Statistics of results per compound compared to an international set of drinking water quality standards,

detection limits and determination limits.												
COMPOUND	DETECTION LIMIT	LIMIT - EU	LIMIT - WHO	LIMIT - CANADA	LIMIT - EPA	LIMIT- NAM	LIMIT - PERU	LIMIT - GROUNDWATE	SET LIMIT	AVG_CONC	MAX_CONC	MIN_CONC
	[µmol/L]						l	I		[arithmetic]		
NOx	3	462.96			92.59		490.74		92.59	0.74	25.00	<lod< th=""></lod<>
NH4	3	27.72							27.72	0.88	44.00	<lod< th=""></lod<>
PO4	0.2								-	0.38	2.30	<lod< th=""></lod<>
Cl	15	7052	7052	7052	7052	7052	7052	7052	7052	48.14	454.00	<lod< th=""></lod<>
SO4	25	2603	5205	5205	2603	2603	2603	2603	2603	147.89	762.00	<lod< th=""></lod<>
Al	0.06	7.41	7.41	7.41	1.85	5.56	7.41		1.85	2.89	10.77	0.36
Ca	0.1					3743			3742.5	324.94	1080.7	10.13
Fe	0.01	3.58		5.37	53.72		5.37		3.58	6.60	171.43	0.09
K	0.05						5115		5115	35.03	702.93	6.11
Li	0.01					251.5			251.51	1.92	21.63	0.04
Mg	0.08					2879			2879	66.77	436.82	1.53
Mn	0.002	9.10	9.10	9.10	9.10	1.82	7.28		1.82	0.58	6.51	0.01
Na	0.3	8699	8699	8699		4350	8699		4350	143.88	651.59	21.16
S	4.5								-	221.84	1019.1	<lod< th=""></lod<>
Si	0.1								-	160.10	449.84	6.83
As	0.2	0.13	0.13	0.13		0.13	0.13		0.13	<lod< th=""><th><lod< th=""><th><lod< th=""></lod<></th></lod<></th></lod<>	<lod< th=""><th><lod< th=""></lod<></th></lod<>	<lod< th=""></lod<>
Be	0.005				0.44	0.22			0.22	0.00	0.02	<lod< th=""></lod<>
Cd	0.01	0.04	0.03	0.04	0.04	0.09	0.03		0.03	0.00	0.01	<lod< th=""></lod<>
Co	0.008					4.24		1.70	1.70	0.01	0.06	<lod< th=""></lod<>
Cu	0.01	31.47	31.47	15.74	20.46	7.87	31.47		7.87	0.02	0.23	<lod< th=""></lod<>
Ni	0.03	0.34	0.34			0.43	0.34		0.34	0.03	0.19	<lod< th=""></lod<>
Sr	0.0002			57.06					57.06	0.78	5.11	0.02
Ti	0.004					2.09			2.09	0.05	1.98	<lod< th=""></lod<>
Zn	0.02		76.44			76.44			76.44	2.48	9.61	<lod< th=""></lod<>
В	0.1	92.51	27.75	462.5		46.25	138.8		27.75	3.55	44.38	<lod< th=""></lod<>
Ba	0.003		2.18	7.28	14.56	3.64	5.10		2.18	0.03	0.23	<lod< th=""></lod<>
Cr	0.02	9.62	9.62	9.62		1.92	9.62		1.92	<lod< th=""><th><lod< th=""><th><lod< th=""></lod<></th></lod<></th></lod<>	<lod< th=""><th><lod< th=""></lod<></th></lod<>	<lod< th=""></lod<>
Ga	0.1								-	0.00	0.12	<lod< th=""></lod<>
In	0.06							0.44	0.44	0.00	0.06	<lod< th=""></lod<>
Мо	0.01					0.52	0.73	0.42	0.42	0.01	0.17	<lod< th=""></lod<>
Pb	0.03	0.05	0.05	0.05		0.72			0.05	<lod< th=""><th><lod< th=""><th><lod< th=""></lod<></th></lod<></th></lod<>	<lod< th=""><th><lod< th=""></lod<></th></lod<>	<lod< th=""></lod<>
Sb	0.1	0.04	0.04	0.05		0.82	1.64		0.04	<lod< th=""><th><lod< th=""><th><lod< th=""></lod<></th></lod<></th></lod<>	<lod< th=""><th><lod< th=""></lod<></th></lod<>	<lod< th=""></lod<>

Used water quality standards:

EU: Water Research Center (2014). Total Dissolved Solids & Water Quality. http://www.water-research.net/index.php/water-treatment/tools/total-dissolved-solids. Visited 14-12-2016

WHO: World Health Organization, 2011: Guidelines for drinking-water quality-4th edition. World Health Organization, Switzerland, 564 pp.

CANADA: Health Canada, 2012: Guidelines for Canadian Drinking Water Quality-Summary Table. Water, Air and Climate Change Bureau, Healthy Environments and Consumer Safety Branch, Health Canada, Ottawa, Ontario, 22 pp. EPA: Environmental Protection Agency (2009). National Primary Drinking Water

Regulations. United States Environmental Protection Agency, US, 6pp.

NAM: Namibia Water Corporation Ltd: (n.d.). Guidelines for the evaluation of drinkingwater for human consumption with regard to chemical, physical and bacteriological quality. Namibia Water Corporation Ltd., Namibia, 5 pp.

PERU: Ministerio de Salud, Peru (2011). Decreto Supremo DS NW 031-2010-SA. Reglamento de la Calidad del Agua para Consumo Humano [Supreme Decree DS NW 031–2010-SA. Drinking-water regulation.

http://www.digesa.minsa.gob.pe/publicaciones/descargas/reglamento_calidad_agua.pdf

GROUNDWATER: Ground Water Quality Standards, (2011): Ground Water Quality Standards - Class IIA by Constituent. New Jersey Dept. of Environmental Protection, 7 pp.

S2 – 20 contain maps of the concentrations measured per specific compound. *Blue* colors indicate that detection limits were not exceeded. *Green* colors indicate that the compound was detected but did not cross any of the water quality limits. *Yellow* colors indicate that one or more of the water qualities were crossed. *Red* colors indicate that all water quality standards were exceeded. *Purple* colors indicate that the compounds concentration was more than twice the upper water quality limit. Figures S18 and S19 contain maps of stable isotope ratios of oxygen and hydrogen. Figure S20 contains a map of presence of iron precipitates in stream beddings.

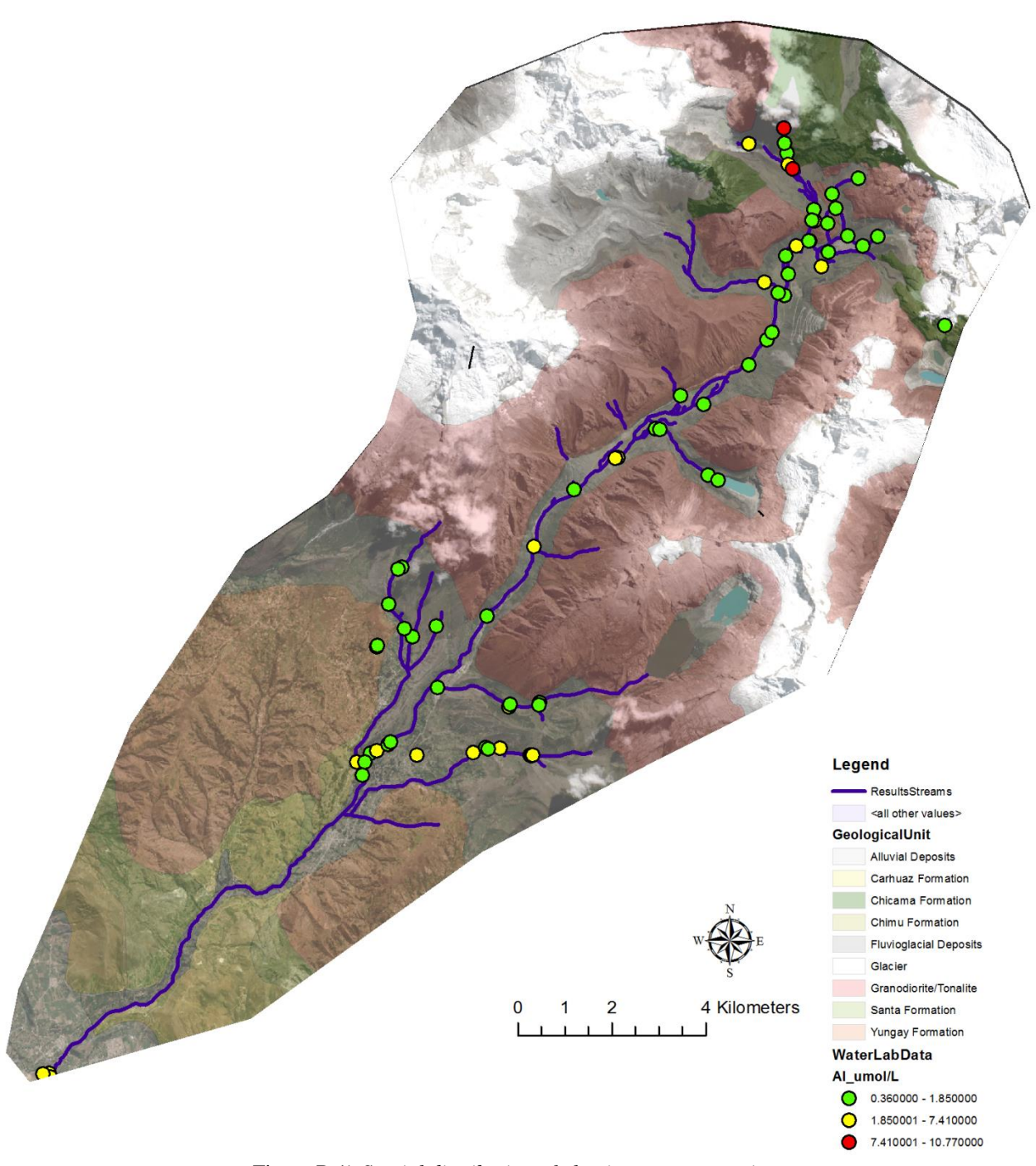


Figure B.1) Spatial distribution of aluminum concentration.

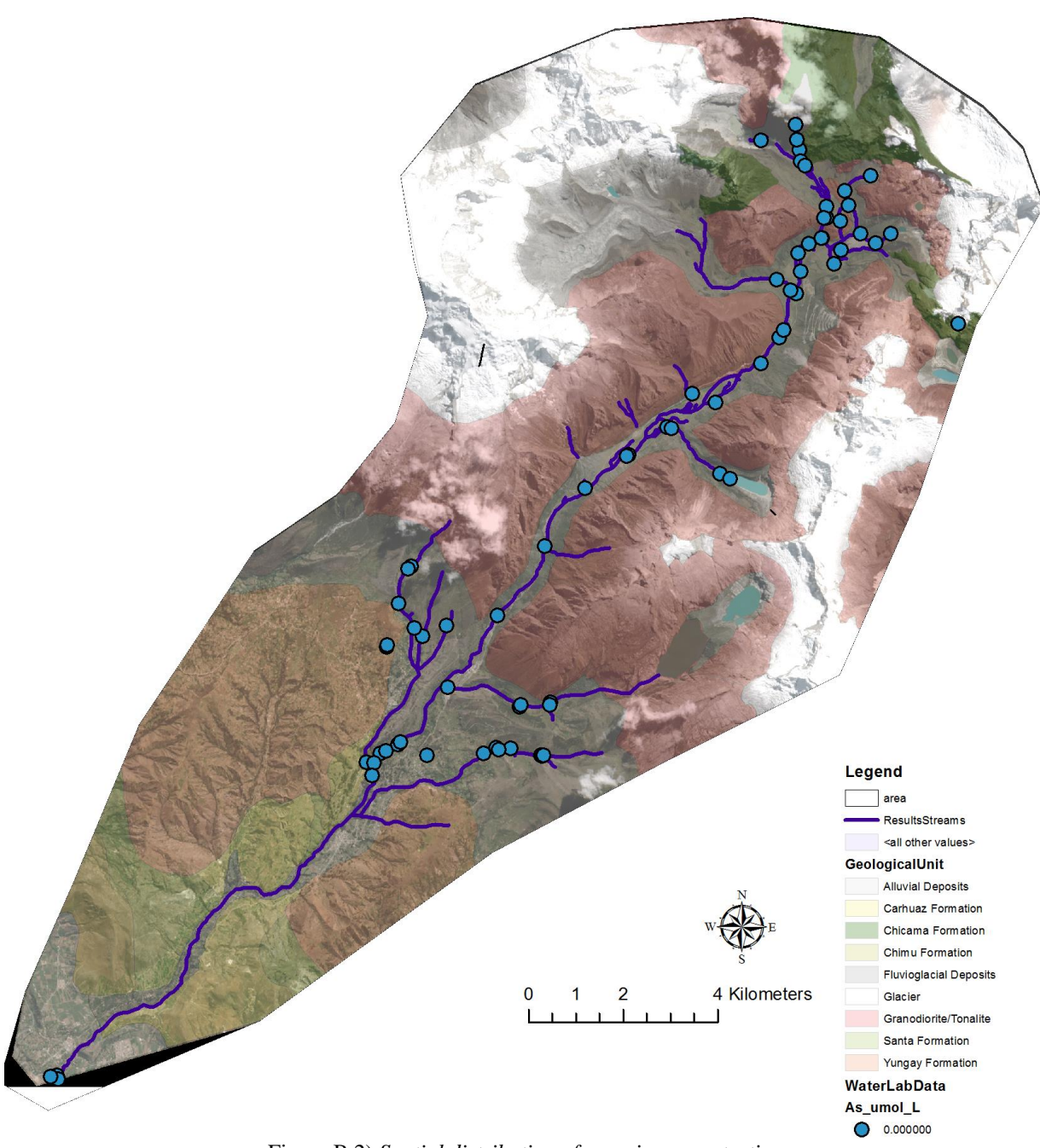


Figure B.2) Spatial distribution of arsenic concentration

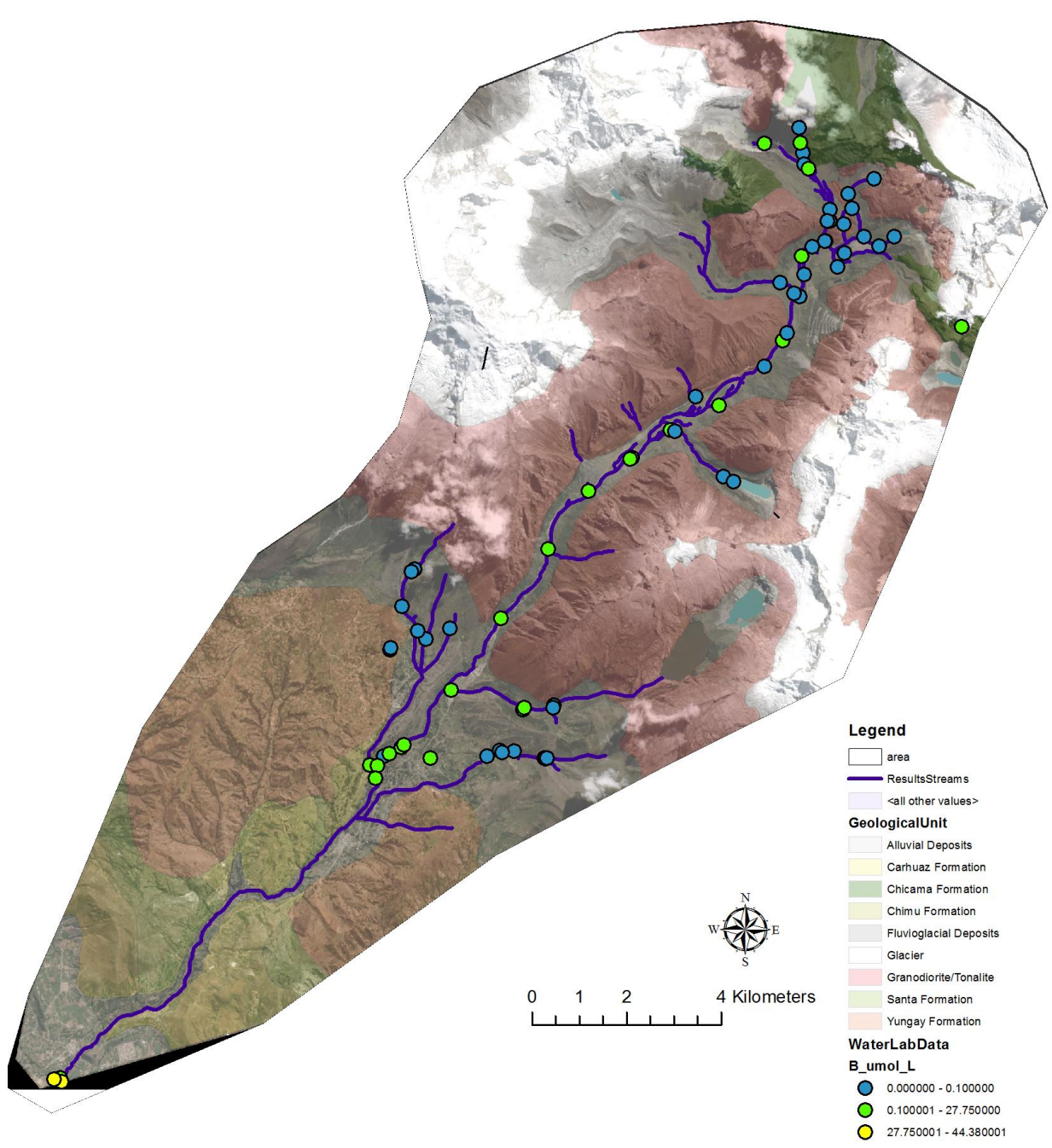
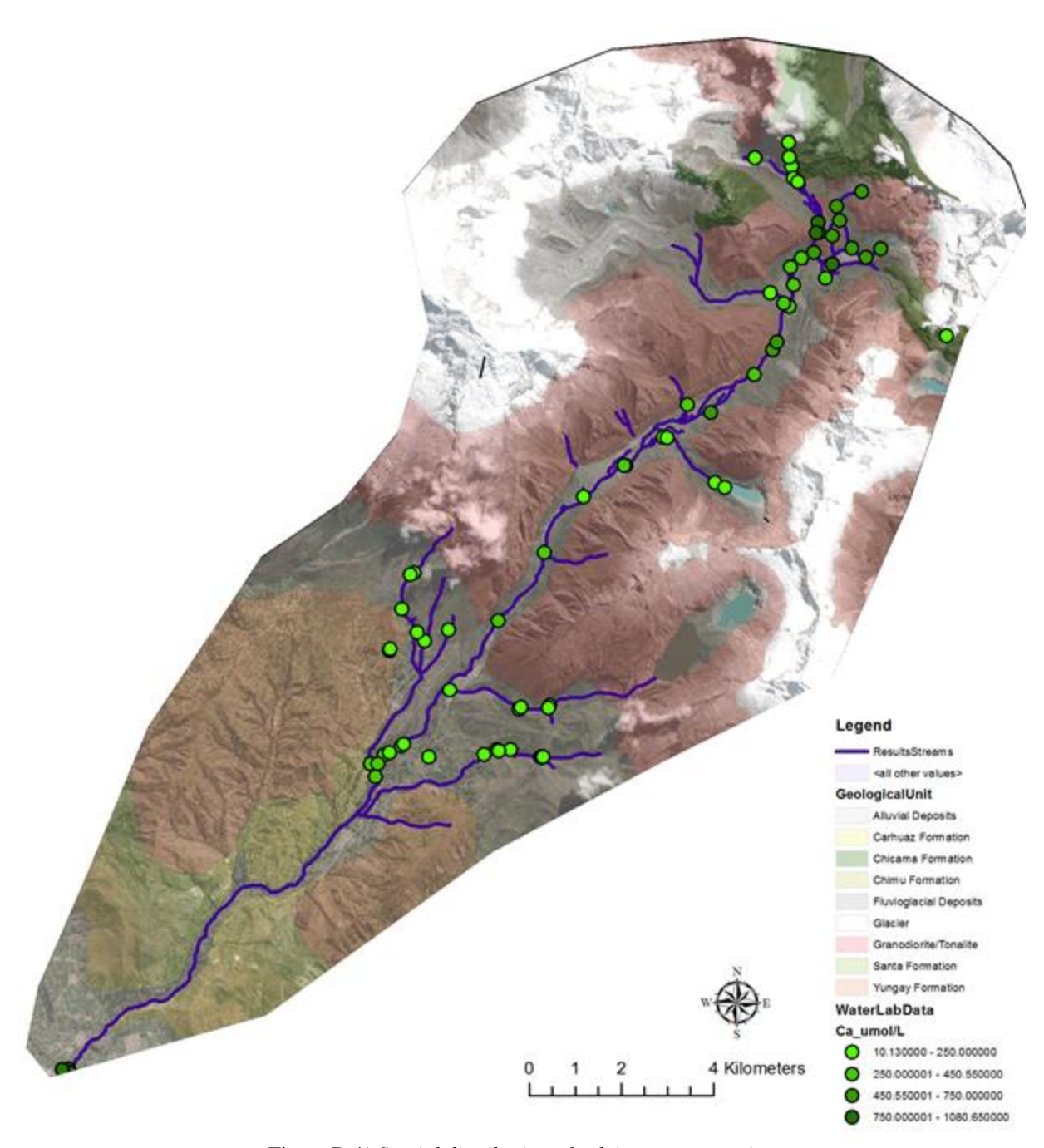


Figure B.3) Spatial distribution of boron concentration



 $\underline{Figure~B.4})~Spatial~distribution~of~calcium~concentration$

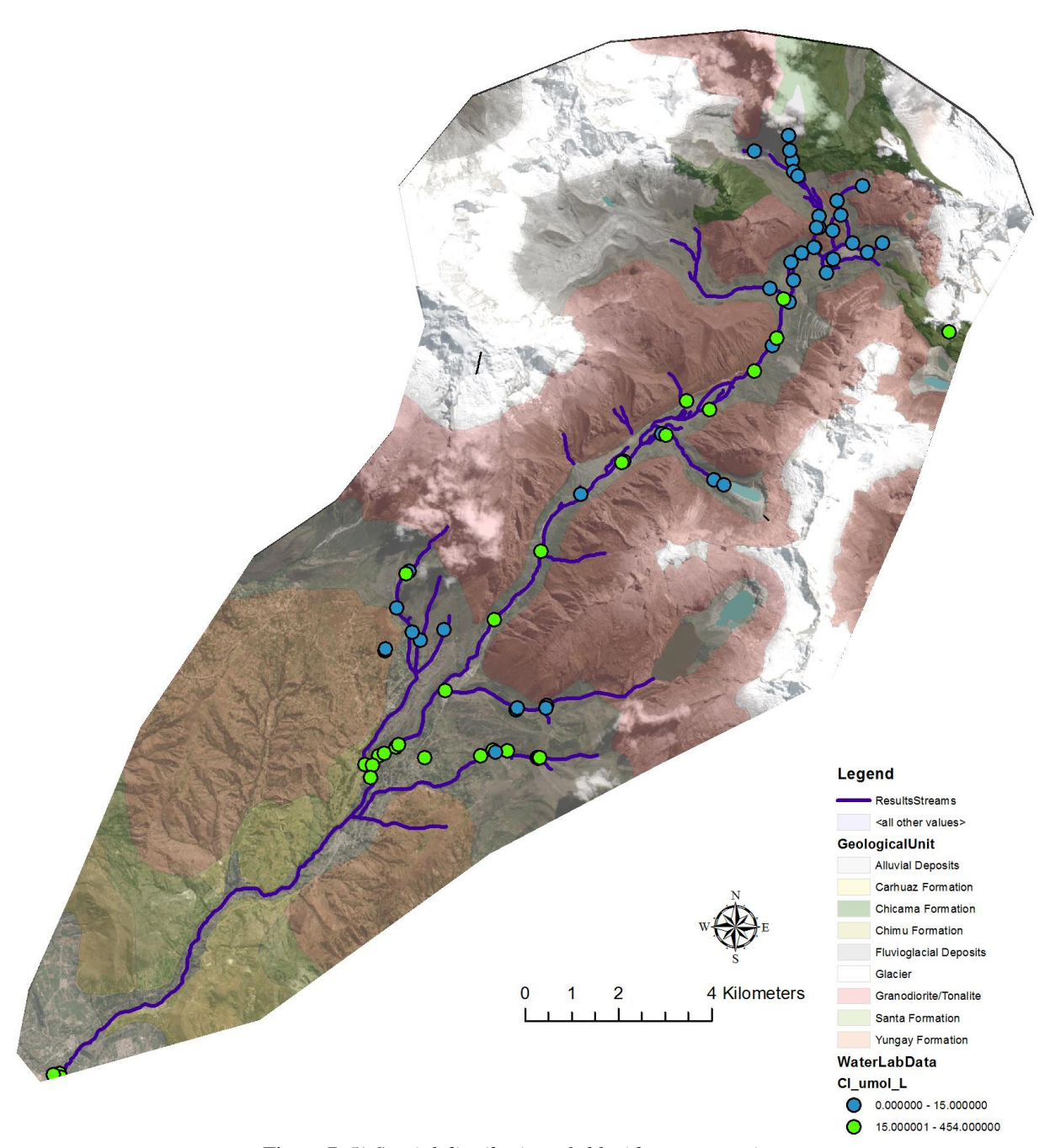


Figure B.5) Spatial distribution of chloride concentration

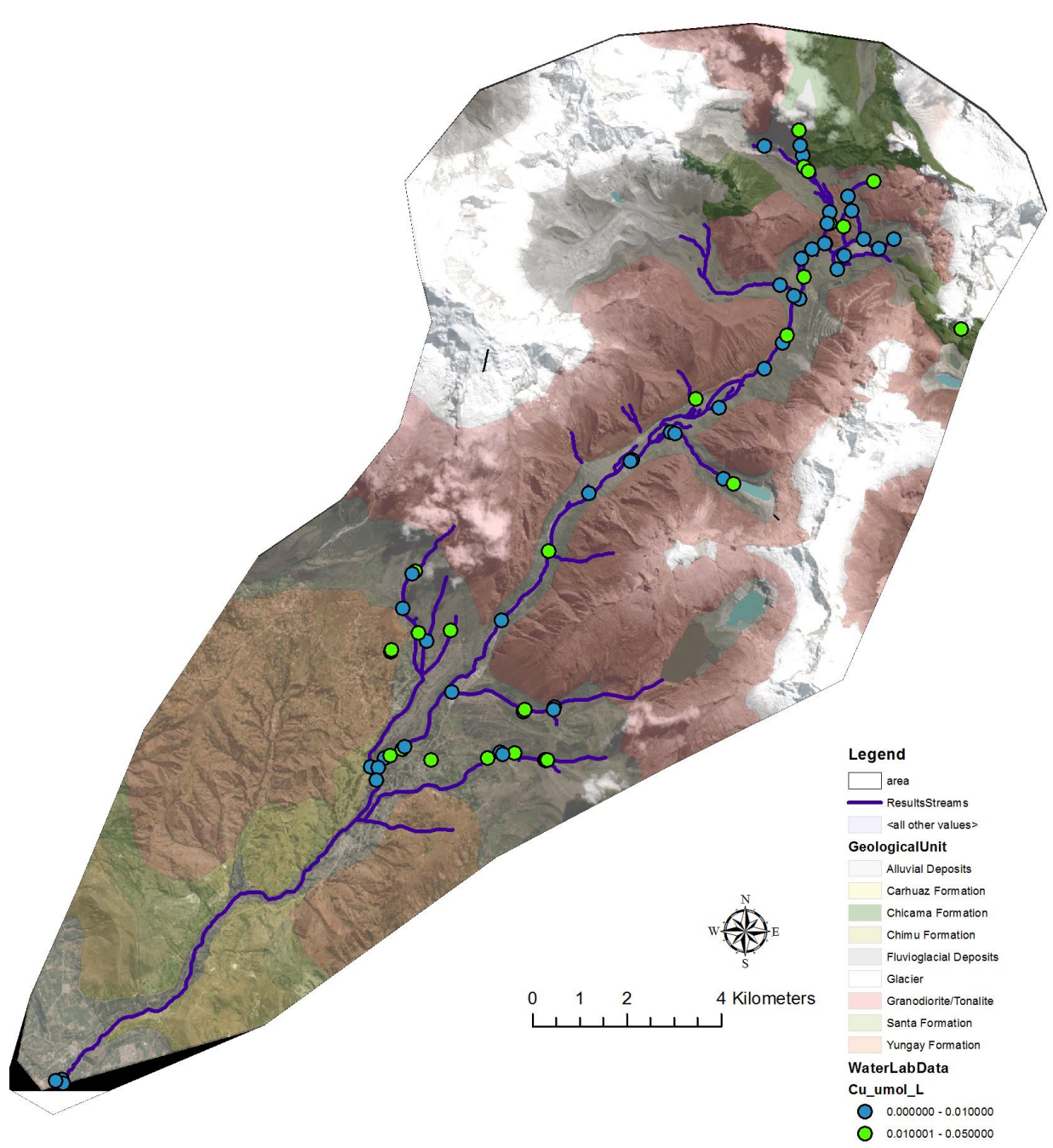


Figure B.6) Spatial distribution of copper concentration

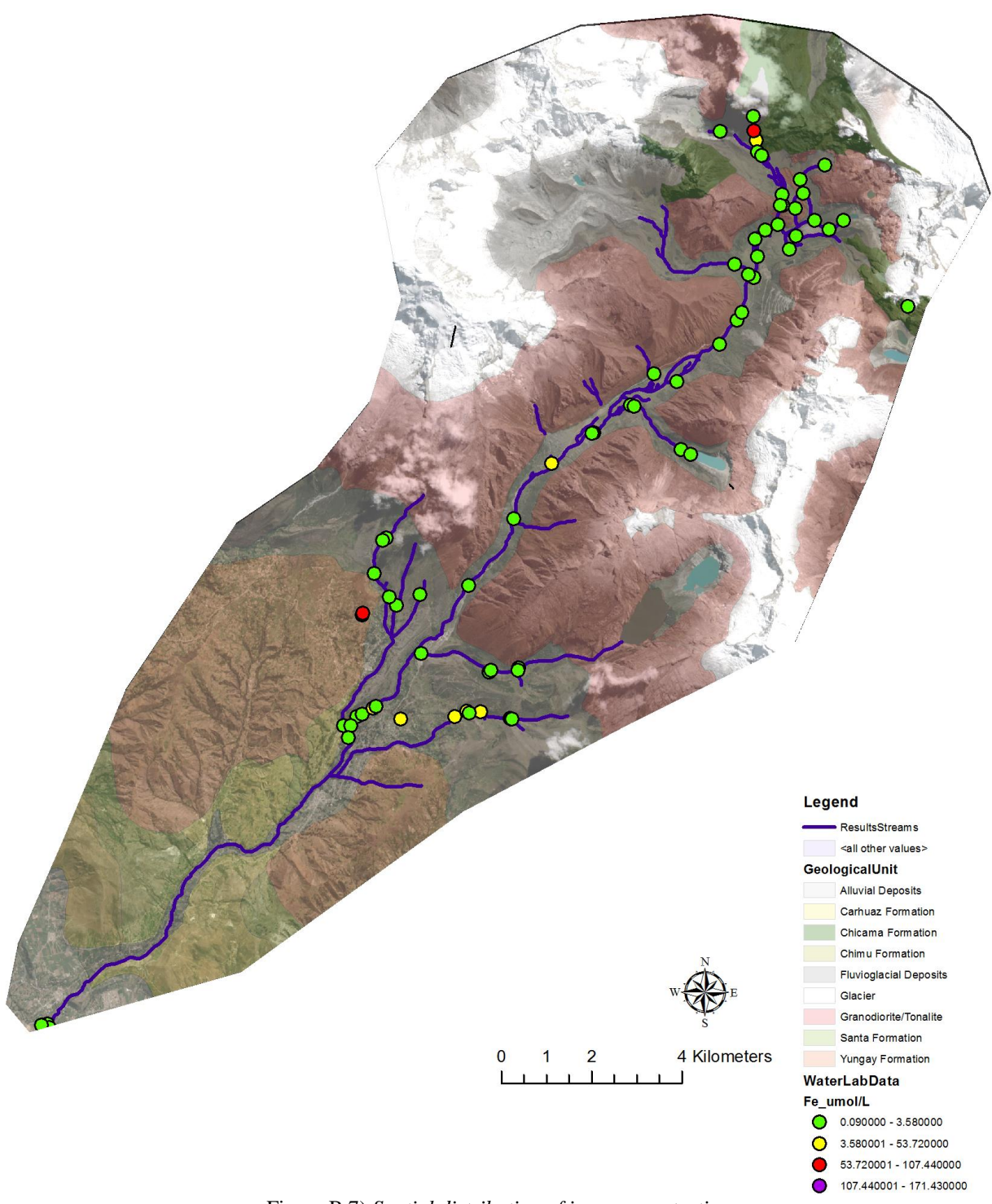


Figure B.7) Spatial distribution of iron concentration

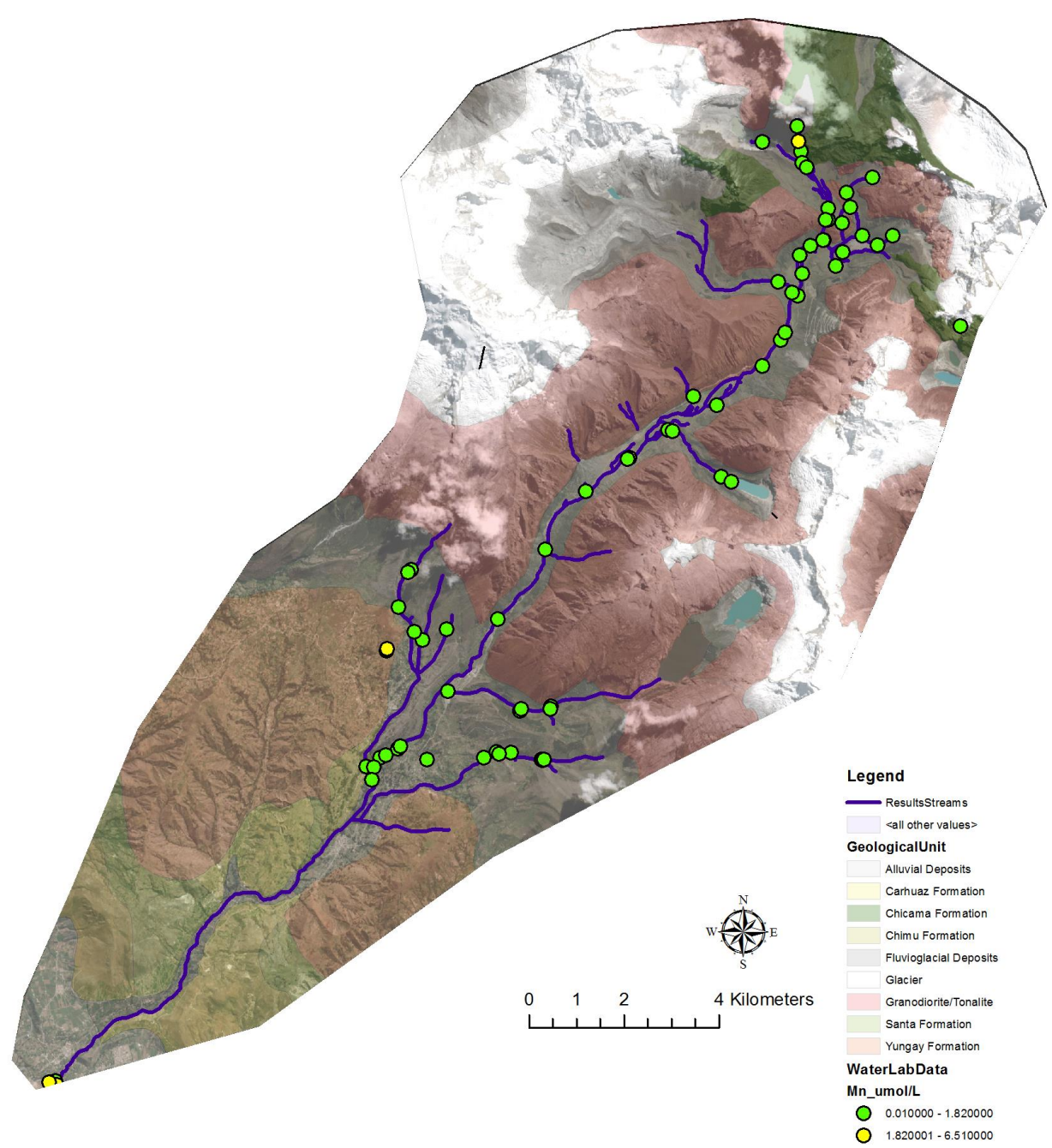


Figure B.8) Spatial distribution of manganese concentration

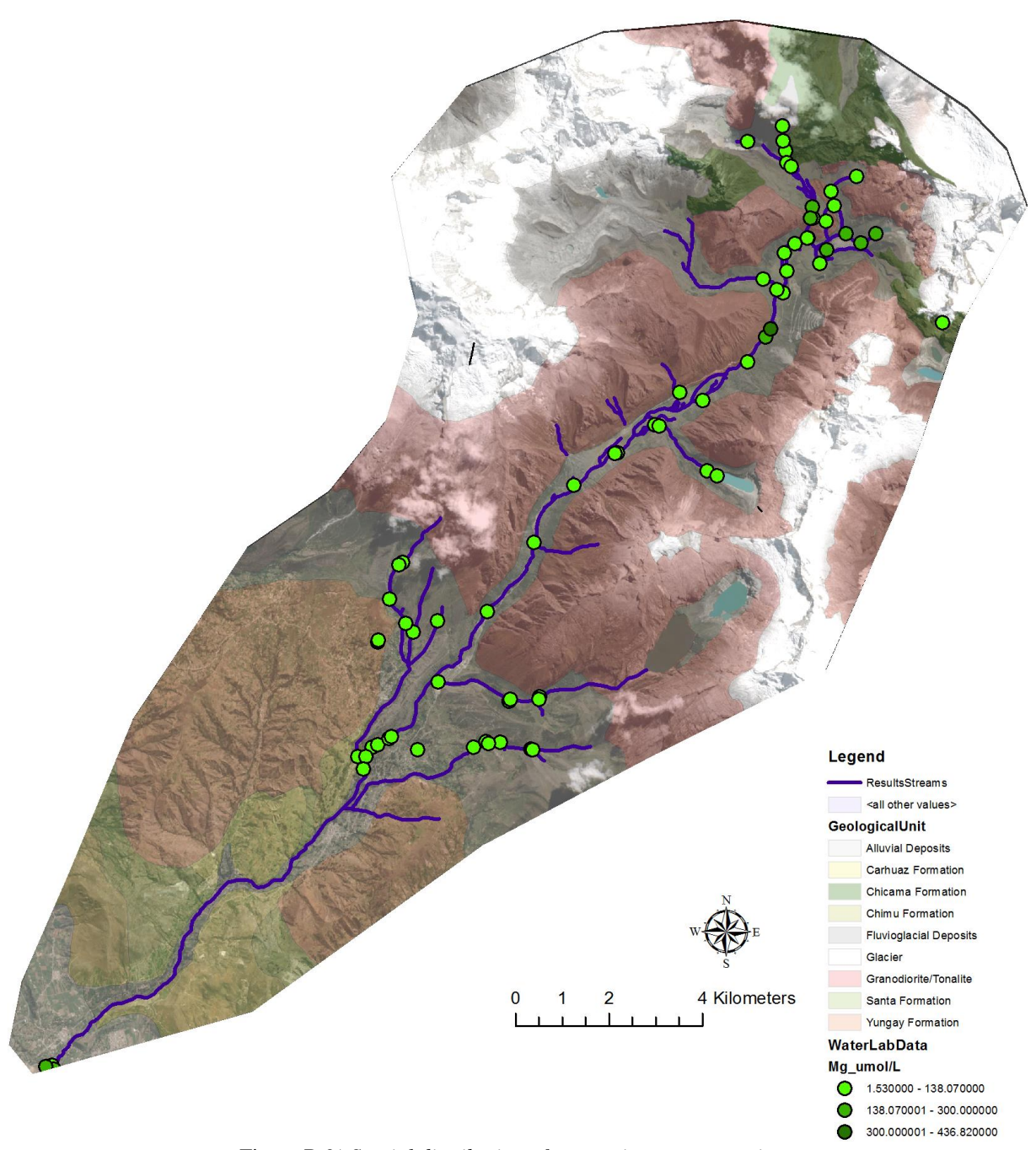


Figure B.9) Spatial distribution of magnesium concentration

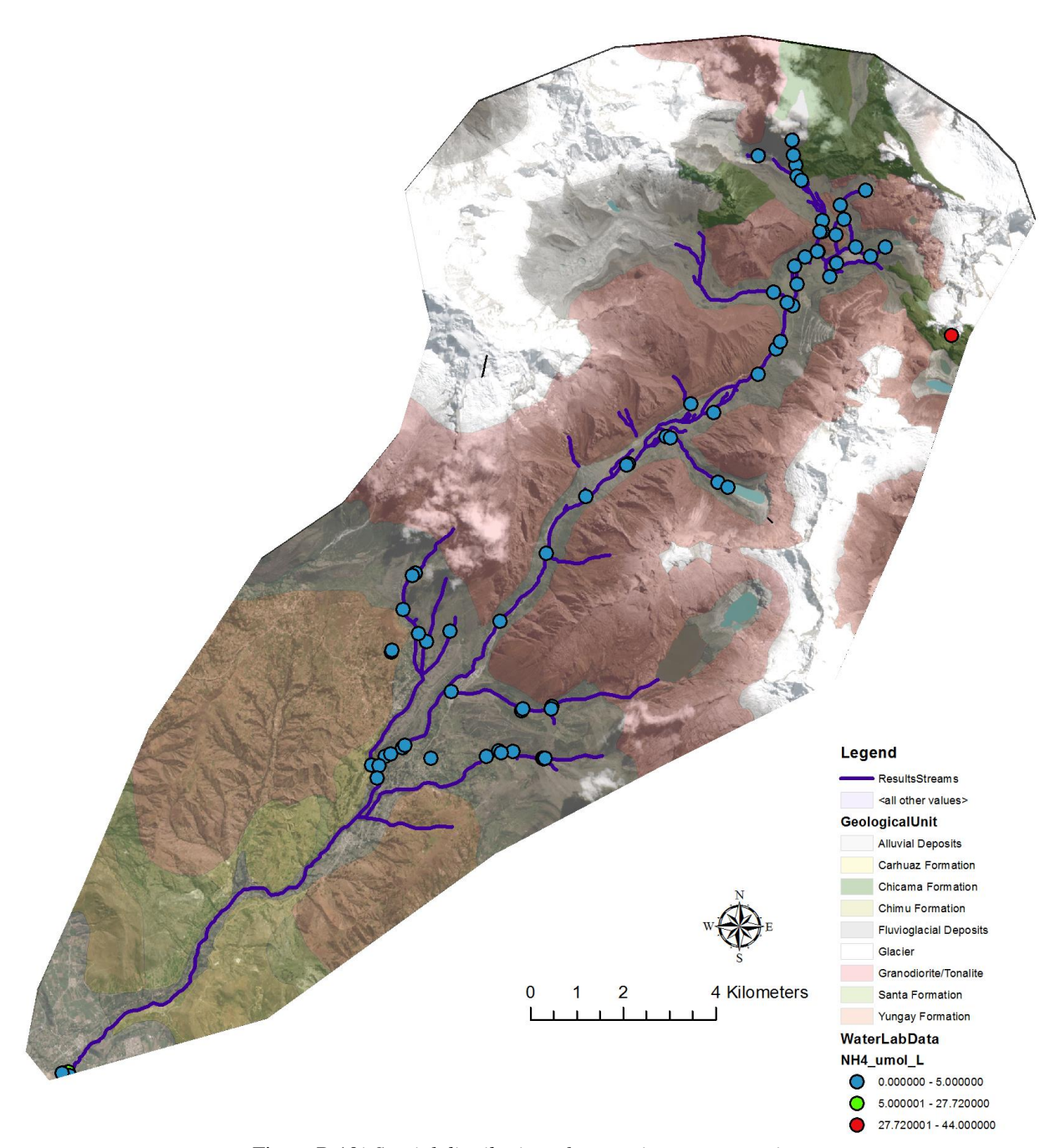


Figure B.10) Spatial distribution of ammonium concentration

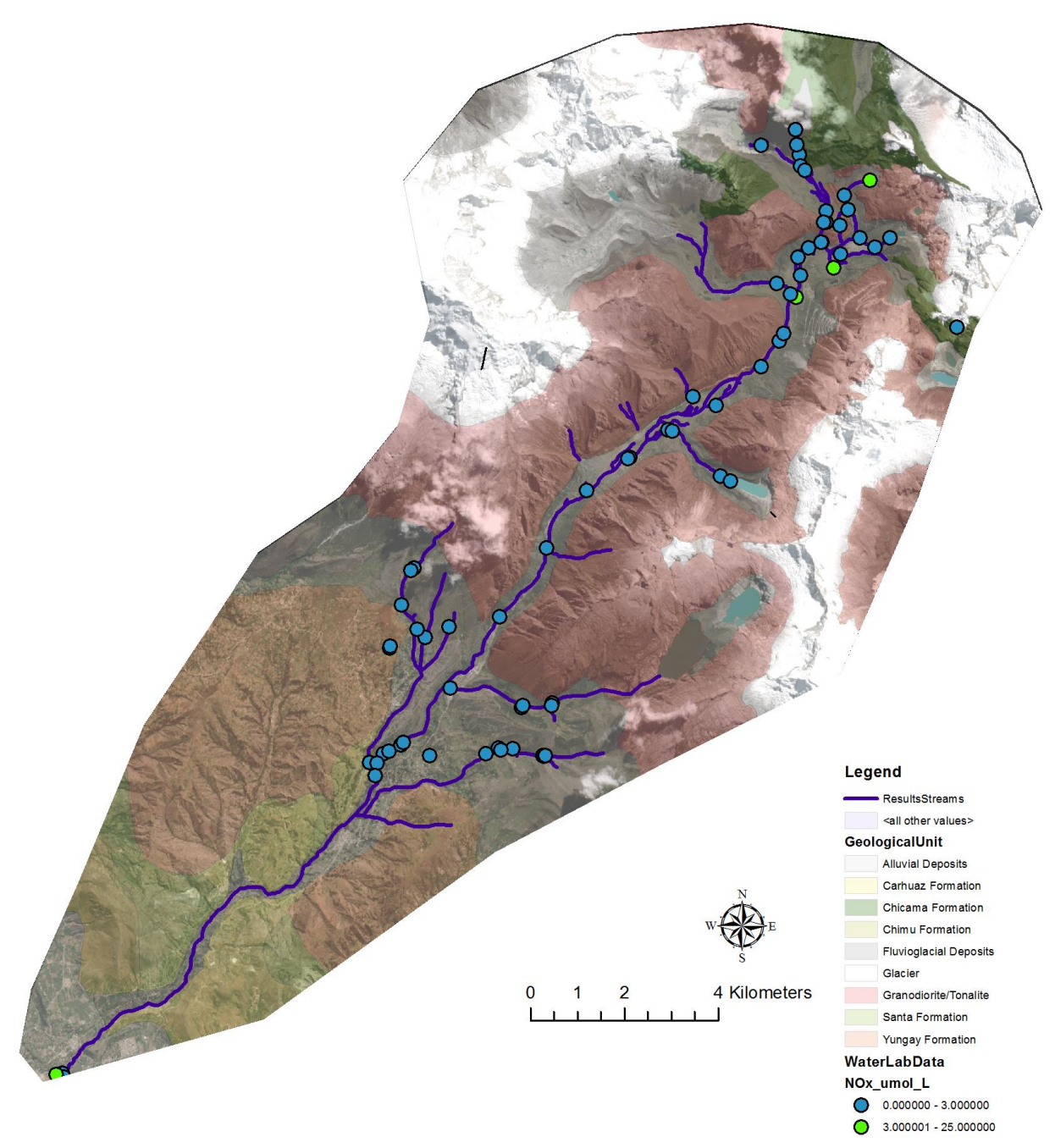
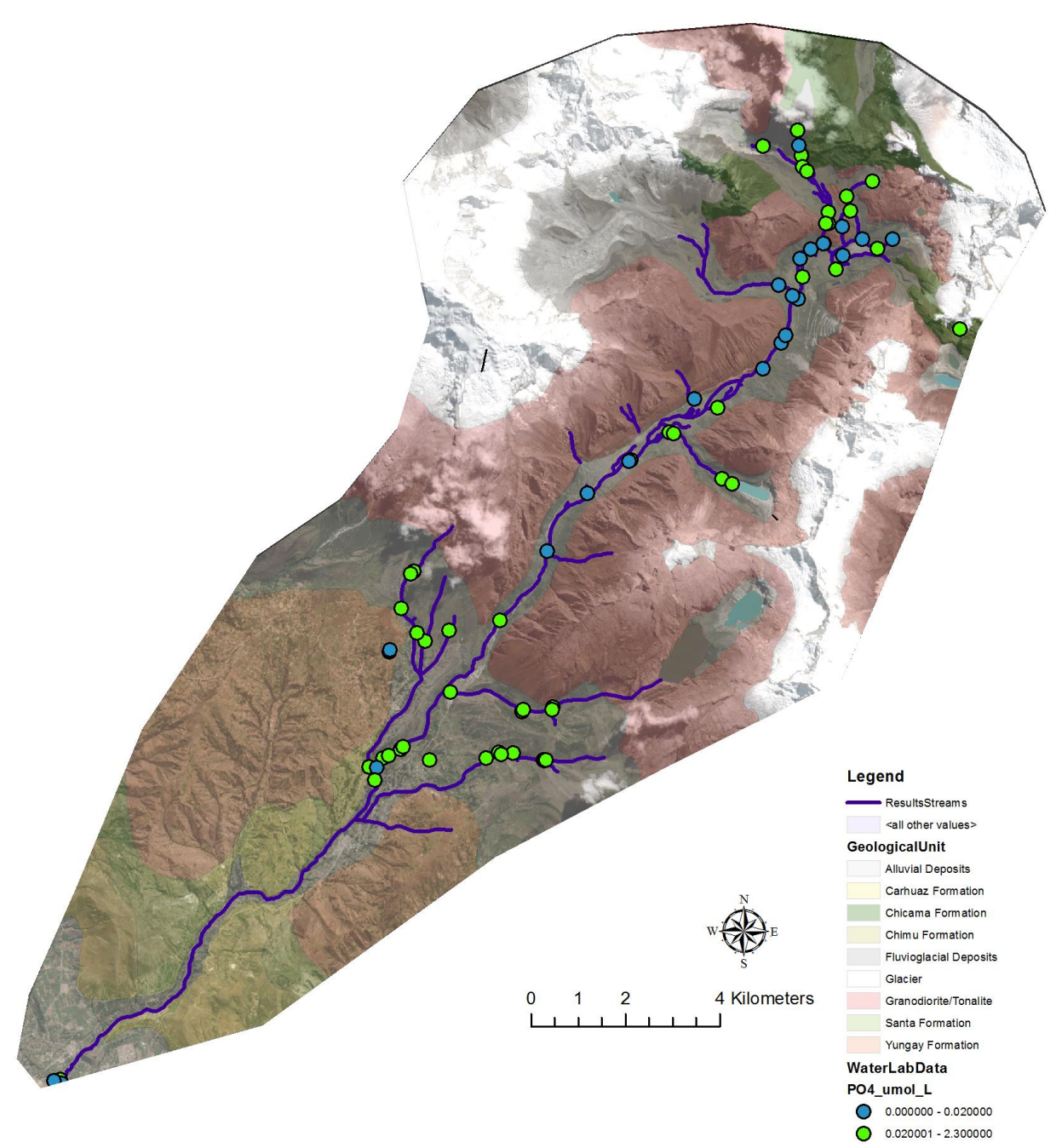
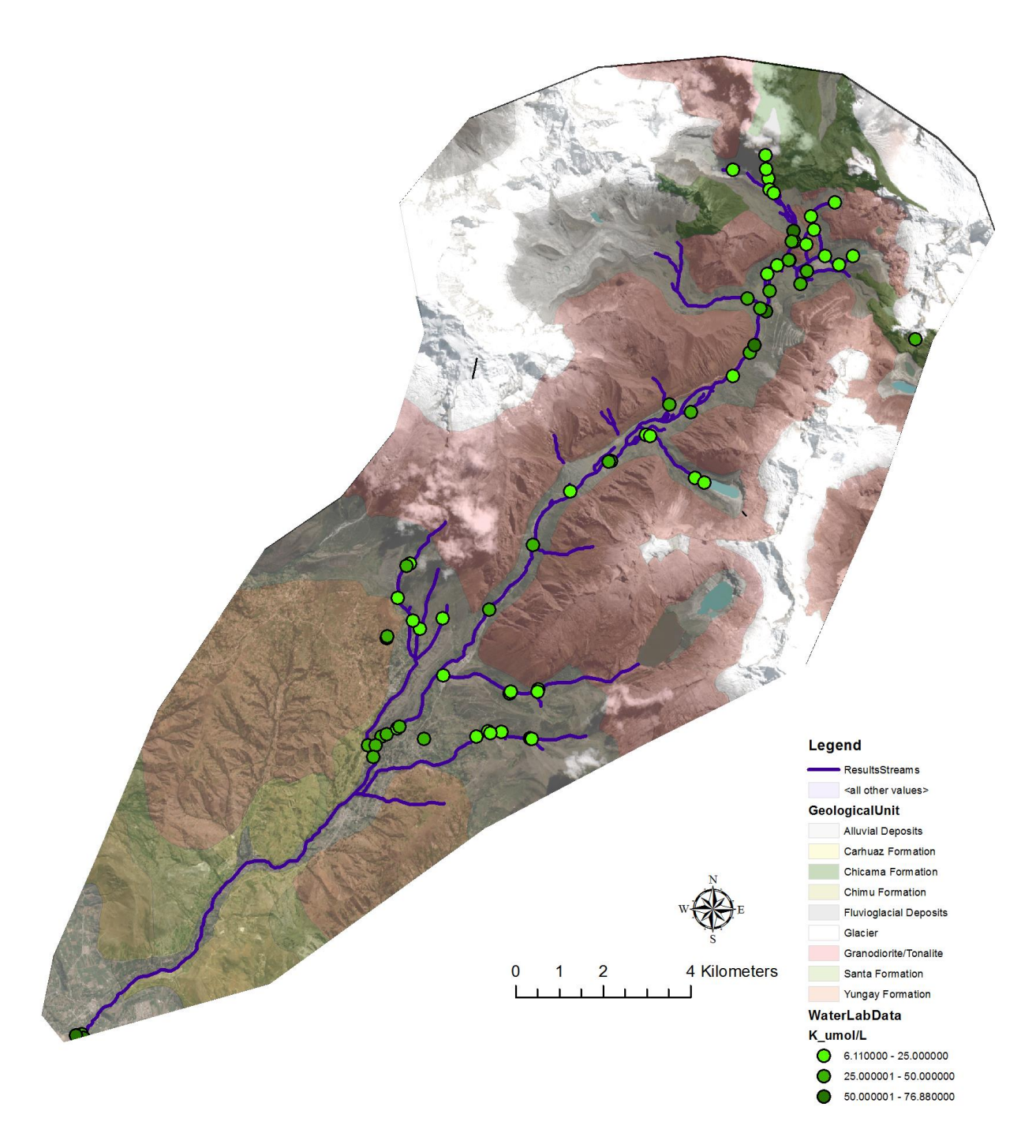


Figure B.11) Spatial distribution of nitrate/nitrite concentration



 $\underline{Figure~B.12})~Spatial~distribution~of~phosphate~concentration$



 $\underline{Figure~B.13})~Spatial~distribution~of~potassium~concentration$

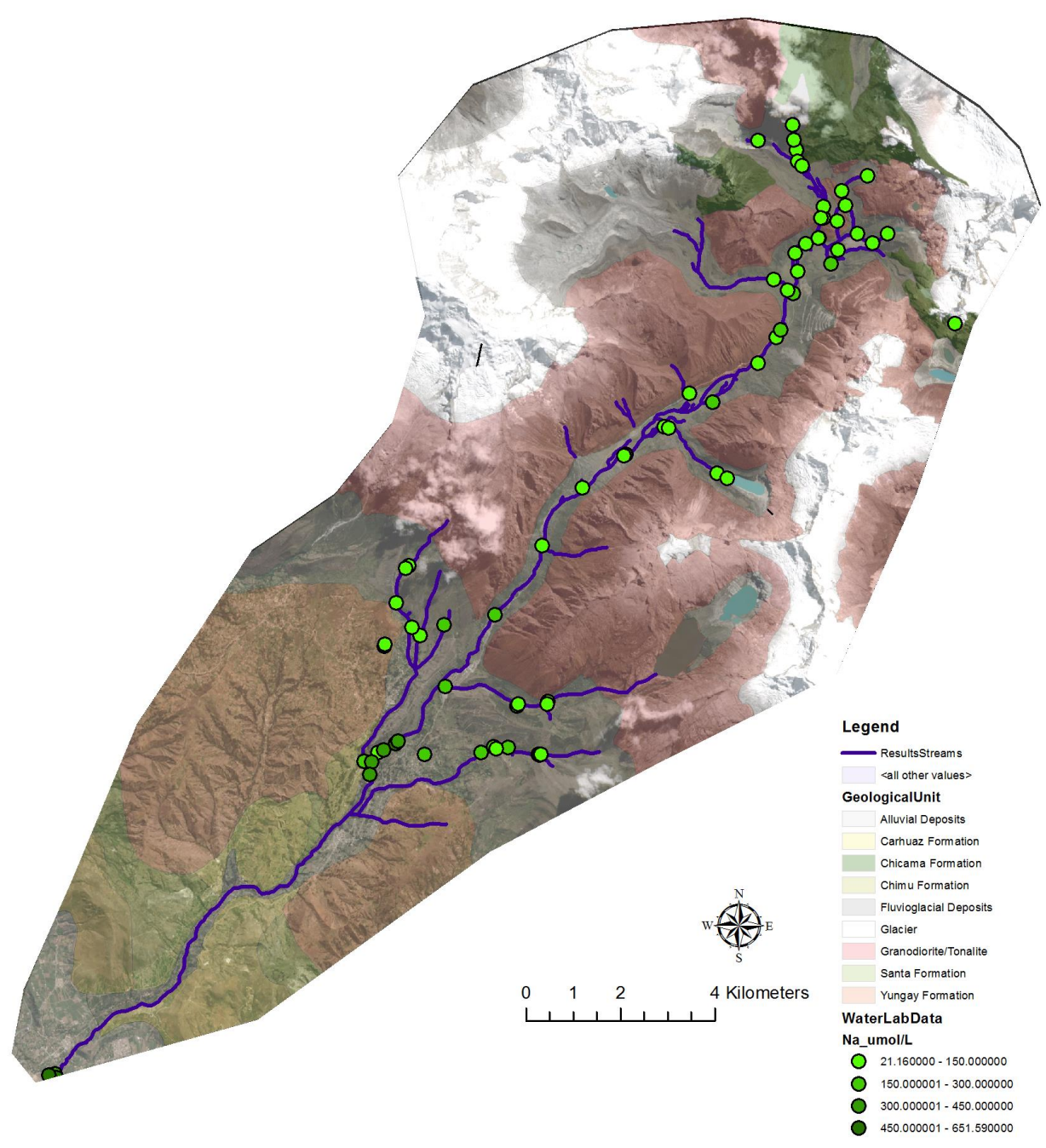


Figure B.14) Spatial distribution of sodium concentration

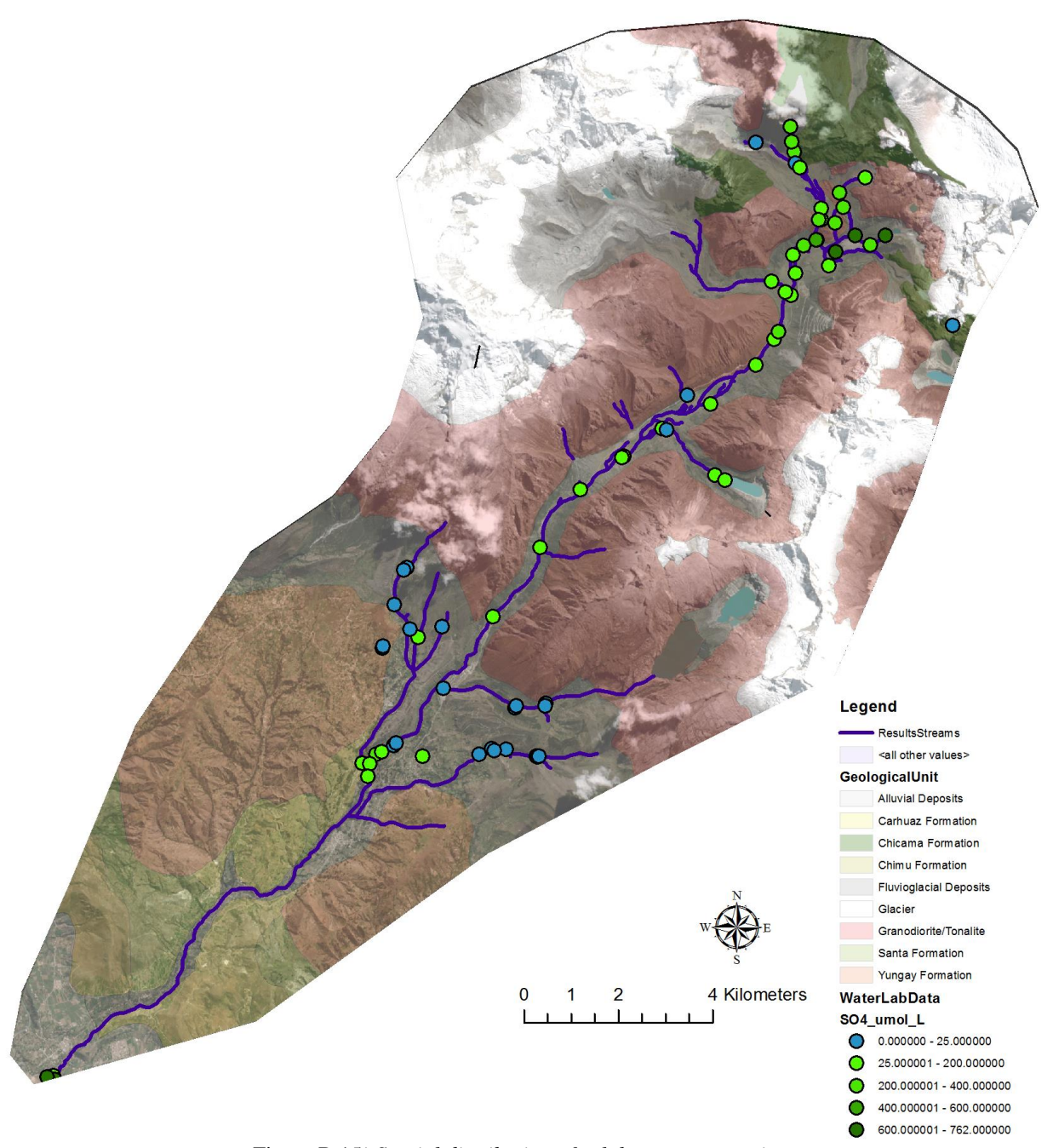


Figure B.15) Spatial distribution of sulphate concentration

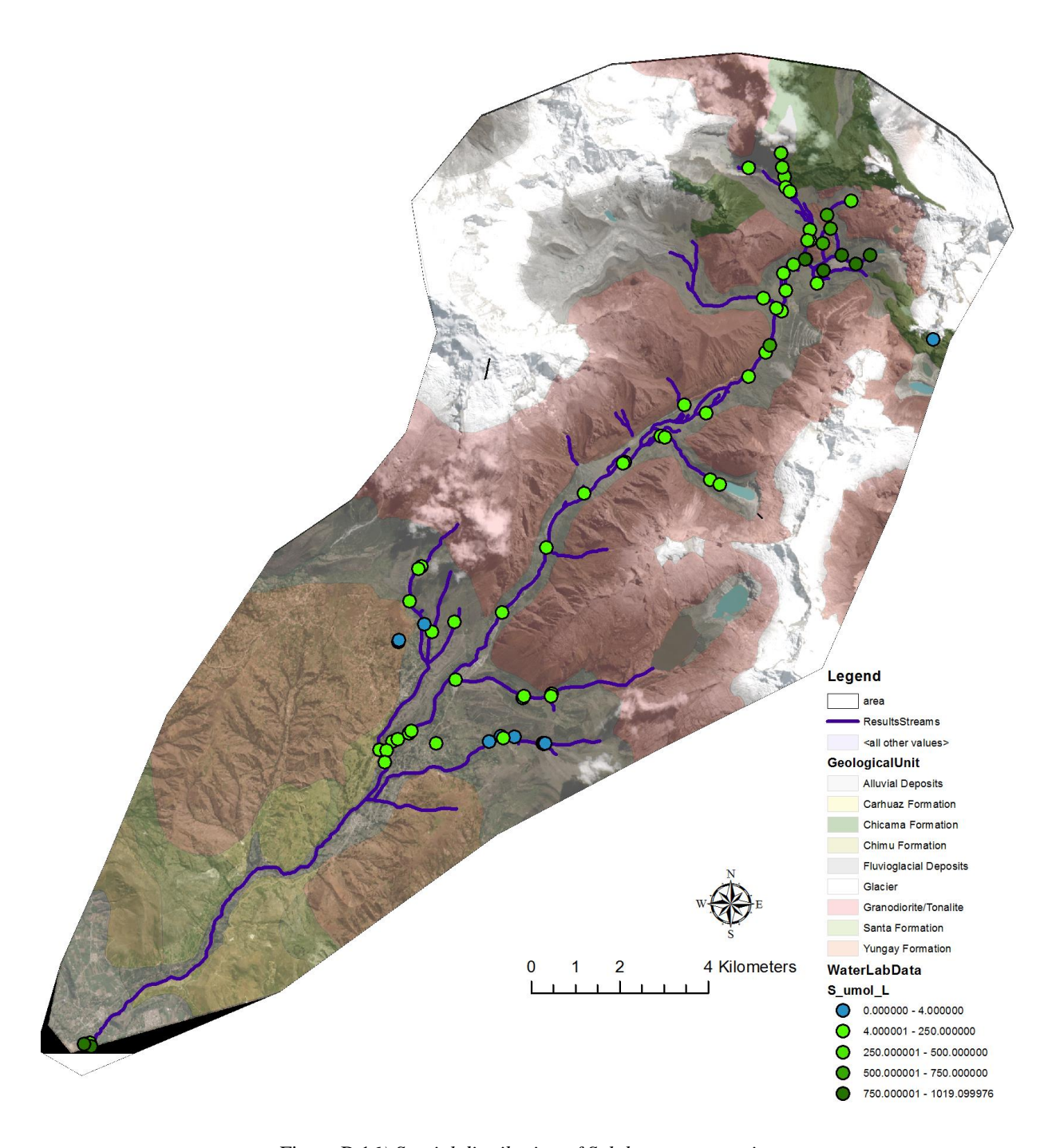


Figure B.16) Spatial distribution of Sulphur concentration

d2H enrichment [o/oo]

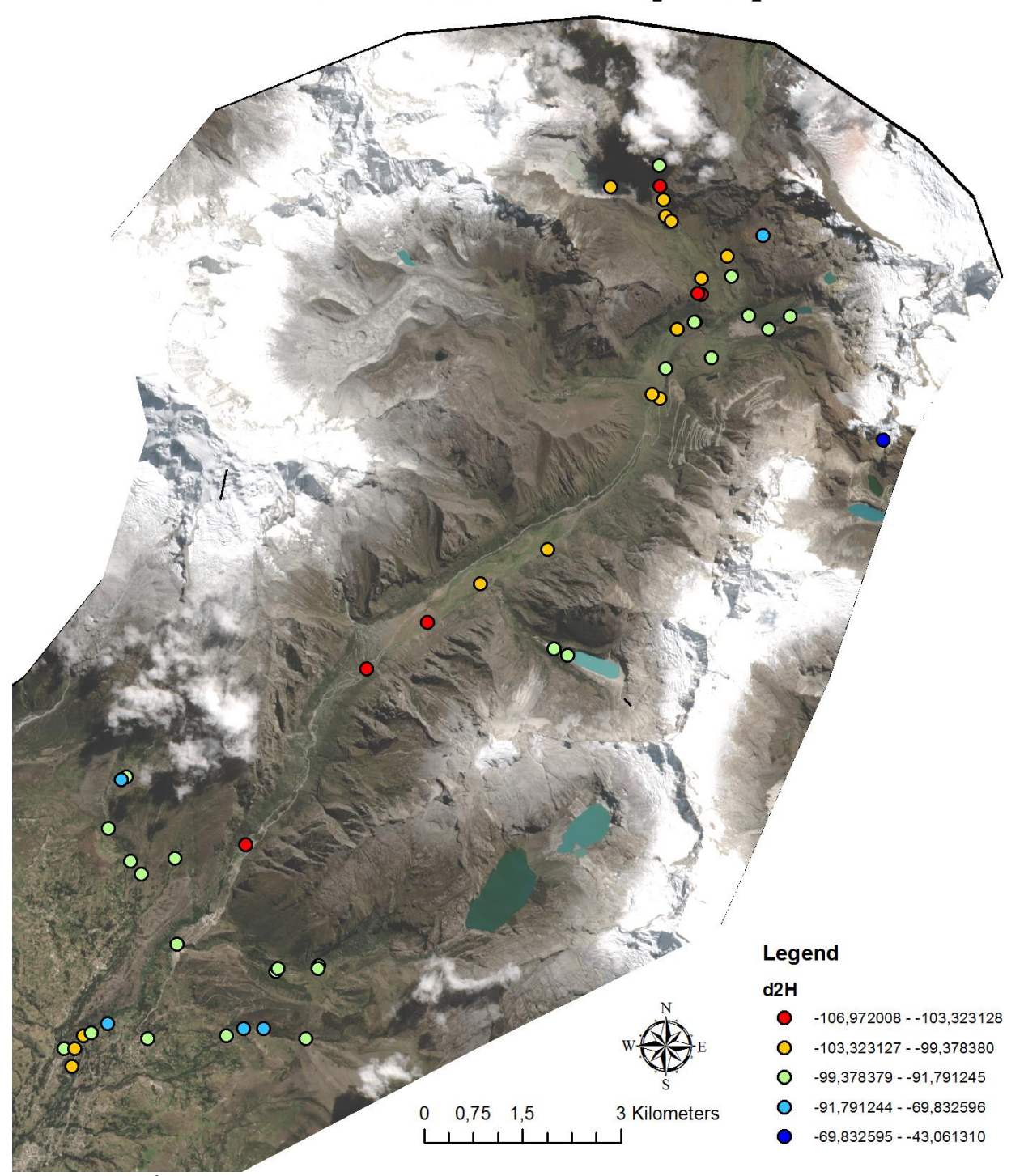


Figure B.17) $\delta^2 H$ enrichment. Red colours indicate high enrichment of heavier isotopes, which in this setting may indicate higher contribution of glacial meltwater. Blue colours indicate higher semblance to ocean water

d18O enrichment [o/oo]

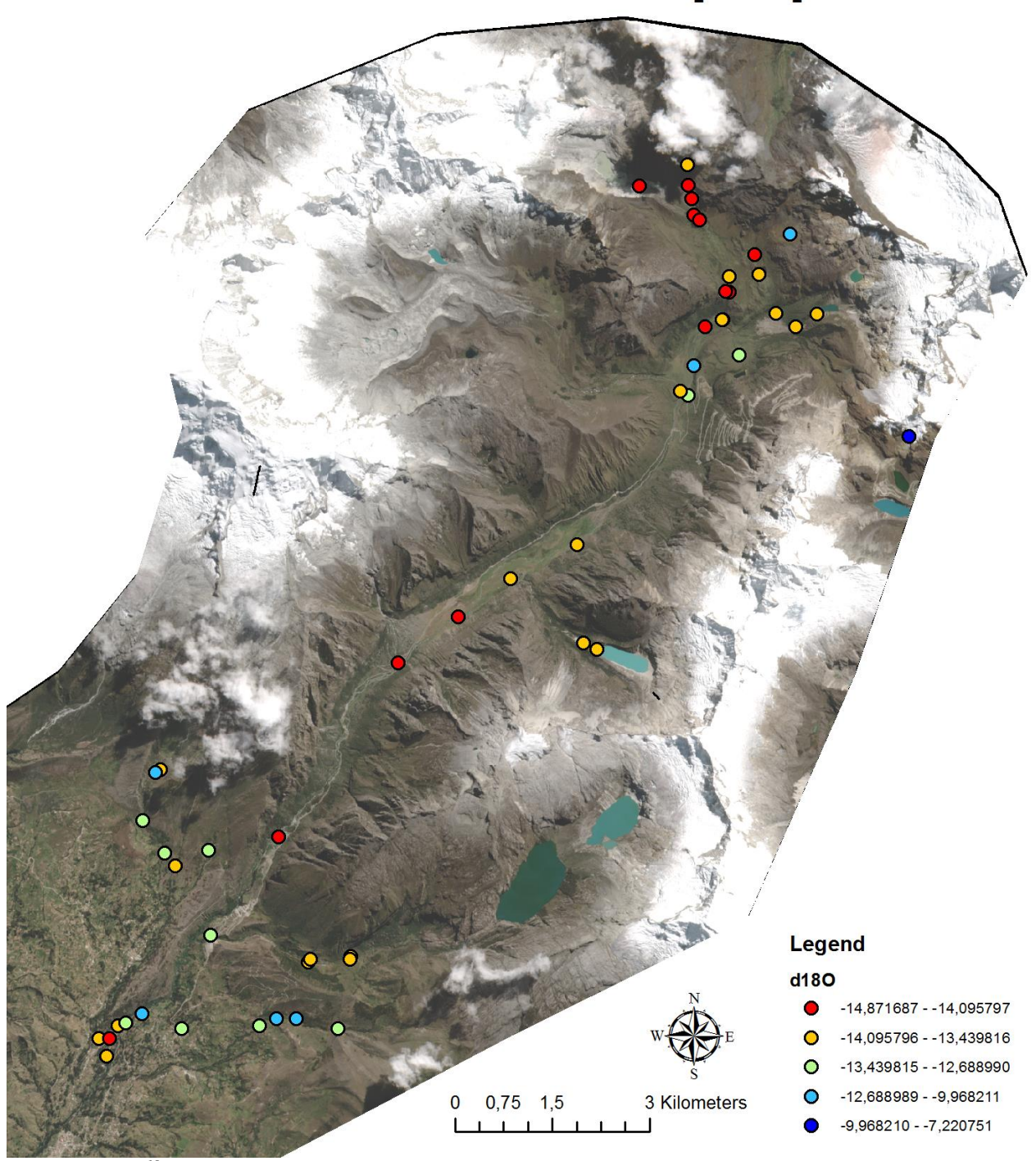
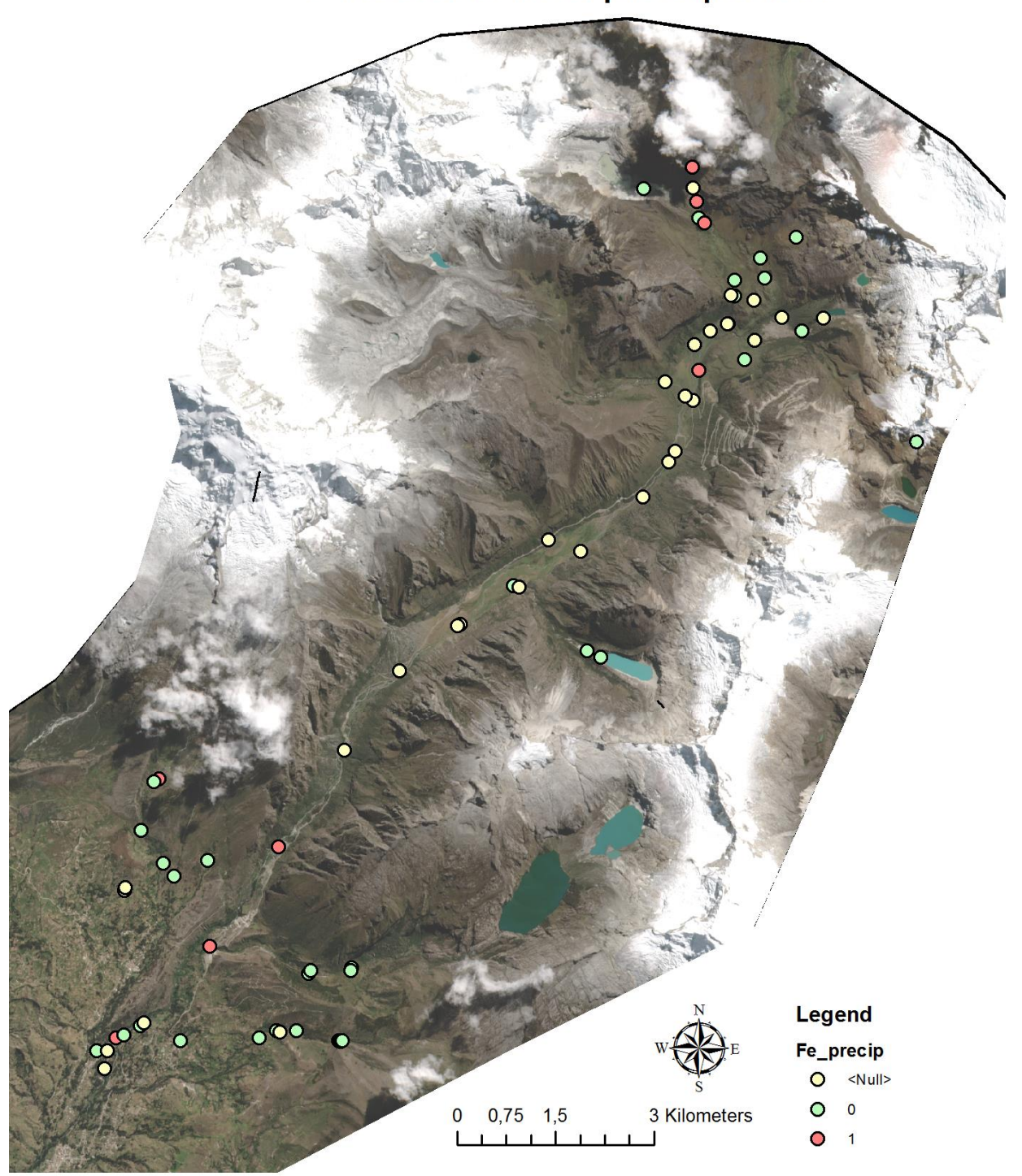


Figure B.18) $\delta^{l8}O$ enrichment. Red colours indicate high enrichment of heavier isotopes, which in this setting may indicate higher contribution of glacial meltwater. Blue colours indicate higher semblance to ocean water.

Presence iron precipitates



<u>Figure B.19</u>) Presence of iron precipitates. Yellow colours indicate no data, red colours indicate presence of iron precipitates. Green colours indicate no iron precipitates.

APPENDIX C MAGNUSSON ET AL. 2017 – DATA

Table C.1) Data for 15 reconstructed paleoglaciers and corresponding Till Samples

Paleo- glacie r	%Chicama -ELA75	%Granitic -ELA75	%Chicama -Subglacial	%Granitic - Subglacial	ELA75 [m]	Est. Age	Soil Sample ID
1	0	100	0	100	4437	Laguna Baja	-
2	0	100	0	100	4339	Laguna Baja	0_22
3	0	100	0	100	4164	Laguna Baja	0_21
4	0	100	14.14	85.86	4237	Rurec	0_5, 0_6, 0_16,
5	0	100	0	100	4347	Rurec	0_17, 4_1, 4_2 0_1, 0_2, 0_3, 0_4
6	0	100	0	100	4556	Holocene	0_12
7	0	100	0	100	4385	Manachaque	0_13
8	11.93	88.07	8.38	91.62	4650	Holocene	0_11
9	58.82	41.18	54.84	45.16	4701	Holocene	0_8
10	16.67	83.33	72.73	27.27	4757	Holocene	0_19, 0_7?
11	64.89	35.11	61.36	38.64	4583	Manachaque	0_18
12	61.36	38.64	27.11	72.89	4330	Laguna Baja	3_3
13	0	100	0	100	4211	Rurec	0_14
14	84.62	15.38	28.42	71.58	4412	Manachaque	0_9, 0_10?
15	100	0	67.07	32.93	4567	Holocene	0_20, 0_7?

Table C.2)	Till Physica	1 Properties							
Locatio n	% sand	% silt	% clay	% gravel	% OM	Ksat SPAW [cm/hr]	%C- CNH S	%N- CNH S	% Chicama fragment
									s
0_1	68.1	16.8	15.1	32.6	4.84	3.12	2.82	0.23	19.5
0_2	55.4	21.9	22.7	49	4.81	2.41	2.8	0.25	8.4
0_3	68.3	18.3	13.4	56.3	0.34	1.47	0.2	0.04	7.8
0_4	70.1	22.9	7	57.7	3.5	3.71	2.04	0.16	3.8
0_5	53.9	34	12.1	39.5	0.08	1.45	0.05	0.02	20.8
0_6	64.8	24.7	10.5	54.9	0.18	1.65	0.11	0.03	1.1
0_7	75.9	20	4.1	63.6	0.8	3.66	0.47	0.05	3.8
0_8	58.4	29.9	11.7	84.8	2.18	1.45	1.27	0.1	98.5
0_9	49.7	30.6	19.7	58	4.48	1.19	2.61	0.25	68.2
0_10	65.9	17.9	16.2	36.7	1.59	1.8	0.93	0.09	36.5
0_11	77	16.5	6.5	57.5	1.57	3.35	0.92	0.09	47.1
0_12	66.4	19.6	14	72.6	0.34	1.02	0.2	0.03	0
0_13	80.7	15.7	3.6	78.9	1.9	4.09	1.11	0.1	0
0_14	63.8	19.1	17.1	62.8	0.58	0.84	0.34	0.06	0
0_16	59.8	22.3	17.9	54.1	2.4	1.14	1.4	0.14	10.0

0_17	65.9	25.9	8.2	53.3	0.11	2.29	0.07	0.02	8.8
0_18	62.6	22.9	14.5	50.7	2.86	1.73	1.67	0.11	40.8
0_19	54.3	37.7	8	75.9	0.36	1.32	0.21	0.03	15.1
0_20	43.8	32.7	23.5	55.8	3.71	0.74	2.16	0.25	100
0_21	76.1	19.1	4.8	71.4	1.63	3.33	0.95	0.09	11.6
0_22	71.9	23.4	4.7	48.8	1.97	4.5	1.15	0.1	1
0_23	57.5	27.1	15.4	52	0.43	1.07	0.25	0.04	1.4
0_24	69.7	16.6	13.7	44.2	0.13	1.73	0.08	0.03	10.6
0_25	42.7	32	25.3	52.8	5.13	0.94	2.99	0.27	5.6
3_3	59.8	36	4.2	70.3	1.19	2.52	0.69	0.07	7.9
4_1	61.9	27	11.1	42.1	2.88	2.95	1.68	0.17	3.1
4_2	60.7	22.8	16.5	34.4	2.64	1.83	1.54	0.14	2.6

		~	
Table C	.3) Till	Chemical	Properties

ID	%Fe- XRF	%As- XRF	%Cu- XRF	%Al- XRF	%Mn- XRF	%Si- XRF	%K- XRF	%Ca- XRF	%Na- ICP	%Mg- ICP	%S- ICP
0_1	3.177	0.004	0	6.364	0.073	16.543	1.493	1.396	0.026	0.348	0.403
0_2	3.171	0.009	0	9.593	0.058	21.926	2.099	0.37	0.077	0.55	0.411
0_3	1.418	0.003	0	7.486	0.017	26.877	2.264	1.13	0.056	0.201	0.172
0_4	0.919	0.001	0	7.908	0	26.654	2.354	1.234	0.044	0.152	0.34
0_5	0.869	0.001	0	7.435	0	27.777	2.421	1.285	0.037	0.111	0.272
0_6	0.892	0.001	0	7.533	0	29.406	2.482	1.287	0.051	0.09	0.186
0_7	1.711	0.001	0	7.646	0	25.531	2.033	2.036	0.03	0.199	0.212
0_8	0.831	0.001	0	7.728	0	29.084	2.354	1.266	0.046	0.118	0.168
0_9	5.977	0.025	0.004	11.586	0.04	20.369	1.999	0.791	0.08	0.847	0.909
0_10	2.544	0.005	0	8.957	0.137	25.598	2.027	1.531	0.12	0.514	0.208
0_11	2.346	0.006	0	7.289	0.036	24.867	2.152	1.136	0.099	0.402	0.45
0_12	1.084	0.003	0	9.014	0.026	27.115	2.969	0.96	0.05	0.155	0.294
0_13	0.881	0.001	0	8.289	0	25.947	2.681	0.958	0.021	0.088	0.135
0_14	1.25	0	0	11.022	0	26.84	2.805	0.766	0.035	0.317	0.344
0_16	2.351	0.002	0	9.183	0.012	26.113	2.226	1.037	0.115	0.307	0.365
0_17	9.85	0.007	0.01	12.322	0.043	20.389	1.565	0.852	0.24	1.183	1.429
0_18	3.928	0.007	0	9.587	0.039	18.67	1.284	1.726	0.088	0.957	0.382
0_19	1.77	0.003	0	9.275	0	28.522	2.391	1.971	0.081	0.344	0.252
0_20	6.392	0.005	0.005	14.388	0.014	22.36	1.668	0.369	0.262	0.672	0.456
0_21	2.31	0.002	0	11.264	0.026	26.256	2.523	1.249	0.035	0.446	0.257
0_22	1.482	0.002	0	9.294	0.017	26.362	2.222	1.581	0.033	0.275	0.611
0_23	1.368	0.001	0	9.225	0.017	29.551	2.301	1.508	0.04	0.394	0.507
0_24	2.198	0.001	0	11.155	0.024	26	1.889	1.65	0.038	0.281	0.126
0_25	2.232	0.003	0	11.28	0.025	24.081	1.853	0.919	0.028	0.391	0.263
3_3	1.55	0.003	0	7.032	0	35.196	2.799	1.288	0.062	0.284	0.054
4_1	1.802	0.004	0	8.438	0.023	33.218	2.659	1.046	0.038	0.261	0.175
4_2	1.22	0.004	0	6.691	0.013	32.75	2.549	1.143	0.028	0.149	0.135

Err max *	1.7%					0.7%			3%	2.8%	101.8%
Err avg*	1.2%	24%	16%	1.3%	24%	0.6%	1.4%	3.4%	1.0%	1.1%	21.2%

^{*)} For XRF, relative errors are calculated as counting error/measured value for each replicate. For ICP, errors are 2* standard deviation of duplicate.

Table C.4) Full Test Statistics for comparison of compound concentrations up- and downstream of morainic ridges of high and low Chicama content. Significance assessed after Bonferroni-Holm correction.

		ce in upstream-down between low and hig				Difference in springwater concentration between low and high Chicama group					
	p value	mean diff (high- low Chicama)	stdev of diff		n	p	V	alue	mean diff (high-low Chicama)	stdev of diff	N
EC	0.71	2.41	66.26	2	3			0.11	24.36	49.46	11
pН	0.36	-0.45	0.94	2	2			1	0	0.52	11
(HCO ₃)	0.96	-0.32	8.11	1	3			0.33	43.68	44.2	11
(SO ₄) ²⁻	0.19	127.9	92.55	1	3			0.01	89.31	25.88	11
Al	0.05	-3.01	2.42	1	3			0.48	-0.42	0.86	11
Ca	0.15	41.39	29.31	1	3			0.05	344.16	251.28	11
Fe	0.08	39.84	37.05	1	3			0.88	-22.51	30.27	11
K	0.91	0.3	3.14 1		3			0.02	22.06	11.92	11
Mg	0.00*	32.59	10.49	1	3			0.05	99.5	53.53	11
Mn	0.27	1.65	1.75	1	3			0.88	-0.58	0.86	11
Na	0.54	-3.74	20.07	1	3			0.9	-73.76	120.82	11
S	0.01	94.67	44.54	1	3			0.01	171.61	58.78	11
Si	0.46	27.66	61.51	1	3			0.9	-9.67	104.74	11
As	1	0	0	1	3			1	0	0	11
Cu	0.05	-0.01	0.01	1	3			0.46	-0.01	0.01	11
В	0.26	0.55	0.53	1	3			0.68	-2.8	3.2	11
TOC	0.46	0.49	0.66	1	3			0.61	-0.21	5.46	11
$\delta^{18}O$	0.08	-1.82	1.27	1	13		0.6		-0.3	0.84	11
δ ² H	0.08	-13.43	9.62	1	3			0.23	-3.88	4.63	11

⁼ p < 0.05= p < 0.01= p < 0.001

⁼ p < 0.1

⁼ significant correlation caused by single outlier

NS = not significant

<u>Table C.5) Correlation matrix of till properties and changes in water quality parameters calculated as upstream value – downstream value.</u> Significance assessed after Bonferroni-Holm correction.

	EC (n=23)	pH (n=22)	HCO3 (n=13)	SO4 (n=13)	Al (n=13)	Ca (n=13)	Fe (n=13)	K (n=13)	Mg (n=13)	Mn (n=13)	Na (n=13)	S (n=13)	Si (n=13)	Cu (n=13)	B (n=13)	TOC (n=13)
Chicama	.107 NS	043 NS	008 NS	.540 NS	315 NS	.494 NS	.450 NS	.249 NS	.649 *	.166 NS	.188 NS	.614 +	.309 NS	387 NS	.156 NS	.196 NS
KSat	118 NS	.215 NS	.044 NS	693 *	.077 NS	407 NS	651 *	.406 NS	582 NS	552 NS	370 NS	486 NS	063 NS	.110 NS	245 NS	.123 NS
Fe							.130 NS									
С																.186 NS
Al					.094 NS											
Ca						516 NS										
Na											.121 NS					
Cu														309 NS		
Mn										.108 NS						
								.272 NS								
Gravel	423 NS															
S		141 NS	516 NS	.274 NS								.558 NS				
Si													034 NS			
Mg									.359 NS							

```
\begin{array}{lll} * & & = p < 0.05 \\ ** & & = p < 0.01 \\ *** & & = p < 0.001 \\ + & & = p < 0.1 \\ \# & & = significant correlation caused by single outlier \\ NS & & = not significant \end{array}
```

<u>Table C.6) Water quality – field measurements</u>

NR	Lat (WGS84)	Long (WGS84)	Mo nth	Day	Hr	Min	FIELD NOTES
gr0_w1	-77.588708	-9.204415	6	28	12	30	spring from morainic ridge
gr0_w2	-77.588417	-9.204019	6	28	13	30	upstream of inflow w1
gr0_w3	-77.582755	-9.203650	6	28	14	0	rio quilcay
gr0_w4	-77.582917	-9.204114	6	28	15	0	tributary from morainic ridge into rio quilcay
gr0_w6	-77.602450	-9.200569	6	29	9	30	rio quilcay after morainic ridge before joining rio buin
gr0_w7	-77.592773	-9.186979	6	29	13	30	rio buin at middle bridge
gr0_w8	-77.618209	-9.214859	6	29	15	30	glacial melwater stream
gr0_w10	-77.534167	-9.098333	6	30	14	0	weird pH
gr0_w11	-77.533889	-9.100556	6	30	14	30	chicama stream, downstream of red waterfall
gr0_w12	-77.533889	-9.097191	6	30	14	0	glacial lake, contaminated sample
gr0_w13	-77.528946	-9.111373	7	2	11	30	stream above steep ridge in upper fieldwork area
gr0_w14	-77.525412	-9.106217	7	2	12	30	stream infiltrated in moraine and talus slope, appears at base
gr0_w5	-77.615504	-9.213154	6	29	9	0	baseline location
gr0_w15	-77.520415	-9.103327	7	2	13	50	moraine dammed lake, small
gr0_w16	-77.534047	-9.121583	7	4	10	0	tributary flowing out of moraine
gr0_w18	-77.527646	-9.120201	7	4	13	30	lots of cows, very slow flowing water
gr0_w19	-77.519154	-9.116093	7	4	14	30	tributary right downstream of mainly granodioritc moraine
gr0_w20	-77.549794	-9.160160	7	5	12	15	from granodiorite moraine
gr0_w21	-77.547867	-9.161129	7	5	12	0	laguna hualcacocha
gr0_w22	-77.559471	-9.151329	7	5	15	40	downstream from morainic ridges, w20
gr0_w23	-77.602593	-9.188773	7	6	11	30	gully 1 at irrigation channel
gr0_w24	-77.607298	-9.190848	7	6	12	0	gully 2 at irrigation channel
gr0_w25	-77.608783	-9.189209	7	6	13	0	gully 3 at irrigation channel
gr0_w26	-77.614392	-9.212697	7	8	10	15	stream, may be from irrigation channel!
gr0_w27	-77.612130	-9.211466	7	8	12	30	stream, may be from irrigation channel!
gr0_w28	-77.606638	-9.213610	7	8	15	20	stream joining Rio Buin
gr0_w29	-77.529002	-9.109232	7	9	11	20	stream coming from morainic material into valley

gr0_w39 -77.584353 -9.213876 7 12 13 15 three samples: 38 is main river, 39 is lower tributary, 40 is upper tributary gr0_w40 -77.584164 -9.213768 7 12 13 30 three samples: 38 is main river, 39 is lower tributary, 40 is upper tributary gr0_w41 -77.595552 -9.212796 7 12 14 30 downstream of 36-40 gr0_w42 -77.503855 -9.131729 7 12 11 30 snow sample (under glacier terminus) gr0_w43 -77.678186 -9.274250 7 14 14 0 Rio Buin, high pH gr0_w44 -77.67905 -9.274403 7 14 14 15 Rio Santa downstream gr2_w1 -77.616711 -9.214881 6 29 10 30 trout farm, lower rio buin gr2_w2 -77.533050 -9.101331 6 30 13 45 outflow from glacial lake gr2_w4 -77.532424 -9.116235 7 4 12 15 glacial melt flow gr3_w4 <td< th=""><th></th><th>•</th><th></th><th></th><th></th><th></th><th></th><th></th></td<>		•						
gr0_w32 -77.541475 -9.096508 7 9 13 30 inflow of glacial lake, purely granitic rock gr0_w33 -77.611809 -9.184520 7 11 11 20 gully 3 higher above irrigation channel gr0_w34 -77.609983 -9.177850 7 11 13 0 gully 3 higher, above first set of moraines gr0_w35 -77.609983 -9.177850 7 11 13 30 wetland stream originating from moraine into gully 3 gr0_w36 -77.593226 -9.212334 7 12 12 0 stream from morainic ridge gr0_w37 -77.590478 -9.212338 7 12 13 0 three samples: 38 is main river, 39 is lower tributary, 40 is upper tributar gr0_w39 -77.584596 -9.213788 7 12 13 30 three samples: 38 is main river, 39 is lower tributary, 40 is upper tributar gr0_w40 -77.584164 -9.213768 7 12 13 30 three samples: 38 is main river, 39 is lower tributary, 40 is upper tributar gr0_w41 -7	gr0_w30	-77.524768	-9.108975	7	9	14	0	lake in wetland
gr0_w33 -77.611809 -9.184520 7 11 11 20 gully 3 higher above irrigation channel gr0_w34 -77.609285 -9.177450 7 11 13 0 gully 3 higher, above first set of moraines gr0_w35 -77.60983 -9.177850 7 11 13 30 wetland stream originating from moraine into gully 3 gr0_w36 -77.593226 -9.212247 7 12 11 30 stream from morainic ridge gr0_w37 -77.59478 -9.213738 7 12 12 0 stream from morainic ridge gr0_w38 -77.584596 -9.213738 7 12 13 0 three samples: 38 is main river, 39 is lower tributary, 40 is upper tributar gr0_w49 -77.584164 -9.213768 7 12 13 30 three samples: 38 is main river, 39 is lower tributary, 40 is upper tributar gr0_w40 -77.584164 -9.213768 7 12 13 30 three samples: 38 is main river, 39 is lower tributary, 40 is upper tributar gr0_w41 -77.538186	gr0_w31	-77.534759	-9.093550	7	9	12	55	lake in wetland
gr0_w34 -77.609285 -9.177450 7 11 13 0 gully 3 higher, above first set of moraines gr0_w35 -77.609983 -9.177850 7 11 13 30 wetland stream originating from moraine into gully 3 gr0_w36 -77.593226 -9.212247 7 12 11 30 stream from morainic ridge gr0_w37 -77.590478 -9.212334 7 12 12 0 stream from morainic ridge gr0_w38 -77.584596 -9.213768 7 12 13 0 three samples: 38 is main river, 39 is lower tributary, 40 is upper tributar gr0_w40 -77.584164 -9.213768 7 12 13 15 three samples: 38 is main river, 39 is lower tributary, 40 is upper tributar gr0_w41 -77.595552 -9.212796 7 12 14 30 downstream of 36-40 gr0_w42 -77.503855 -9.131729 7 12 11 30 snow sample (under glacier terminus) gr0_w43 -77.678186 -9.274250 7 14 <td>gr0_w32</td> <td>-77.541475</td> <td>-9.096508</td> <td>7</td> <td>9</td> <td>13</td> <td>30</td> <td>inflow of glacial lake, purely granitic rock</td>	gr0_w32	-77.541475	-9.096508	7	9	13	30	inflow of glacial lake, purely granitic rock
gT_w35 -77.609983 -9.177850 7 11 13 30 wetland stream originating from moraine into gully 3 gTO_w36 -77.593226 -9.212247 7 12 11 30 stream from morainic ridge gTO_w37 -77.590478 -9.212334 7 12 12 0 stream from morainic ridge gTO_w38 -77.584596 -9.213738 7 12 13 0 three samples: 38 is main river, 39 is lower tributary, 40 is upper tributar gTO_w49 -77.584164 -9.213768 7 12 13 30 three samples: 38 is main river, 39 is lower tributary, 40 is upper tributar gTO_w40 -77.584164 -9.213768 7 12 13 30 three samples: 38 is main river, 39 is lower tributary, 40 is upper tributar gTO_w40 -77.584164 -9.213768 7 12 14 30 downstream of 36-40 gTO_w42 -77.503855 -9.131729 7 12 11 30 snow sample (under glacier terminus) gTO_w43 -77.678186 -9.27450	gr0_w33	-77.611809	-9.184520	7	11	11	20	gully 3 higher above irrigation channel
gr0_w36 -77.593226 -9.212247 7 12 11 30 stream from morainic ridge gr0_w37 -77.590478 -9.212334 7 12 12 0 stream from morainic ridge gr0_w38 -77.584596 -9.213738 7 12 13 0 three samples: 38 is main river, 39 is lower tributary, 40 is upper tributary gr0_w39 -77.584353 -9.213768 7 12 13 30 three samples: 38 is main river, 39 is lower tributary, 40 is upper tributary gr0_w40 -77.584164 -9.213768 7 12 13 30 three samples: 38 is main river, 39 is lower tributary, 40 is upper tributary gr0_w41 -77.595552 -9.212796 7 12 14 30 downstream of 36-40 gr0_w42 -77.503855 -9.131729 7 12 11 30 snow sample (under glacier terminus) gr0_w43 -77.678186 -9.274250 7 14 14 0 Rio Buin, high pH gr2_w1 -77.679441 -9.274403 7 14 <td>gr0_w34</td> <td>-77.609285</td> <td>-9.177450</td> <td>7</td> <td>11</td> <td>13</td> <td>0</td> <td>gully 3 higher, above first set of moraines</td>	gr0_w34	-77.609285	-9.177450	7	11	13	0	gully 3 higher, above first set of moraines
gr0_w37 -77.590478 -9.212334 7 12 12 0 stream from morainic ridge gr0_w38 -77.584596 -9.213738 7 12 13 0 three samples: 38 is main river, 39 is lower tributary, 40 is upper tributar gr0_w39 -77.584353 -9.213768 7 12 13 30 three samples: 38 is main river, 39 is lower tributary, 40 is upper tributar gr0_w40 -77.584164 -9.213768 7 12 14 30 downstream of 36-40 gr0_w41 -77.595552 -9.212796 7 12 14 30 downstream of 36-40 gr0_w42 -77.503855 -9.131729 7 12 11 30 snow sample (under glacier terminus) gr0_w43 -77.678186 -9.274250 7 14 14 0 Rio Buin, high pH gr0_w44 -77.67905 -9.274976 7 14 14 15 Rio Santa downstream gr2_w1 -77.69441 -9.214881 6 29 10 30 trout farm, l	gr0_w35	-77.609983	-9.177850	7	11	13	30	wetland stream originating from moraine into gully 3
gr0_w38 -77.584596 -9.213738 7 12 13 0 three samples: 38 is main river, 39 is lower tributary, 40 is upper tributary gr0_w40 -77.584164 -9.213768 7 12 13 15 three samples: 38 is main river, 39 is lower tributary, 40 is upper tributary gr0_w40 -77.584164 -9.213768 7 12 13 30 three samples: 38 is main river, 39 is lower tributary, 40 is upper tributary gr0_w41 -77.595552 -9.212796 7 12 14 30 downstream of 36-40 gr0_w42 -77.503855 -9.131729 7 12 11 30 snow sample (under glacier terminus) gr0_w43 -77.678186 -9.274250 7 14 14 0 Rio Buin, high pH gr0_w44 -77.67905 -9.274403 7 14 14 15 Rio Santa downstream gr2_w1 -77.616711 -9.214881 6 29 10 30 trout farm, lower rio buin gr2_w2 -77.533050 -9.101331 6 30 13 45 outflow from glacial lake <t< td=""><td>gr0_w36</td><td>-77.593226</td><td>-9.212247</td><td>7</td><td>12</td><td>11</td><td>30</td><td>stream from morainic ridge</td></t<>	gr0_w36	-77.593226	-9.212247	7	12	11	30	stream from morainic ridge
gr0_w39 -77.584353 -9.213876 7 12 13 15 three samples: 38 is main river, 39 is lower tributary, 40 is upper tributary gr0_w40 -77.584164 -9.213768 7 12 13 30 three samples: 38 is main river, 39 is lower tributary, 40 is upper tributary gr0_w41 -77.595552 -9.212796 7 12 14 30 downstream of 36-40 gr0_w42 -77.503855 -9.131729 7 12 11 30 snow sample (under glacier terminus) gr0_w43 -77.678186 -9.274250 7 14 14 0 Rio Buin, high pH gr0_w44 -77.67905 -9.274403 7 14 14 15 Rio Santa downstream gr2_w1 -77.616711 -9.214881 6 29 10 30 trout farm, lower rio buin gr2_w2 -77.533050 -9.101331 6 30 13 45 outflow from glacial lake gr2_w4 -77.532424 -9.116235 7 4 12 15 glacial melt flow gr3_w4 <td< td=""><td>gr0_w37</td><td>-77.590478</td><td>-9.212334</td><td>7</td><td>12</td><td>12</td><td>0</td><td>stream from morainic ridge</td></td<>	gr0_w37	-77.590478	-9.212334	7	12	12	0	stream from morainic ridge
gr0_w40 -77.584164 -9.213768 7 12 13 30 three samples: 38 is main river, 39 is lower tributary, 40 is upper tributary gr0_w41 -77.595552 -9.212796 7 12 14 30 downstream of 36-40 gr0_w42 -77.503855 -9.131729 7 12 11 30 snow sample (under glacier terminus) gr0_w43 -77.678186 -9.274250 7 14 14 0 Rio Buin, high pH gr0_w44 -77.67905 -9.274976 7 14 14 15 Rio Santa downstream gr2_w1 -77.679441 -9.274403 7 14 14 30 Rio Santa upstream gr2_w1 -77.616711 -9.214881 6 29 10 30 trout farm, lower rio buin gr2_w2 -77.533050 -9.101331 6 30 13 45 outflow from glacial lake gr2_w3 -77.516715 -9.114496 7 2 14 5 outflow from glacial lake gr3_w4 -77.53278 -9.21254	gr0_w38	-77.584596	-9.213738	7	12	13	0	three samples: 38 is main river, 39 is lower tributary, 40 is upper tributary
gr0_w41 -77.595552 -9.212796 7 12 14 30 downstream of 36-40 gr0_w42 -77.503855 -9.131729 7 12 11 30 snow sample (under glacier terminus) gr0_w43 -77.678186 -9.274250 7 14 14 0 Rio Buin, high pH gr0_w44 -77.679795 -9.274403 7 14 14 15 Rio Santa downstream gr0_w45 -77.679441 -9.274403 7 14 14 30 Rio Santa downstream gr2_w1 -77.616711 -9.214881 6 29 10 30 trout farm, lower rio buin gr2_w2 -77.533050 -9.101331 6 30 13 45 outflow from glacial lake gr2_w3 -77.516715 -9.114496 7 2 14 5 outflow from glacial lake gr3_w1 -77.532424 -9.116235 7 4 12 15 glacial melt flow gr3_w4 -77.53487 -9.12575 <td>gr0_w39</td> <td>-77.584353</td> <td>-9.213876</td> <td>7</td> <td>12</td> <td>13</td> <td>15</td> <td>three samples: 38 is main river, 39 is lower tributary, 40 is upper tributary</td>	gr0_w39	-77.584353	-9.213876	7	12	13	15	three samples: 38 is main river, 39 is lower tributary, 40 is upper tributary
gr0_w42 -77.503855 -9.131729 7 12 11 30 snow sample (under glacier terminus) gr0_w43 -77.678186 -9.274250 7 14 14 0 Rio Buin, high pH gr0_w44 -77.677905 -9.274403 7 14 14 15 Rio Santa downstream gr2_w1 -77.616711 -9.214881 6 29 10 30 trout farm, lower rio buin gr2_w2 -77.533050 -9.101331 6 30 13 45 outflow from glacial lake gr2_w3 -77.516715 -9.114496 7 2 14 5 outflow from glacial lake gr2_w4 -77.532424 -9.116235 7 4 12 15 glacial melt flow gr3_w4 -77.53456 -9.11807 6 30 14 20 spring from morainic ridge gr3_w6 -77.53597 -9.12516 6 30 13 0 tributary from morainic ridge gr3_w8 -77.53867 -9	gr0_w40	-77.584164	-9.213768	7	12	13	30	three samples: 38 is main river, 39 is lower tributary, 40 is upper tributary
gr0_w43 -77.678186 -9.274250 7 14 14 0 Rio Buin, high pH gr0_w44 -77.677905 -9.274976 7 14 14 15 Rio Santa downstream gr0_w45 -77.679441 -9.274403 7 14 14 30 Rio Santa downstream gr2_w1 -77.616711 -9.214881 6 29 10 30 trout farm, lower rio buin gr2_w2 -77.533050 -9.101331 6 30 13 45 outflow from glacial lake gr2_w3 -77.516715 -9.114496 7 2 14 5 outflow from glacial lake gr2_w4 -77.532424 -9.116235 7 4 12 15 glacial melt flow gr3_w1 -77.59278 -9.21254 6 29 14 30 tributary gr3_w4 -77.53487 -9.12575 6 30 11 45 main stream Río Buín gr3_w6 -77.53867 -9.12516 6 <t< td=""><td>gr0_w41</td><td>-77.595552</td><td>-9.212796</td><td>7</td><td>12</td><td>14</td><td>30</td><td>downstream of 36-40</td></t<>	gr0_w41	-77.595552	-9.212796	7	12	14	30	downstream of 36-40
gr0_w44 -77.677905 -9.274976 7 14 14 15 Rio Santa downstream gr0_w45 -77.679441 -9.274403 7 14 14 30 Rio Santa upstream gr2_w1 -77.616711 -9.214881 6 29 10 30 trout farm, lower rio buin gr2_w2 -77.533050 -9.101331 6 30 13 45 outflow from glacial lake gr2_w3 -77.516715 -9.114496 7 2 14 5 outflow from glacial lake gr2_w4 -77.532424 -9.116235 7 4 12 15 glacial melt flow gr3_w1 -77.59278 -9.21254 6 29 14 30 tributary gr3_w4 -77.53456 -9.11807 6 30 14 20 spring from morainic ridge gr3_w5 -77.53597 -9.12516 6 30 13 0 tributary from morainic ridge gr3_w7 -77.53867 -9.12312 6 30 13 30 spring from ground moraine gr3_w8	gr0_w42	-77.503855	-9.131729	7	12	11	30	snow sample (under glacier terminus)
gr0_w45 -77.679441 -9.274403 7 14 14 30 Rio Santa upstream gr2_w1 -77.616711 -9.214881 6 29 10 30 trout farm, lower rio buin gr2_w2 -77.533050 -9.101331 6 30 13 45 outflow from glacial lake gr2_w3 -77.516715 -9.114496 7 2 14 5 outflow from glacial lake gr2_w4 -77.532424 -9.116235 7 4 12 15 glacial melt flow gr3_w1 -77.59278 -9.21254 6 29 14 30 tributary gr3_w4 -77.53456 -9.11807 6 30 14 20 spring from morainic ridge gr3_w5 -77.53487 -9.12575 6 30 11 45 main stream Río Buín gr3_w7 -77.53867 -9.12312 6 30 13 30 spring from ground moraine gr3_w8 -77.5299 -9.11521 6	gr0_w43	-77.678186	-9.274250	7	14	14	0	Rio Buin, high pH
gr2_w1 -77.616711 -9.214881 6 29 10 30 trout farm, lower rio buin gr2_w2 -77.533050 -9.101331 6 30 13 45 outflow from glacial lake gr2_w3 -77.516715 -9.114496 7 2 14 5 outflow from glacial lake gr2_w4 -77.532424 -9.116235 7 4 12 15 glacial melt flow gr3_w1 -77.59278 -9.21254 6 29 14 30 tributary gr3_w4 -77.53456 -9.11807 6 30 14 20 spring from morainic ridge gr3_w5 -77.53487 -9.12575 6 30 11 45 main stream Río Buín gr3_w6 -77.53867 -9.12312 6 30 13 30 spring from ground moraine gr3_w8 -77.5299 -9.11521 6 30 15 15 tributary	gr0_w44	-77.677905	-9.274976	7	14	14	15	Rio Santa downstream
gr2_w2 -77.533050 -9.101331 6 30 13 45 outflow from glacial lake gr2_w3 -77.516715 -9.114496 7 2 14 5 outflow from glacial lake gr2_w4 -77.532424 -9.116235 7 4 12 15 glacial melt flow gr3_w1 -77.59278 -9.21254 6 29 14 30 tributary gr3_w4 -77.53456 -9.11807 6 30 14 20 spring from morainic ridge gr3_w5 -77.53487 -9.12575 6 30 11 45 main stream Río Buín gr3_w6 -77.53597 -9.12516 6 30 13 0 tributary from morainic ridge gr3_w7 -77.53867 -9.12312 6 30 13 30 spring from ground moraine gr3_w8 -77.5299 -9.11521 6 30 15 15 tributary	gr0_w45	-77.679441	-9.274403	7	14	14	30	Rio Santa upstream
gr2_w3 -77.516715 -9.114496 7 2 14 5 outflow from glacial lake gr2_w4 -77.532424 -9.116235 7 4 12 15 glacial melt flow gr3_w1 -77.59278 -9.21254 6 29 14 30 tributary gr3_w4 -77.53456 -9.11807 6 30 14 20 spring from morainic ridge gr3_w5 -77.53487 -9.12575 6 30 11 45 main stream Río Buín gr3_w6 -77.53597 -9.12516 6 30 13 0 tributary from morainic ridge gr3_w7 -77.53867 -9.12312 6 30 13 30 spring from ground moraine gr3_w8 -77.5299 -9.11521 6 30 15 15 tributary	gr2_w1	-77.616711	-9.214881	6	29	10	30	trout farm, lower rio buin
gr2_w4 -77.532424 -9.116235 7 4 12 15 glacial melt flow gr3_w1 -77.59278 -9.21254 6 29 14 30 tributary gr3_w4 -77.53456 -9.11807 6 30 14 20 spring from morainic ridge gr3_w5 -77.53487 -9.12575 6 30 11 45 main stream Río Buín gr3_w6 -77.53597 -9.12516 6 30 13 0 tributary from morainic ridge gr3_w7 -77.53867 -9.12312 6 30 13 30 spring from ground moraine gr3_w8 -77.5299 -9.11521 6 30 15 15 tributary	gr2_w2	-77.533050	-9.101331	6	30	13	45	outflow from glacial lake
gr3_w1 -77.59278 -9.21254 6 29 14 30 tributary gr3_w4 -77.53456 -9.11807 6 30 14 20 spring from morainic ridge gr3_w5 -77.53487 -9.12575 6 30 11 45 main stream Río Buín gr3_w6 -77.53597 -9.12516 6 30 13 0 tributary from morainic ridge gr3_w7 -77.53867 -9.12312 6 30 13 30 spring from ground moraine gr3_w8 -77.5299 -9.11521 6 30 15 15 tributary	gr2_w3	-77.516715	-9.114496	7	2	14	5	outflow from glacial lake
gr3_w4	gr2_w4	-77.532424	-9.116235	7	4	12	15	glacial melt flow
gr3_w5	gr3_w1	-77.59278	-9.21254	6	29	14	30	tributary
gr3_w6	gr3_w4	-77.53456	-9.11807	6	30	14	20	spring from morainic ridge
gr3_w7	gr3_w5	-77.53487	-9.12575	6	30	11	45	main stream Río Buín
gr3_w8 -77.5299 -9.11521 6 30 15 15 tributary	gr3_w6	-77.53597	-9.12516	6	30	13	0	tributary from morainic ridge
S -	gr3_w7	-77.53867	-9.12312	6	30	13	30	spring from ground moraine
2 0 77 50006 0 11502 6 20 15 20 11 1	gr3_w8	-77.5299	-9.11521	6	30	15	15	tributary
gr3_w9 -77.52996 -9.11523 6 30 15 30 tributary, many red rocks	gr3_w9	-77.52996	-9.11523	6	30	15	30	tributary, many red rocks
gr3_w10 -77.52943 -9.11133 7 2 11 10 tributary from slope	gr3_w10	-77.52943	-9.11133	7	2	11	10	tributary from slope
gr3_w11 -77.52633 -9.11195 7 2 12 20 tributary from ground moraine/pampa	gr3_w11	-77.52633	-9.11195	7	2	12	20	tributary from ground moraine/pampa
gr3_w12 -77.52248 -9.11439 7 2 14 5 tributary from morainic ridge	gr3_w12	-77.52248	-9.11439	7	2	14	5	tributary from morainic ridge
gr3_w13 -77.52629 -9.11748 7 2 15 0 tributary from alongside morainic ridge	gr3_w13	-77.52629	-9.11748	7	2	15	0	tributary from alongside morainic ridge
gr3_w14 -77.53826 -9.13425 7 4 10 40 tributary from slope	gr3_w14	-77.53826	-9.13425	7	4	10	40	tributary from slope

gr3_w15	-77.54185	-9.13906	7	4	11	45	small tributary, grazing area
gr3_w16	-77.55057	-9.14651	7	4	14	30	tributary from mountainside
gr3_w17	-77.55507	-9.14485	7	4	15	20	tributary, disappears into alluvial fan
gr3_w18	-77.53734	-9.13274	7	4	9	50	tributary from slope
gr3_w19	-77.56733	-9.15667	7	5	13	30	morainic ridge tributary, very red
gr3_w20	-77.57578	-9.16274	7	5	15	20	main river
gr3_w21	-77.61423	-9.19276	7	9	12	20	non-moraine tributary
gr3_w22	-77.61412	-9.19241	7	9	12	50	non-moraine tributary
gr3_w23	-77.61717	-9.21736	7	8	9	35	lowest measurement point of Rio Buin
gr3_w24	-77.61162	-9.21104	7	8	13	35	tributary (irrigation?) from rose field
gr3_w25	-77.53465	-9.09642	7	11	12	15	red waterfall, source area with a lot of chicama
gr4_w5	-77.55872	-9.15079	7	6	13	20	from waterfall
gr4_w7	-77.56773	-9.15676	7	6	13	35	main river after waterfall
gr4_w9	-77.58177	-9.17397	7	6	14	48	main river
x_1					9	30	
x_2					9	15	
x_3					13	0	
x_4					14	0	
x_5					14	20	
x_6					14	40	
x_7					13	0	
x_8					11	40	
x_9					11	0	
x_10					11	40	
x_11					9	30	
x_12					16	0	
x_13					16	0	
x_14					14	30	
x_15					14	0	
x_16					11	15	
x_17					11	30	
. –						- 1	

x_18 x_19 x_20 x_21 x_22 x_23 x_24 x_25 x_26 x_27 x_28 x_29 x_30 x_31 x_32 x_33 x_34 x_35 x_36 x_37 x_38 x_39 x_40 x_41 x_42 x_43 x_44 x_45 x_46			
x_19 x_20 x_21 x_22 x_23 x_24 x_25 x_26 x_27 x_28 x_29 x_30 x_31 x_32 x_33 x_34 x_35 x_36 x_37 x_38 x_39 x_40 x_41 x_42 x_43 x_44 x_45 x_46	x_18	11	50
x_20 x_21 x_22 x_23 x_24 x_25 x_26 x_27 x_28 x_29 x_30 x_31 x_32 x_33 x_34 x_35 x_36 x_37 x_38 x_39 x_40 x_41 x_42 x_43 x_44 x_45 x_46		10	0
x_21 x_22 x_23 x_24 x_25 x_26 x_27 x_28 x_29 x_30 x_31 x_32 x_33 x_34 x_35 x_36 x_37 x_38 x_39 x_40 x_41 x_42 x_43 x_44 x_45 x_46		9	45
x_22 x_23 x_24 x_25 x_26 x_27 x_28 x_29 x_30 x_31 x_32 x_33 x_34 x_35 x_36 x_37 x_38 x_39 x_40 x_41 x_42 x_43 x_44 x_45 x_46		14	30
x_23 x_24 x_25 x_26 x_27 x_28 x_29 x_30 x_31 x_32 x_33 x_34 x_35 x_36 x_37 x_38 x_39 x_40 x_41 x_42 x_43 x_44 x_45 x_46		13	40
x_24 x_25 x_26 x_27 x_28 x_29 x_30 x_31 x_32 x_33 x_34 x_35 x_36 x_37 x_38 x_39 x_40 x_41 x_42 x_43 x_44 x_45 x_46		13	10
x_25 x_26 x_27 x_28 x_29 x_30 x_31 x_32 x_33 x_34 x_35 x_36 x_37 x_38 x_39 x_40 x_41 x_42 x_43 x_44 x_45 x_46		13	30
x_26 x_27 x_28 x_29 x_30 x_31 x_32 x_33 x_34 x_35 x_36 x_37 x_38 x_39 x_40 x_41 x_42 x_43 x_44 x_45 x_46		12	20
x_27 x_28 x_29 x_30 x_31 x_32 x_33 x_34 x_35 x_36 x_37 x_38 x_39 x_40 x_41 x_42 x_43 x_44 x_45 x_46		11	30
x_28 x_29 x_30 x_31 x_32 x_33 x_34 x_35 x_36 x_37 x_38 x_39 x_40 x_41 x_42 x_43 x_44 x_45 x_46		10	30
x_29 x_30 x_31 x_32 x_33 x_34 x_35 x_36 x_37 x_38 x_39 x_40 x_41 x_42 x_43 x_44 x_45 x_46		10	15
x_30 x_31 x_32 x_33 x_34 x_35 x_36 x_37 x_38 x_39 x_40 x_41 x_42 x_43 x_44 x_45 x_46		9	15
x_31 x_32 x_33 x_34 x_35 x_36 x_37 x_38 x_39 x_40 x_41 x_42 x_43 x_44 x_45 x_46		12	40
x_32 x_33 x_34 x_35 x_36 x_37 x_38 x_39 x_40 x_41 x_42 x_43 x_44 x_45 x_46		15	0
x_33 x_34 x_35 x_36 x_37 x_38 x_39 x_40 x_41 x_42 x_43 x_44 x_45 x_46		15	10
x_34 x_35 x_36 x_37 x_38 x_39 x_40 x_41 x_42 x_43 x_44 x_45 x_46		12	35
x_35 x_36 x_37 x_38 x_39 x_40 x_41 x_42 x_43 x_44 x_45 x_46		13	0
x_36 x_37 x_38 x_39 x_40 x_41 x_42 x_43 x_44 x_45 x_46		11	45
x_37 x_38 x_39 x_40 x_41 x_42 x_43 x_44 x_45 x_46		12	45
x_38 x_39 x_40 x_41 x_42 x_43 x_44 x_45 x_46		13	45
x_39 x_40 x_41 x_42 x_43 x_44 x_45 x_46		14	30
x_40 x_41 x_42 x_43 x_44 x_45 x_46		15	0
x_41 x_42 x_43 x_44 x_45 x_46		11	10
x_42 x_43 x_44 x_45 x_46		11	0
x_43 x_44 x_45 x_46		11	30
x_44 x_45 x_46		9	20
x_45 x_46		10	20
x_46		11	5
		11	20
v 17	x_40 x_47	13	35
x_47 x_48		13	20
		12	30
x_49	X_49	14	30

x_50	12	30
x_51	14	30
x_52	14	35
x_53	14	50
x_54	15	45
x_55	12	25
x_56	14	45
x_57	15	0
x_58	12	45
x_59	14	15
x_60	10	30
x_61	13	30
x_62	10	50
x_63	10	0
x_64	11	0
x_65	9	45
x_66	12	30
x_67	14	10

<u>Table C.6) Continued: Water quality – field measurements</u>

NR	Туре	Algal mats [y/n]	Fe-precip [y/n]	Temp.	EC	Distance to Glacier	Detrended EC	pН	CO3 [mg/L]	HCO3 [mg/L]	CaCO3-eq [mg/L]
gr0_w1	S	0	0	16.2	49.7		49.7	6.5	0	38.3	31.4
gr0_w2	MS	0	0	11.2	30	6200	44.74	6.5	0	15.7	12.9
gr0_w3	MS	0	0	9.8	15.6	5600	22.74	6.4	0	9.9	8.1
gr0_w4	S	0	0	10	26.1		26.1	6.4	0	10.2	8.4
gr0_w6	MS	0	a bit	7.7	58	7700	127.61	6.3	0	26	21.3
gr0_w7	MS	0	1	9.9	69.1	13500	119.88	6.3	0	30.6	25.1
gr0_w8	MS	0	0	11.9	68.4	7200	97.57	6.9	0	36.2	29.7
gr0_w10	MS	0 / a bit	: 1	6.8	51.6	1900	68.24	8	0	10.2	8.4

gr0_w11	MS	0	0	4.3	25.8	1600	33.66	7.5	0	17	14
gr0_w12	L	0	0	4	35.5			7.6	0	15.7	12.9
gr0_w13	MS	0	0	6.1	55	3300	79.44	7.7	0	15.3	12.6
gr0_w14	MS	0	0	5.9	139.8	1500	190.11	7.6	0	9.4	7.7
gr0_w5	MS	0	a bit	6.4	81.1	18500	256.25	5.8	0	51.2	41.9
gr0_w15	L	0	0	9.7	102.1	900	132.35	7.7	0	2.9	2.1
gr0_w16	S	0	1	10.1	94.7		94.7	7	0	26.7	21.9
gr0_w18	S	0	0	23.9	129		129	7.4	0	56.2	46.1
gr0_w19	MS	0	0	6.4	157.5	1200	197.63	7.6	0	9.4	7.9
gr0_w20	MS	0	0	9.3	41.5	1700	60.71	7.4	0	20.7	17
gr0_w21	L	0	0	8.3	42	1200	61.98	7.3	0	25.5	21
gr0_w22	MS	0	0	7.3	41	3200	53.71	7.4	0	29	32.8
gr0_w23	S	0	0	8.6	38.4		38.4	6.8	0	25.5	21
gr0_w24	MS	0	0	12	41.9	4100	58.67	7.2	0	20.6	16.9
gr0_w25	MS	0	0	12	26.8	4400	35.47	7.2	0	15.7	12.9
gr0_w26	S	0	0	10.5	72.2		72.2	8	0	28.1	23.1
gr0_w27	S	0	0	13.5	116		116	6.7	0	47.9	39.3
gr0_w28	IC	0	0	12.4	75.6		75.6	7.2	0	25.5	21
gr0_w29	L	0	0	7	168.2		168.2	7.4	0	109.6	90
gr0_w30	L	0	0	?	110.9		110.9	7.1	0	20.7	17
gr0_w31	MS	0	1	6.2	62.3	1300	98.9	5.2	0	6.4	4.2
gr0_w32	MS	0	0	1.9	25.5	800	39.5	7.2	0	15.7	12.9
gr0_w33	MS	0	0	7.4	14.2	3900	19.28	7.2	0	6.7	5.5
gr0_w34	MS	0	slightly	12.5	18.3	2900	22.72	7.3	0	9.1	7.4
gr0_w35	S	0	0	24.1	24.8		24.8	7.6	0	15.3	12.6
gr0_w36	S	0	0	8.8	29		29	6.7	0	15.8	12.9
gr0_w37	S	0	0	21.2	30.4	5200	44.1	7	0	23.4	19.2
gr0_w38	MS	0	0	11.2	22.6	4500	31.39	7.3	0	15.3	12.6
gr0_w39	MS	0	1	10.5	21.4	4500	29.37	7.1	0	17.9	14.7
gr0_w40	MS	0	0	11.5	23.7	4500	32.14	7.5	0	15.3	12.6
gr0_w41	S	0	0	11.5	30.1		30.1	7.2	0	23.9	19.6
gr0_w42	GI	0	0	0	27.2		27.2	6.7	0	0.2	0.1

gr0_w43	MS	0	0	15.5	188	27000	188	9.3	6	66.9	65.5
gr0_w44	R	0	0	14.8	282		282	8	0.1	71.4	58.7
gr0_w45	R	0	0	15.4	290		290	7.7	0.1	76.4	62.8
gr2_w1	MS	0	?	9	82.8	18700	223.25	7.6	0	36.1	29.7
gr2_w2	MS	0	slightly			2000					
gr2_w3	MS	?	?			900			0	17.5	14.3
gr2_w4	MS	0	?			3500			0	20.5	16.9
gr3_w1	S	?	?	?	27.2		27.2	6.6			
gr3_w4	S	?	?	?	118.7		118.7	7.2			
gr3_w5	S	?	?	?	90.8		90.8	6.5			
gr3_w6	S	?	?	?	65		65	6.53			
gr3_w7	MS	?	?	?	35.2	3300	47.15	7.03			
gr3_w8	S	?	?	?	140.2		140.2	6.65			
gr3_w9	MS	?	?	?	134.1	2600	168.88	6.6			
gr3_w10	S	?	?	?	170		170	8.3	0	117.9	96.7
gr3_w11	S	?	?	?	123.5		123.5	7.3	0	31	25.4
gr3_w12	MS	?	?	?	145.3	1600	187.32	7.2	0	15.3	12.6
gr3_w13	MS	?	?	?	153	2100	191.98	7.2	0	15.4	12.6
gr3_w14	S	?	?	?	123.6		123.6	7.2			
gr3_w15	S	?	?	?	60.2		60.2	6.7			
gr3_w16	S	?	?	?	111.5		111.5	6.2			
gr3_w17	MS	?	?	?	45.1	2300	55.24	6.8			
gr3_w18	S	?	?	?	181.9		181.9	7.2			
gr3_w19	S	?	?	?	225		225	5.9	0	146.5	120.1
gr3_w20	MS	?	?	?	39.1		39.1	6.6	0	25.5	21
gr3_w21		?	?	?	16.7		16.7	6.2	0	13.7	11.2
gr3_w22		?	?	?	62		62	6.3	0	31.9	26.2
gr3_w23	MS	?	?	?	98.9	19000	219.24	7.3			
gr3_w24	S	?	?	?	110.5		110.5	7			
gr3_w25	MS	?	?	?	88	1700	111.49	6	0	2.8	0
gr4_w5	MS	?	?	?	26.7	3300	34.65	7.5			
gr4_w7	MS	?	?	?	68	10200	91.28	7.4			

gr4_w9	MS	c	?	?	?	71.2	12200	90.01	7.4
x_1	MS				9.8	112.1	18900	249.44	7.7
x_2	MS				9	114.1	18000	255.81	7.8
x_3	MS				11.5	101.5	5200	166.3	7.8
x_4	MS					52.8	5300	67.06	7.2
x_5	MS					58.3	5300	73.09	7.1
x_6	MS					57.4	4100	71.08	7.2
x_7	MS					45.5		60.11	6.7
x_8	S					40.2		40.2	7.2
x_9	IC					63		63	6.9
x_10	S					64.2	13700	64.2	6.7
x_11	MS					77	10900	153.66	6.7
x_12	MS					69.7		89.14	6.9
x_13	S					33	9800	33	6.2
x_14	MS					70	9300	96.11	6.6
x_15	MS					43.2	1500	60.9	6.6
x_16	MS					36.1	8600	55.38	6.6
x_17	MS					70.4	8700	116.88	6.7
x_18	MS					70.4	3500	114.14	6.7
x_19	MS					45.5	8300	76.07	6.2
x_20	MS					54		100.5	6.5
x_21	S					104.5	6400	104.5	6.7
x_22	MS					66.1	6300	85.99	6.2
x_23	MS					66.5		88.44	6.5
x_24	S					26.4	6000	26.4	6.3
x_25	MS					64.2	5300	89.19	6.5
x_26	MS					62.8	5100	90.89	6.5
x_27	MS					57.9	5000	88.55	6.6
x_28	MS					57	4800	88.34	6.4
x_29	MS					83.8	4000	137	6.8
x_30	MS					82.2	3400	115.56	6.7
x_31	MS					53.8	3100	68.3	6.6

Ī	I					I
x_32	MS		49.5		62.64	6.5
x_33	MS		16.7		16.7	6.2
x_34			58.7		58.7	6.4
x_35		10.5	44.4		44.4	7.1
x_36	S	12	57.5	4600	57.5	6.9
x_37	MS	10.8	58.8	4800	75.33	7.3
x_38	MS	10.4	58.3	4800	72.59	7.1
x_39	MS	10.1	58.8		72.04	7.3
x_40	S	8.5	30.3		30.3	7.2
x_41	S	11.5	102		102	7.7
x_42	S	8.5	96.8	7800	96.8	7.4
x_43	MS		78.8		136.44	7.2
x_44	S		72.7		72.7	7.3
x_45	S		102.7		102.7	7.4
x_46	S		96.8		96.8	7.4
x_47	IC		77		77	7.3
x_48			114.5	5000	114.5	7.2
x_49	MS		52.8		65.76	7.2
x_50	IC		35.1		35.1	7
x_51	IC		26.8	5300	26.8	7.1
x_52	MS		58.3		72.41	7.1
x_53	S		70.4	5400	70.4	7.2
x_54	MS		57.4	7000	68.52	7.2
x_55	MS		53.2		85.69	6.7
x_56	S		79.3	5600	79.3	6.4
x_57	MS		17.6		24.57	6.5
x_58	IC		26		26	6.1
x_59	S		30		30	6.5
x_60	MS		40.5		79.35	6.6
x_61	S		26.8		26.8	6.6
x_62	S		207		207	5.9
x_63	S		45.5	4700	45.5	6.2

x_64	MS	61.1	96.53	6.7
x_65	S	98.9	98.9	7
x_66	L	44	44	8.5
x_67	L	14.5	14.5	

<u>Table C.6) Continued: Water quality – laboratory measurements</u>

NR	NOx [µmol/ L]	NH4 [µmol/ L]	PO4 [μmol/ L]	Cl [µmol/ L]	SO4 [µmol/ L]	Al (µmol/ L)	Ca (µmol/ L)	Fe (µmol/ L)	K (μmol/ L)	Li (µmol/ L)	Mg (μmol/ L)	Mn (μmol/ L)	Na (μmol/ L)	S (µmol/ L)	Si (µmol/ L)
gr0_w 1	<3	5	2.3	<17	16	2.55	153.58	0.93	42.46	0.59	26.53	0.03	182.50	24.5	389.0
gr0_w 2	<3	<5	0.4	<17	17	0.63	118.27	0.96	14.14	1.31	14.02	0.31	88.09	30.8	119.9
gr0_w 3	<3	<5	0.5	<17	18	0.52	79.93	0.26	9.39	0.30	7.13	0.06	43.83	27.3	87.7
gr0_w 4	<3	<5	0.5	<17	15	0.36	83.94	0.35	9.91	0.25	6.86	0.01	32.94	26.1	68.1
gr0_w	<3	<5	0.5	206	18	0.64	170.08	0.88	23.98	8.97	21.14	0.13	296.06	32.0	139.4
gr0_w 7	<3	<5	0.3	104	122	1.24	308.18	1.14	25.47	5.79	46.57	0.22	210.84	186.6	130.3
gr0_w 8	<3	<5	0.9	76	113	3.18	279.69	2.22	42.07	0.65	66.91	0.21	188.89	159.4	210.8
gr0_w 10	<3	<5	0.5	<17	218	0.93	202.56	10.91	9.06	0.52	54.80	1.50	38.63	297.7	110.1
gr0_w 11	<3	<5	0.5	<17	25	5.06	133.47	2.56	23.76	0.19	8.84	0.11	29.37	46.1	39.8
gr0_w 12	<3	<5	0.5	<17	20	81.12	160.83	36.63	702.93	1.15	43.49	1.35	69.26	41.0	129.7
gr0_w 13	<3	<5	0.6	<17	144	4.12	243.72	3.48	41.29	0.32	35.79	0.73	41.62	195.9	82.8
gr0_w 14	<3	<5	0.4	<17	304	0.75	651.16	0.29	15.79	0.12	77.12	0.03	40.97	734.1	103.5
gr0_w 5	<3	<5	0.5	18	262	0.44	347.38	0.52	45.76	0.16	94.65	0.06	141.73	149.4	243.2
gr0_w 15	9	<5	0.3	<17	72	0.88	537.97	0.28	13.19	0.28	48.59	0.03	29.47	490.5	31.3

1 0	ı					Ī									
gr0_w 16	<3	<5	0.5	<17	147	0.71	259.29	0.72	42.53	0.18	38.54	0.35	117.02	190.0	235.3
gr0_w 18	25	<5	0.7	<17	72	1.88	338.01	0.62	45.74	0.43	71.97	0.04	202.91	135.2	367.0
gr0_w 19	<3	<5	0.6	<17	257	0.96	640.92	0.18	24.48	0.68	165.85	0.17	56.84	812.4	52.8
gr0_w 20	<3	<5	0.6	<17	45	1.61	219.00	0.30	10.65	0.32	44.07	0.02	25.26	80.1	39.7
gr0_w 21	<3	<5	0.6	<17	41	1.32	197.57	0.37	10.75	0.30	37.65	0.02	22.87	47.7	34.0
gr0_w 22	<3	<5	0.6	<17	28	0.98	200.22	0.25	11.26	0.26	27.75	0.02	59.58	42.0	114.0
gr0_w 23	<3	<5	0.6	<17	16		133.48			0.26					288.1
gr0_w						1.03	133.48	1.67	7.37	0.05	23.86	0.33	178.72	20.1	288.1
24	<3	<5	0.4	<17	32	0.49	124.71	0.35	6.11	0.05	14.19	0.02	133.46	31.6	251.6
gr0_w 25	<3	<5	0.7	<17	15	0.98	58.78	0.63	9.45	0.12	8.29	0.02	122.55	<4	211.7
gr0_w 26	<3	<5	0.8	203	30	2.23	162.62	1.49	41.22	6.45	28.70	0.03	313.45	46.0	206.4
gr0_w 27	<3	<5	0.9	151	23	0.83	94.86	10.46	23.95	2.93	33.23	0.37	585.41	41.0	359.1
gr0_w 28	<3	<5	0.7	31	154	2.24	179.18	6.30	36.40	1.05	79.17	1.40	202.87	211.5	284.4
gr0_w 29	<3	<5	0.6	<17	75	0.96	783.26	0.80	50.56	0.29	187.98	0.17	111.76	270.7	167.6
gr0_w	<3	<5	0.6	<17	350										
30	\\ 3	\3	0.0	\17	330	0.78	590.30	0.99	17.27	0.13	80.71	0.05	55.79	530.9	120.7
gr0_w 31	<3	<5	0.2	<17	240	7.86	222.89	2.01	9.42	0.62	60.15	1.66	31.08	346.8	97.5
gr0_w 32	<3	<5	0.6	<17	18	4.77	129.89	1.99	18.89	0.19	8.23	0.13	21.16	39.4	37.0
gr0_w 33	<3	<5	0.4	<17	15	1.02	56.94	0.27	11.00	0.12	4.84	0.02	45.16	12.9	106.1
gr0_w 34	<3	<5	0.4	<17	15	0.69	71.27	0.57	7.73	0.12	5.66	0.03	49.87	8.9	116.4
gr0_w 35	<3	<5	0.5	18	15	1.05	73.21	0.33	37.70	0.25	8.48	0.03	128.46	4.4	256.9
gr0_w	2	_	0.7	20	1.5	1.03	13.41	0.55	31.10	0.23	0.40	0.03	120.40	7.7	230.9
36	<3	<5	0.7	29	15	1.53	68.88	11.98	9.40	0.10	10.23	0.14	161.10	<4	294.9

I ~~0 *** I															
gr0_w 37	<3	<5	0.6	25	15	1.96	86.15	4.94	8.60	0.09	10.55	1.53	160.28	<4	141.6
gr0_w 38	<3	<5	0.6	32	15	1.34	62.34	1.90	9.72	0.12	6.96	0.28	131.12	<4	262.0
gr0_w 39	<3	<5	1	39	15	10.77	54.83	10.65	9.50	0.29	12.47	0.46	123.31	<4	313.1
gr0_w 40	<3	<5	0.7	38	15	1.99	72.67	1.09	7.01	0.13	7.75	0.06	132.26	<4	272.8
gr0_w 41	<3	<5	0.8	29	15	3.71	84.44	4.16	10.37	0.19	10.87	0.19	163.07	<4	291.4
gr0_w 42	<3	44	0.4	165	15	0.64	10.13	0.35	46.98	0.04	1.53	0.20	102.48	<4	6.8
gr0_w	<3	12	0.4	203	333										
43 gr0_w						2.81	770.84 1022.3	1.48	44.63	7.18	130.39	0.09	370.21	443.6	154.8
44	<3	3	<0,2	452	657	3.62	4	1.15	71.09	20.85	242.23	4.60	628.49	938.3	160.6
gr0_w 45	6	<3	<0,2	454	674	2.93	1080.6 5	3.52	69.61	21.63	246.20	4.40	651.59	961.1	168.6
gr2_w 1	<3	<3	<0,2	254	122	1.40	311.62	0.79	30.00	10.81	46.91	0.20	354.48	173.0	139.5
gr2_w 2	<3	<3	0.3	<15	31	8.08	138.75	3.16	20.76	0.55	9.56	0.10	33.70	36.4	42.6
gr2_w	<3	<3	<0,2	<15	673	1.32	646.53	0.20	18.48	0.76	172.95	0.55	46.78	859.5	47.5
gr2_w	<3	<3	<0,2	<15	367	2.02	450.55	1.07	22.80	0.36	94.28	0.35	48.79	472.8	75.1
gr3_w	<3	<3	0.3	<15	23	0.52	88.17	1.06	11.20	0.16	11.77	0.08	127.20	28.4	243.9
gr3_w	<3	<3	<0,2	<15	101	0.73	438.41	0.12	13.88	0.27	42.92	0.01	125.77	88.4	208.4
gr3_w	14	<3	<0,2	<15	103										
5 gr3_w						0.48	379.63	1.71	59.03	0.19	105.77	0.17	161.80	148.3	280.6
6	<3	<3	<0,2	17	43	0.50	289.91	0.28	39.66	0.11	40.23	0.01	142.92	53.0	261.9
gr3_w 7	<3	<3	<0,2	<15	75	4.25	199.17	1.25	28.57	0.42	12.09	0.06	50.49	89.2	79.6
gr3_w 8	<3	<3	0.8	22	587	0.76	702.31	1.09	14.63	0.33	125.59	0.05	54.80	767.8	119.1
gr3_w 9	<3	<3	<0,2	<15	528	1.28	604.58	1.22	28.58	0.49	138.07	0.24	62.88	751.2	87.8

				ı	ı									
<3	<3	0.2	<15	235	0.84	922.28	0.15	33.58	0.27	227.61	0.03	112.08	345.6	174.8
<3	<3	<0,2	<15	394	0.74	564.78	0.95	18.08	0.13	75.58	0.05	54.04	557.7	123.9
<3	<3	<0,2	<15	668	1.06	714.58	0.13	23.01	0.80	193.29	0.19	49.77	965.0	53.9
<3	<3	<0,2	<15	762	0.63	806.34	0.09	27.14	0.38	175.96	0.24	73.04	1019.1	93.6
<3	<3	<0,2	<15	116	1.27	724.59	0.33	27.39	0.61	164.95	0.11	48.99	184.5	52.8
<3	<3	<0,2	18	76	0.71	322.42	0.11	10.91	0.32	88.13	0.03	22.40	125.4	33.7
<3	<3	0.2	26	62							0.01			243.4
<3	<3	<0,2	25	22										174.1
<3	<3	<0,2	160	330										84.2
<3	<3	0.4	57	43										449.8
<3	<3	<0,2	<15	59										94.5
<3	<3	<0,2	<15	<25										132.3
<3	<3	<0,2	<15	<25										210.0
<3	<3	0.3	278	112										162.6
<3	<3	0.3	218	<25										177.8
<3	<3	<0,2	<15	303										136.8
<3	<3	0.2	99	<25										154.4
<3	<3	<0,2	29	117										125.5
<3	<3	<0,2	38	123										124.5
	<3 <3 <3 <3 <3 <3 <3 <3 <3 <3 <3 <3 <3 <3 <3 <3 <3 <3 <3 <3 <3 <3 <3 <3 <3 <3 <3 <3 <3 <3 <3 <3 <3 <3 <3 <3 <3 <3 <3 <3 <3 <3 <3 <3 <3 <3 <3 <3 <3 <3 <3	3 3 3 3	<3	<3	<3	<3	<3	3 3 <0,2	3 3 <0,2	3 3 <0,2	3 3 <0,2	3 3 40,2 415 394 0.74 564.78 0.95 18.08 0.13 75.58 0.05 3 3 40,2 415 668 1.06 714.58 0.13 23.01 0.80 193.29 0.19 3 3 40,2 415 762 0.63 806.34 0.09 27.14 0.38 175.96 0.24 3 3 40,2 415 116 1.27 724.59 0.33 27.39 0.61 164.95 0.11 3 3 40,2 18 76 0.71 322.42 0.11 10.91 0.32 88.13 0.03 3 3 40,2 26 62 1.38 551.27 0.10 26.08 1.86 60.15 0.01 3 3 40,2 25 22 0.75 286.86 0.13 27.25 0.27 11.33 0.02 3 3 40,2 415	3 3 40,2 415 394 0.74 564.78 0.95 18.08 0.13 75.58 0.05 54.04 3 3 40,2 415 668 1.06 714.58 0.13 23.01 0.80 193.29 0.19 49.77 3 3 40,2 415 762 0.63 806.34 0.09 27.14 0.38 175.96 0.24 73.04 3 3 40,2 415 116 1.27 724.59 0.33 27.39 0.61 164.95 0.11 48.99 3 3 40,2 18 76 0.71 322.42 0.11 10.91 0.32 88.13 0.03 22.40 3 3 40,2 25 22 0.75 286.86 0.13 27.25 0.27 11.33 0.02 93.75 3 3 40,2 15 59 0.63 216.17 5.83 11.35 0.91 <td< td=""><td> </td></td<>	

Table C.6) Continued: Water quality – laboratory measurements

NR	As (µmol /L)	Be (µmol /L)	Cd (µmol /L)	Co (µmol /L)	Cu (µmol /L)	Ni (µmol /L)	Sr (µmol /L)	Ti (µmol /L)	Zn (µmol /L)	B (μmol /L)	Ba (µmol /L)	Cr (µmol /L)	Ga (µmol /L)	In (µmol /L)	Mo (μmol /L)	Pb (μmol /L)	Sb (µmol /L)
gr0_ w1	<0,2	<0,00 5	<0,00 5	<0,00 8	<0,01	<0,03	0.515	0.059	<0,02	0.88	0.032	<0,02	<0,1	<0,06	0.02	<0,03	<0,1
gr0_ w2	<0,2	<0,00 5	<0,00 5	<0,00 8	0.02	<0,03	0.257	0.006	0.03	2.41	0.013	<0,02	<0,1	<0,06	<0.01	<0,03	<0,1
gr0_	, , ,	<0,00		<0,00		,,,,,		<0,00				, , , ,	, ,	,,,,,,,,,,,,,,,,,,,,,,,,,,,,,,,,,,,,,,,		,	, ,
w3	<0,2	5	0.005	8	0.01	<0,03	0.188	4	<0,02	<0,1	0.009	<0,02	< 0,1	<0,06	0.01	<0,03	< 0,1
gr0_		<0,00	<0,00	<0,00				<0,00									
w4	<0,2	5	5	8	0.01	<0,03	0.192	4	<0,02	<0,1	0.015	<0,02	<0,1	<0,06	<0,01	<0,03	<0,1
gr0_ w6	<0,2	<0,00	<0,00	<0,00 8	0.01	<0,03	0.574	<0,00 4	0.05	21.04	0.034	<0,02	<0,1	<0,06	<0,01	<0,03	<0,1
gr0_	<0,2	<0,00	<0,00	<0,00	0.01	<0,03	0.574	4	0.03	21.04	0.034	<0,02	<0,1	<0,00	<0,01	<0,03	<0,1
w7	<0,2	5	5	8	<0,01	0.03	0.930	0.018	0.06	11.32	0.025	<0,02	<0,1	<0,06	0.01	<0,03	< 0,1
gr0_	ĺ	<0,00	<0,00	<0,00	ĺ							ĺ	,	,		,	,
w8	<0,2	5	5	8	0.01	<0,03	0.770	0.016	0.02	0.96	0.041	<0,02	< 0,1	<0,06	< 0,01	< 0,03	< 0,1
gr0_		<0,00	<0,00					<0,00									
w10	<0,2	5 <0,00	5	0.031 < 0.00	0.01	0.08	0.305	4	0.15	<0,1	0.010	<0,02	<0,1	<0,06	<0,01	<0,03	<0,1
gr0_ w11	<0,2	5	0.005	8	0.02	<0,03	0.233	0.152	0.04	<0,1	0.020	<0,02	<0,1	<0,06	0.02	<0,03	<0,1
gr0_	٧٥,2	<0,00	0.005	U	0.02	۷٥,05	0.233	0.132	0.01	νο,1	0.020	10,02	٧٥,1	٧٥,٥٥	0.02	νο,οσ	<0,1
w12	<0,2	5	0.005	0.017	0.23	0.05	0.321	1.980	0.47	0.81	0.230	<0,02	0.12	< 0,06	< 0,01	< 0,03	< 0,1
gr0_		<0,00															
w13	<0,2	5	0.005	0.009	0.02	0.03	0.346	0.103	0.04	<0,1	0.022	<0,02	<0,1	<0,06	0.02	< 0,03	<0,1
gr0_ w14	<0,2	<0,00 5	<0,00 5	0.012	<0,01	0.08	0.501	<0,00 4	0.05	<0,1	0.018	<0,02	ر0 1	<0.06	<0,01	<0,03	ر n 1
gr0_	<0,2	<0.00	<0.00	<0.012	<0,01	0.08	0.301	<0.00	0.03	<0,1	0.018	<0,02	<0,1	<0,06	<0,01	<0,03	<0,1
w5	<0,2	5	5	8	0.01	<0,03	0.460	4	0.02	<0,1	0.047	<0.02	<0,1	<0,06	0.01	<0,03	<0,1
gr0_	ĺ	<0,00	<0,00	<0,00		,		<0,00		,		ĺ	,	,		,	,
w15	<0,2	5	5	8	0.02	0.05	0.261	4	0.06	< 0,1	0.011	<0,02	< 0,1	<0,06	< 0,01	< 0,03	< 0,1
gr0_	0.0	<0,00	<0,00	<0,00	0.00	0.04	0.700	<0,00	0.05	0.4	0.055	0.00	0.4	0.05	0.04	0.00	0.4
w16	<0,2	5 <0,00	5 <0,00	8 <0,00	0.02	0.04	0.580	4	0.07	<0,1	0.066	<0,02	<0,1	<0,06	<0,01	<0,03	<0,1
gr0_ w18	<0,2	<0,00 5	<0,00 5	<0,00 8	0.01	<0,03	0.797	0.007	<0,02	<0,1	0.054	<0,02	<0,1	<0,06	0.01	<0,03	<0,1
gr0_	10,2	<0.00	<0,00	J	0.01	10,03	0.171	<0,00	10,02	\O,1	0.057	10,02	\U,1	10,00	0.01	\0,0 <i>3</i>	\U,1
w19	<0,2	5	5	0.009	0.01	0.15	0.527	4	0.17	< 0,1	0.054	<0,02	< 0,1	<0,06	< 0,01	< 0,03	<0,1
gr0_		<0,00	<0,00	<0,00													
w20	<0,2	5	5	8	0.01	<0,03	0.612	0.005	0.04	< 0,1	0.025	< 0,02	< 0,1	< 0,06	< 0,01	<0,03	< 0,1

gr0_		<0,00	<0,00	<0,00													
w21	<0,2	5	5	8	0.02	<0,03	0.625	0.008	0.05	< 0,1	0.025	< 0,02	< 0,1	< 0,06	< 0,01	< 0,03	< 0,1
gr0_		<0,00	<0,00	<0,00				<0,00									
w22	<0,2	5	5	8	0.01	<0,03	0.566	4	<0,02	0.37	0.019	<0,02	<0,1	<0,06	<0,01	<0,03	< 0,1
gr0_ w23	<0,2	<0,00 5	<0,00 5	<0,00 8	0.02	<0,03	0.445	0.008	<0.02	<0,1	0.012	<0.02	<0,1	<0.06	<0.01	<0.03	<0,1
gr0_	<0,2	<0.00	< 0.00	<0.00	0.02	<0,03	0.443	<0,00	<0,02	<0,1	0.012	<0,02	<0,1	<0,00	<0,01	<0,03	<0,1
w24	<0,2	5	5	8	<0,01	<0,03	0.476	4	<0,02	<0,1	0.004	<0,02	< 0,1	<0,06	<0,01	<0,03	< 0,1
gr0_	,_	<0,00	<0,00	<0,00	,	,			,	,-		,	,-	,	,	,	,-
w25	<0,2	5	5	8	0.04	<0,03	0.193	0.014	< 0,02	<0,1	0.008	< 0,02	< 0,1	< 0,06	< 0,01	<0,03	< 0,1
gr0_		<0,00	<0,00														
w26	<0,2	5	5	0.009	0.02	<0,03	0.592	0.014	0.06	18.94	0.020	<0,02	<0,1	<0,06	< 0,01	<0,03	< 0,1
gr0_	-0.2	<0,00 5	<0,00 5	<0,00	0.02	-0.02	0.207	0.020	0.05	17.07	0.017	-0.02	ر ۱ د	٠٥.٥٢	-0.01	-0.02	ر ۱ د
w27 gr0_	<0,2	<0.00	<0.00	8	0.02	<0,03	0.397	0.020	0.05	17.87	0.017	<0,02	<0,1	<0,06	<0,01	<0,03	<0,1
w28	<0,2	5	5	0.018	0.02	0.05	0.642	0.011	0.12	0.72	0.054	<0,02	<0,1	<0,06	<0,01	<0,03	< 0,1
gr0_	10,2	<0,00		<0,00	0.02	0.02	0.0.2	<0,00	0.12	0.7.2	0.00	10,02	10,1	10,00	10,01	10,00	10,1
w29	<0,2	5	0.008	8	< 0,01	<0,03	1.259	4	0.05	< 0,1	0.011	< 0,02	< 0,1	< 0,06	0.12	<0,03	< 0,1
gr0_		<0,00	<0,00	<0,00				<0,00									
w30	<0,2	5	5	8	<0,01	0.04	0.518	4	0.05	<0,1	0.021	< 0,02	<0,1	<0,06	< 0,01	< 0,03	<0,1
gr0_ w31	-0.2	<0,00 5	<0,00 5	0.059	0.02	0.14	0.311	<0,00	0.23	<0,1	0.008	<0,02	<0,1	0.06	<0.01	<0,03	<0,1
gr0_	<0,2	<0,00	<0,00	<0.039	0.02	0.14	0.511	4	0.23	<0,1	0.008	<0,02	<0,1	0.00	<0,01	<0,03	<0,1
w32	<0,2	5	5	8	0.01	0.04	0.231	0.174	0.03	0.42	0.018	<0,02	<0,1	<0,06	<0,01	<0,03	<0,1
gr0_	, ,	<0,00	<0,00	<0,00								, , ,	, ,	, , , , ,	, , ,	, , , , , ,	,
w33	<0,2	5	5	8	0.01	<0,03	0.108	0.020	0.02	< 0,1	0.004	< 0,02	< 0,1	< 0,06	< 0,01	<0,03	< 0,1
gr0_		<0,00	<0,00	<0,00													
w34	<0,2	5	5	8	0.02	<0,03	0.174	0.015	<0,02	<0,1	0.009	<0,02	<0,1	<0,06	<0,01	<0,03	< 0,1
gr0_ w35	<0,2	<0,00 5	<0,00	<0,00 8	0.01	<0,03	0.255	0.007	0.05	<0,1	0.004	<0,02	<0,1	0.06	<0,01	<0,03	<0,1
gr0_	<0,2	<0.00	<0.00	<0,00	0.01	<0,03	0.233	0.007	0.03	<0,1	0.004	<0,02	<0,1	0.00	<0,01	<0,03	<0,1
w36	<0,2	5	5	8	0.01	<0,03	0.226	0.019	0.03	<0,1	0.025	<0,02	<0,1	<0,06	<0,01	<0,03	< 0,1
gr0_	,_	<0,00	<0,00	<0,00		,,,,				- ,-		,	- ,-	,,,,	,,,	,	,-
w37	<0,2	5	5	8	0.02	<0,03	0.362	0.024	0.03	< 0,1	0.030	< 0,02	< 0,1	< 0,06	< 0,01	<0,03	< 0,1
gr0_		<0,00	<0,00	<0,00			0.5										
w38	<0,2	5	5	8	0.02	<0,03	0.242	0.032	0.05	<0,1	0.006	<0,02	<0,1	<0,06	<0,01	<0,03	<0,1
gr0_ w39	<0,2	<0,00 5	<0,00	<0,00 8	0.01	<0,03	0.228	0.467	0.10	<0,1	0.023	<0.02	<0,1	<0.06	<0,01	<0.03	<0,1
gr0_	<0,2	<0,00	<0,00	<0,00	0.01	<0,03	0.228	0.407	0.10	<0,1	0.023	<0,02	<0,1	<0,00	<0,01	<0,03	<0,1
w40	<0,2	5	5	8	0.02	<0,03	0.252	0.034	0.05	<0,1	0.009	<0,02	<0,1	<0,06	<0,01	<0,03	<0,1
	,_	-	_	_		,00				,•	0.007	,	,-	,00	,01	,00	,-

W41	gr0_		<0,00	<0,00	<0,00													
Variable Variable		<0,2				0.02	<0,03	0.300	0.058	6.04	<0,1	0.026	< 0,02	< 0,1	< 0,06	< 0,01	< 0,03	< 0,1
gr0_ w44 w44 w45 w45	gr0_		<0,00	<0,00	<0,00							<0,00						
w44 gr0		<0,2	•	•		0.04	<0,03	0.016	0.011	0.54	0.30	3	< 0,02	< 0,1	0.06	< 0,01	< 0,03	< 0,1
gr0_ w44			,															
w44 c0,2 c0,005 c0,006 c0,006 c0,006 c0,001 c0,003 c0,016 c0,007 c0,007		<0,2	5	5	8	0.01	<0,03	2.512		3.70	16.75	0.056	<0,02	<0,1	<0,06	0.01	<0,03	<0,1
gr0_ w45		0.0	0.00.	0.006	0.046	0.04	0.10	2 20 4		4.00	10.05	0.4.40	0.00	0.4	0.04	0.04	0.00	0.4
w4 0,2 5 5 8 0,01 0,00		<0,2			0.046	0.01	0.13	2.304		4.90	42.06	0.142	<0,02	<0,1	<0,06	<0,01	<0,03	<0,1
gr2		<0.2			0.020	<0.01	0.00	2 174	1	4.41	11 29	0.140	<0.02	∠0.1	<0.06	<0.01	<0.02	∠0.1
$ \begin{array}{c ccccccccccccccccccccccccccccccccccc$		<0,2	-	-		<0,01	0.09	2.174	4	4.41	44.36	0.149	<0,02	<0,1	<0,00	<0,01	<0,03	<0,1
$ \begin{array}{c ccccccccccccccccccccccccccccccccccc$		<0.2	· · · · · · · · · · · · · · · · · · ·	· · · · · · · · · · · · · · · · · · ·		<0.01	0.03	1 163	0.028	0.22	26.06	0.034	<0.02	<0.1	< 0.06	0.02	<0.03	<0.1
W2		\0,2	-	_		<0,01	0.03	1.105	0.020	0.22	20.00	0.031	\0,02	\0,1	νο,οο	0.02	<0,05	\0,1
$ \begin{array}{c ccccccccccccccccccccccccccccccccccc$		<0.2		· · · · · · · · · · · · · · · · · · ·		0.02	0.03	0.270	0.301	0.06	1.04	0.026	< 0.02	< 0.1	< 0.06	0.01	< 0.03	< 0.1
W3		, ,	<0,00	<0,00									, .	,	, , , , ,		,	,
$ \begin{array}{c ccccccccccccccccccccccccccccccccccc$		<0,2	5	5	0.038	0.01	0.19	0.522	4	0.25	< 0,1	0.052	< 0,02	< 0,1	< 0,06	< 0,01	< 0,03	< 0,1
$ \begin{array}{c ccccccccccccccccccccccccccccccccccc$	gr2_		<0,00	< 0,00														
$ \begin{array}{c ccccccccccccccccccccccccccccccccccc$		<0,2	-	_		< 0,01	0.06	0.458	0.044	0.05	< 0,1	0.027	< 0,02	< 0,1	< 0,06	< 0,01	<0,03	< 0,1
$ \begin{array}{c ccccccccccccccccccccccccccccccccccc$				· · · · · · · · · · · · · · · · · · ·														
w4 <0,2		<0,2		-		0.01	<0,03	0.245		5.84	<0,1	0.016	< 0,02	<0,1	0.06	< 0,01	< 0,03	< 0,1
$ \begin{array}{c ccccccccccccccccccccccccccccccccccc$	-	0.0		· · · · · · · · · · · · · · · · · · ·	,	0.04	0.00	4.000			0.40	0.040	0.00	0.4	0.04	0.40	0.00	0.4
W5		<0,2	5	_		<0,01	<0,03	1.282		7.51	0.43	0.040	<0,02	<0,1	<0,06	0.10	<0,03	<0,1
$ \begin{array}{c ccccccccccccccccccccccccccccccccccc$		-O 2	0.005	′		<0.01	<0.02	0.560		0.20	c0 1	0.055	<0.02	c0 1	<0.06	0.01	<0.02	ر د ۱ د
$ \begin{array}{c ccccccccccccccccccccccccccccccccccc$		<0,2		_		<0,01	<0,03	0.360		9.20	<0,1	0.033	<0,02	<0,1	<0,00	0.01	<0,03	<0,1
$ \begin{array}{c ccccccccccccccccccccccccccccccccccc$		<0.2		· · · · · · · · · · · · · · · · · · ·		0.01	<0.03	0 999		9.44	<0.1	0.020	<0.02	<0.1	<0.06	<0.01	<0.03	<0.1
$ \begin{array}{c ccccccccccccccccccccccccccccccccccc$		\0,2		-		0.01	<0,03	0.777	Т	7.44	\0,1	0.020	<0,02	\0,1	<0,00	<0,01	<0,03	\0,1
$ \begin{array}{c ccccccccccccccccccccccccccccccccccc$		<0.2	· · · · · · · · · · · · · · · · · · ·	′		< 0.01	< 0.03	0.287	0.100	6.39	< 0.1	0.005	< 0.02	< 0.1	< 0.06	0.07	< 0.03	< 0.1
$ \begin{array}{c ccccccccccccccccccccccccccccccccccc$	gr3_	,	<0,00	<0,00	< 0,00	,	,				,		,	ĺ	,		,	,
$ \begin{array}{c ccccccccccccccccccccccccccccccccccc$		<0,2	5	5	8	< 0,01	0.03	0.753	4	0.24	< 0,1	0.052	< 0,02	< 0,1	< 0,06	< 0,01	< 0,03	< 0,1
$ \begin{array}{c ccccccccccccccccccccccccccccccccccc$			<0,00	< 0,00					< 0,00									
$ \begin{array}{ c c c c c c c c c c c c c c c c c c c$		<0,2		-		0.01	0.10	0.537		0.12	< 0,1	0.045	< 0,02	< 0,1	< 0,06	< 0,01	< 0,03	< 0,1
$ \begin{array}{ c c c c c c c c c c c c c c c c c c c$																		
$ \begin{array}{ c c c c c c c c c c c c c c c c c c c$		<0,2	-	-	8	<0,01	<0,03	1.522		0.06	<0,1	0.006	<0,02	<0,1	<0,06	0.17	<0,03	<0,1
$ \begin{vmatrix} gr3\\w12\\gr3 \end{vmatrix} < 0,2 5 5 0.017 < 0,01 0.14 0.528 4 5.65 <0,1 0.053 <0,02 <0,1 <0,06 <0,01 <0,03 <0,1 \\ <0,00 <0,00 <0,00 <0,00 <0,00 <0,00 <0,00 <0,00 <0,00 <0,00 <0,00 <0,00 <0,00 <0,00 <0,00 <0,00 <0,00 <0,00 <0,00 <0,00 <0,00 <0,00 <0,00 <0,00 <0,00 <0,00 <0,00 <0,00 <0,00 <0,00 <0,00 <0,00 <0,00 <0,00 <0,00 <0,00 <0,00 <0,00 <0,00 <0,00 <0,00 <0,00 <0,00 <0,00 <0,00 <0,00 <0,00 <0,00 <0,00 <0,00 <0,00 <0,00 <0,00 <0,00 <0,00 <0,00 <0,00 <0,00 <0,00 <0,00 <0,00 <0,00 <0,00 <0,00 <0,00 <0,00 <0,00 <0,00 <0,00 <0,00 <0,00 <0,00 <0,00 <0,00 <0,00 <0,00 <0,00 <0,00 <0,00 <0,00 <0,00 <0,00 <0,00 <0,00 <0,00 <0,00 <0,00 <0,00 <0,00 <0,00 <0,00 <0,00 <0,00 <0,00 <0,00 <0,00 <0,00 <0,00 <0,00 <0,00 <0,00 <0,00 <0,00 <0,00 <0,00 <0,00 <0,00 <0,00 <0,00 <0,00 <0,00 <0,00 <0,00 <0,00 <0,00 <0,00 <0,00 <0,00 <0,00 <0,00 <0,00 <0,00 <0,00 <0,00 <0,00 <0,00 <0,00 <0,00 <0,00 <0,00 <0,00 <0,00 <0,00 <0,00 <0,00 <0,00 <0,00 <0,00 <0,00 <0,00 <0,00 <0,00 <0,00 <0,00 <0,00 <0,00 <0,00 <0,00 <0,00 <0,00 <0,00 <0,00 <0,00 <0,00 <0,00 <0,00 <0,00 <0,00 <0,00 <0,00 <0,00 <0,00 <0,00 <0,00 <0,00 <0,00 <0,00 <0,00 <0,00 <0,00 <0,00 <0,00 <0,00 <0,00 <0,00 <0,00 <0,00 <0,00 <0,00 <0,00 <0,00 <0,00 <0,00 <0,00 <0,00 <0,00 <0,00 <0,00 <0,00 <0,00 <0,00 <0,00 <0,00 <0,00 <0,00 <0,00 <0,00 <0,00 <0,00 <0,00 <0,00 <0,00 <0,00 <0,00 <0,00 <0,00 <0,00 <0,00 <0,00 <0,00 <0,00 <0,00 <0,00 <0,00 <0,00 <0,00 <0,00 <0,00 <0,00 <0,00 <0,00 <0,00 <0,00 <0,00 <0,00 <0,00 <0,00 <0,00 <0,00 <0,00 <0,00 <0,00 <0,00 <0,00 <0,00 <0,00 <0,00 <0,00 <$		-0.2	· · · · · · · · · · · · · · · · · · ·		0.011	0.04	0.04	0.554		C 40	-0.1	0.025	₄ 0,02	₄ 0 1	-0.06	0.01	₂ 0.02	₄ 0 1
w12 <0,2		<0,2	-	_	0.011	0.04	0.04	0.554		0.40	<0,1	0.035	<0,02	<0,1	<0,06	0.01	<0,03	<0,1
gr3_ <0,00 <0,00 <0,00 <0,00 <0,00		<0.2			0.017	<0.01	0.14	0.529		5 65	<0.1	0.053	<0.02	<0.1	<0.06	<0.01	<0.03	<0.1
		<0,∠				₹0,01	0.14	0.328		5.05	<0,1	0.055	₹0,02	<0,1	₹0,00	<0,01	₹0,03	\0,1
	w13	<0,2	5	5	8	<0,01	0.05	0.938	4	7.19	<0,1	0.038	<0,02	<0,1	<0,06	<0,01	<0,03	<0,1

gr3_		<0,00	<0,00	<0,00				<0,00									
w14	<0,2	5	5	8	< 0,01	< 0,03	3.341	4	9.05	0.30	0.085	< 0,02	< 0,1	< 0,06	0.02	< 0,03	< 0,1
gr3_		<0,00		<0,00				<0,00									
w15	<0,2	5	0.006	8	< 0,01	< 0,03	1.013	4	9.12	< 0,1	0.019	< 0,02	< 0,1	< 0,06	0.02	<0,03	< 0,1
gr3_		<0,00	<0,00	<0,00				<0,00									
w16	<0,2	5	5	8	<0,01	<0,03	2.243	4	9.61	0.11	0.030	<0,02	<0,1	<0,06	<0,01	<0,03	<0,1
gr3_	.0.0	<0,00	0.005	<0,00	0.02	.0.02	0.022	0.004	7.50	.0.1	0.000	.0.00	.0.1	0.06	0.02	0.02	.0.1
w17	<0,2	5	0.005	8	0.02	<0,03	0.822	0.004 <0.00	7.58	<0,1	0.008	<0,02	<0,1	<0,06	0.02	<0,03	<0,1
gr3_ w18	<0,2	<0,00 5	<0,00 5	<0,00 8	0.05	0.05	5.107	<0,00 4	9.14	<0,1	0.081	<0,02	<0,1	<0,06	0.06	<0,03	<0,1
gr3_	<0,2	3	<0,00	<0,00	0.03	0.03	3.107	<0.00	9.14	<0,1	0.061	<0,02	<0,1	<0,00	0.00	<0,03	<0,1
w19	<0,2	0.017	5	8	<0,01	<0,03	4.834	4	5.84	3.14	0.135	<0,02	<0.1	<0,06	<0,01	<0,03	<0,1
gr3_	10,2	0.017	<0.00	<0.00	10,01	10,05	1.05 1	<0.00	2.01	5.11	0.133	10,02	10,1	10,00	10,01	10,05	(0,1
w20	<0,2	0.005	5	8	0.01	0.04	0.453	4	5.85	0.76	0.003	<0,02	< 0,1	<0,06	0.03	<0,03	<0,1
gr3_		<0,00	< 0,00														,
w21	<0,2	5	5	0.008	0.01	<0,03	0.167	0.021	6.94	< 0,1	0.006	< 0,02	< 0,1	< 0,06	< 0,01	<0,03	< 0,1
gr3_		<0,00	<0,00														
w22	<0,2	5	5	0.049	0.02	<0,03	0.512	0.006	7.34	<0,1	0.078	< 0,02	< 0,1	<0,06	<0,01	<0,03	<0,1
gr3_		<0,00	<0,00	<0,00	0.04	0.02	1.000	0.040	4.70	0.4.00	0.044	0.00	0.4	0.04	0.04	0.00	0.4
w23	<0,2	5	5	8	0.01	0.03	1.230	0.019	4.59	24.82	0.041	<0,02	<0,1	<0,06	<0,01	<0,03	<0,1
gr3_ w24	<0,2	<0,00 5	<0,00	<0,00 8	<0,01	<0,03	0.602	0.010	4.67	21.15	0.028	<0,02	<0,1	<0,06	<0,01	<0,03	<0,1
gr3_	<0,2	<0,00	<0,00	0	<0,01	<0,03	0.002	<0,00	4.07	21.13	0.028	<0,02	<0,1	<0,00	<0,01	<0,03	<0,1
w25	<0,2	5	5	0.012	0.01	<0,03	0.198	4	7.51	1.03	0.007	<0,02	<0,1	<0,06	<0,01	<0,03	<0,1
gr4_	10,2	<0,00	<0,00	<0,00	0.01	10,05	3.170	·	,1	1.05	0.007	10,02	٠,1	10,00	(0,01	10,03	ν,,,
w5	<0,2	5	5	8	0.01	0.04	0.231	0.008	4.57	<0,1	0.006	<0,02	<0,1	<0,06	<0,01	<0,03	<0,1
gr4_		< 0,00	<0,00							,		,	,	,		,	,
w7	<0,2	5	5	0.009	0.01	0.04	0.766	0.059	4.32	0.18	0.017	< 0,02	< 0,1	< 0,06	0.03	< 0,03	< 0,1
gr4_		< 0,00	<0,00														
w9	<0,2	5	5	0.010	0.02	0.04	0.785	0.045	4.70	1.18	0.020	< 0,02	<0,1	<0,06	0.01	<0,03	< 0,1

Table C.6) Continued: Water quality – laboratory measurements

NR	[H+]	TOC (mg/L)	TOC (μeq/L)	pK	K	DOC RCOO (μeq/L)	Elevation [m]	d18O [o/oo]	std d18O (n=2)	d2H [o/oo]	std d2H (n=2)
	3.16228E-				6.88256E-						_
gr0_w1	07	1.117	11.17	5.16225	06	10.67933	3566	-13.61	0.03	-98.19	0.03
	3.16228E-				6.88256E-						
gr0_w2	07	1.724	17.24	5.16225	06	16.48268	3575	-13.44	0.01	-97.17	0.11

ı	1	3.98107E-	Ī			7.54119E-		1				
	or() 11/2	3.98107E- 07	1.1	11	5.12256	7.54119E- 06	10.44842	3613	-13.48	0	-97.76	0.02
	gr0_w3	3.98107E-	1.1	11	3.12230	7.54119E-	10.44642	3013	-13.46	U	-97.70	0.02
	gr0_w4	3.98107E- 07	1.071	10.71	5.12256	7.54119E- 06	10.17296	3607	-13.54	0.03	-97.19	0.16
	g10_w4	5.01187E-	1.071	10.71	3.12230	8.27771E-	10.17290	3007	-13.34	0.03	-37.13	0.10
	gr0_w6	5.01187E- 07	1.541	15.41	5.08209	0.27771E- 06	14.53024	3432	-13.37	0	-96.89	0.38
	gro_wo	5.01187E-	1.541	13.41	3.00209	8.27771E-	14.55024	3432	-13.37	U	-30.03	0.56
	gr0_w7	07	0.8424	8.424	5.08209	06 06	7.943074	3559	-14.5	0.01	-103.32	0.04
	510_W /	1.25893E-	0.0424	0.424	3.00207	4.86172E-	7.743074	3337	14.5	0.01	103.32	0.04
	gr0_w8	07	4.323	43.23	5.31321	06	42.13883	3177	-13.74	0.08	-98.86	0.07
	gr0_w10	0.00000001	1.367	13.67	5.664	2.1677E-06	13.60723	4382	-14.13	0.03	-99.38	0.08
	g10_w10	3.16228E-	1.307	13.07	3.004	3.04614E-	13.00723	4362	-14.13	0.03	-99.36	0.08
	gr0_w11	08	0.5816	5.816	5.51625	06	5.756243	4317	-14.51	0.04	-102.62	0.01
	g10_W11	2.51189E-	0.5010	3.010	3.31023	2.83557E-	3.730243	4317	14.51	0.04	102.02	0.01
	gr0_w12	08	0.8415	8.415	5.54736	06	8.34111		-14.56	0	-103.17	0.19
	810_111	1.99526E-	0.0.10	01.10	0.0.700		0.0 .111		1	· ·	100117	0.15
	gr0_w13	08	0.6072	6.072	5.57769	2.6443E-06	6.026527	4190	-14.47	0.01	-103.36	0.16
	<i>v</i> –	2.51189E-				2.83557E-						
	gr0_w14	08	0.6685	6.685	5.54736	06	6.626301	4228	-14.19	0.03	-100.4	0.08
		1.58489E-				1.35506E-						
	gr0_w5	06	1.249	12.49	4.86804	05	11.18213	3179	-13.7	0.02	-102.38	0.21
		1.99526E-										
	gr0_w15	08	1.161	11.61	5.57769	2.6443E-06	11.52305	4495	-9.97	0.01	-69.83	0.25
						4.47713E-						
	gr0_w16	0.0000001	1.782	17.82	5.349	06	17.43067	3997	-12.18	0.02	-91.79	0.08
	0 10	3.98107E-			o	3.27823E-		400				
	gr0_w18	08	2.461	24.61	5.48436	06	24.31472	4092	-12.69	0.02	-96.21	0.05
	0 10	2.51189E-	0.6626		5.5450.6	2.83557E-	c 577701	1017	12.02	0	00.01	0
	gr0_w19	08	0.6636	6.636	5.54736	06	6.577731	4217	-13.83	0	-98.91	0
	~"0 ***20	3.98107E- 08	0.8179	8.179	5.48436	3.27823E- 06	8.080866	4310	-13.65	0.03	-98.27	0.07
	gr0_w20	5.01187E-	0.8179	0.179	3.46430	3.53435E-	8.080800	4310	-13.03	0.03	-90.27	0.07
	gr0_w21	08	0.7527	7.527	5.45169	3.33433E- 06	7.421756	4346	-13.74	0.02	-98.56	0.09
	g10_w21	3.98107E-	0.7327	1.321	3.73107	3.27823E-	7.421730	7570	-13.74	0.02	-76.50	0.07
	gr0_w22	08	0.5879	5.879	5.48436	06	5.808462	3803	-14.04	0.02	-100.64	0.17
	810=	1.58489E-	0.0075	2.075	21.0.00	5.28883E-	2.000.02	2002	1	0.02	100.0	0.17
	gr0_w23	07	1.202	12.02	5.27664	06	11.67028	3640	-13.36	0.02	-98.36	0.04
		6.30957E-				3.81733E-						
	gr0_w24	08	0.9452	9.452	5.41824	06	9.298311	3554	-13.51	0.01	-98.51	0.06

Ī		6.30957E-				3.81733E-						
	gr0_w25	08	1.874	18.74	5.41824	06	18.43529	3553	-13.11	0.07	-95.82	0.79
	gr0_w26	0.00000001	3.002	30.02	5.664	2.1677E-06	29.88215	3191	-12.92	0.01	-95.33	0.14
		1.99526E-				5.76381E-						
	gr0_w27	07	5.449	54.49	5.23929	06	52.66683	3217	-12.19	0.03	-90.34	0.04
	0 20	6.30957E-	2.02	20.2	5 41004	3.81733E-	10.06002	2271	12.0	0.01	02.21	0.06
	gr0_w28	08 3.98107E-	2.03	20.3	5.41824	06 3.27823E-	19.96992	3371	-12.8	0.01	-93.21	0.06
	gr0_w29	08	2.113	21.13	5.48436	3.27823E- 06	20.87648	4206	-13.67	0.03	-99.38	0.04
	810_1127	7.94328E-	2.113	21.13	5.10150	4.13038E-	20.07010	1200	13.07	0.03	77.50	0.01
	gr0_w30	08	0.9045	9.045	5.38401	06	8.874334	4212	-13.77	0.02	-98.44	0.12
	o –	6.30957E-				2.59753E-						
	gr0_w31	06	0.7934	7.934	4.58544	05	6.383422	4508	-13.49	0.05	-97.4	0.15
	0 00	6.30957E-	0.5005	.	~ 440 2 4	3.81733E-	.			0.00	100.00	0.00
	gr0_w32	08 6.30957E-	0.5905	5.905	5.41824	06	5.808985	4544	-14.4	0.08	-102.23	0.02
	gr0_w33	6.3095/E- 08	0.9204	9.204	5.41824	3.81733E- 06	9.054343	3657	-13.22	0.06	-95.29	0.01
	g10_w33	5.01187E-	0.9204	9.204	J.41024	3.53435E-	7.034343	3037	-13.22	0.00	-93.29	0.01
	gr0_w34	08	0.6948	6.948	5.45169	06	6.850852	3814	-13.67	0.04	-97.54	0.13
	<i>C</i> –	2.51189E-				2.83557E-						
	gr0_w35	08	1.977	19.77	5.54736	06	19.59641	3806	-11.86	0.03	-88.71	0.16
		1.99526E-				5.76381E-						
	gr0_w36	07	3.378	33.78	5.23929	06	32.64976	3567	-11.67	0.01	-87.58	0.08
	or0 w27	0.0000001	2.262	22.62	5.349	4.47713E- 06	22.1258	3597	-11.82	0.01	-87.43	0.1
	gr0_w37	5.01187E-	2.202	22.02	3.349	3.53435E-	22.1236	3391	-11.62	0.01	-07.43	0.1
	gr0_w38	08	1.566	15.66	5.45169	06	15.44104	3670	-12.98	0.02	-95.62	0.05
	8	7.94328E-				4.13038E-						
	gr0_w39	08	1.474	14.74	5.38401	06	14.46188	3669				
		3.16228E-				3.04614E-						
	gr0_w40	08	1.089	10.89	5.51625	06	10.77811	3678				
	41	6.30957E-	1 444	1 4 4 4	£ 41004	3.81733E-	14 20521	2520	12.05	0.05	02.00	0.05
	gr0_w41	08 1.99526E-	1.444	14.44	5.41824	06 5.76381E-	14.20521	3528	-12.95	0.05	-93.99	0.05
	gr0_w42	07	2.1	21	5.23929	06	20.29737	4925	-7.22	0.06	-43.06	0.12
	S10_11 12	5.01187E-	2.1	21	0.20727	1.10436E-	20.27.37	1,723	7.22	0.00	13.00	0.12
	gr0_w43	10	2.696	26.96	5.95689	06	26.94777	2583	-13.65	0.05	-98.09	0.04
	gr0_w44	0.00000001	1.455	14.55	5.664	2.1677E-06	14.48319	2583	-13.51	0.01	-98.44	0.15
		1.99526E-										
	gr0_w45	08	1.805	18.05	5.57769	2.6443E-06	17.91482	2580	-13.54	0.03	-98.63	0.14

1	2.51189E-				2.83557E-]				
gr2_w1	08	1.102	11.02	5.54736	06	10.92324	3168	-14.1	0.01	-100.52	0.01
gr2_w2		0.5993	5.993	0.96	0.10964782		4278	-14.32	0.01	-101.64	0.06
gr2_w3		0.7418	7.418	0.96	0.10964782		4310	-13.91	0.03	-98.9	0.07
gr2_w4		0.8814	8.814	0.96	0.10964782		4012	-14.12	0.05	-100.24	0.04
812_**	2.51189E-	0.0011	0.011	0.70	6.29274E-		1012	11.12	0.03	100.21	0.01
gr3_w1	07	4.301	43.01	5.20116	06	41.35906	3572				
	6.30957E-				3.81733E-						
gr3_w4	08	9.688	96.88	5.41824	06	95.30473	3998				
2 5	3.16228E-	0.007	00.07	5 1 6005	6.88256E-	05.0222	20.66	12.25	0.02	100.21	0.00
gr3_w5	07 2.95121E-	8.987	89.87	5.16225	06 6.69877E-	85.9222	3966	-13.35	0.03	-100.31	0.09
gr3_w6	07	7.255	72.55	5.174005	0.0987712-	69.48861	3952	-13.6	0.04	-100.84	0.17
g13_w6	9.33254E-	7.233	72.55	3.17 1003	4.36933E-	02.10001	3732	13.0	0.01	100.01	0.17
gr3_w7	08	3.896	38.96	5.359585	06	38.14525	3995				
	2.23872E-				6.02112E-						
gr3_w8	07	1.233	12.33	5.220323	06	11.88799	4019	-13.89	0.02	-99.47	0.09
2 0	2.51189E-	0.6012	6.012	5.00116	6.29274E-	6.551.402	4010	10.75	0.01	07.07	0.10
gr3_w9	07 5.01187E-	0.6813	6.813	5.20116	06 1.80597E-	6.551483	4019	-13.75	0.01	-97.87	0.18
gr3_w10	3.0118/E- 09	1.415	14.15	5.74329	1.8039/E- 06	14.11084	4189	-14.41	0	-105.16	0.04
g13_w10	5.01187E-	1.413	14.13	3.1432)	3.53435E-	14.11004	4107	17.71	V	103.10	0.04
gr3_w11	08	3.423	34.23	5.45169	06	33.75139	4186				
	6.30957E-				3.81733E-						
gr3_w12	08	2.299	22.99	5.41824	06	22.61618	4121	-13.99	0.05	-98.74	0.02
	6.30957E-				3.81733E-		4000				
gr3_w13	08	2.883	28.83	5.41824	06	28.36122	4090				
gr3_w14	6.30957E- 08	14.62	146.2	5.41824	3.81733E- 06	143.8228	3955				
g13_w14	1.99526E-	14.02	140.2	3.41024	5.76381E-	143.0220	3733				
gr3_w15	07	6.666	66.66	5.23929	06	64.42964	3892				
8	6.30957E-										
gr3_w16	07						3825	-14.02	0	-101.72	0.02
	1.58489E-				5.28883E-						
gr3_w17	07	6.773	67.73	5.27664	06	65.7594	3857				
~m2 ···10	6.30957E-	18.23	102.2	5 41004	3.81733E-	170 2259	3940				
gr3_w18	08 1.25893E-	10.23	182.3	5.41824	06 1.22346E-	179.3358	3940				
gr3_w19		21.53	215.3	4.91241	05	195.2128	3804	-14.61	0.07	-106.06	0.01
1 6			- · -								

	2.51189E-				6.29274E-						
gr3_w20	07	4.072	40.72	5.20116	06	39.15696	3769	-14.87	0.02	-106.97	0
	6.30957E-				9.10249E-						
gr3_w21	07	3.25	32.5	5.04084	06	30.39323	3539				
	5.01187E-				8.27771E-						
gr3_w22	07	7.552	75.52	5.08209	06	71.20856	3543				
	5.01187E-										
gr3_w23	08						3153	-13.98	0.02	-101.56	0
					4.47713E-						
gr3_w24	0.0000001	2.679	26.79	5.349	06	26.2047	3224				
					1.10662E-						
gr3_w25	0.000001	1.189	11.89	4.956	05	10.90461	4424	-14.6	0.02	-105.05	0.14
	3.16228E-				3.04614E-						
gr4_w5	08	4.175	41.75	5.51625	06	41.32104	3815				
	3.98107E-				3.27823E-						
gr4_w7	08	5.205	52.05	5.48436	06	51.42549	3801				
	3.98107E-				3.27823E-						
gr4_w9	08	3.921	39.21	5.48436	06	38.73955	3685				

APPENDIX D MAGNUSSON ET AL. 2017 – PROTOCOLS

D1. GIS PROTOCOLS	p. 1
D2. LAB PROTOCOLS	p. 5
D3. DATA PROCESSING	p.11

D1. GIS Protocols

Polygon Watershed Delineation

In order to reconstruct paleoglaciers from DTM analysis, several pre-processing steps had to be completed using ArcHydro Tools. The proposed workflow from the ESRI ArcHydro tutorial (ESRI, 2011) was used and a more elaborate description of the process can be found in this document.

- 1) Level DEM in lakes using a lake feature class based on field mapping and Sentinel data from May 2016.
- 2) Using the DEM reconditioning tools, stream features were burned into the DTM (this feature class was based on field mapping and Sentinel data May 2016, see 7.1). Default settings for river buffer zone were used.
- 3) Sink Prescreening was carried out followed by sink evaluation to generate a shapefile of sinks to be removed
- 4) *Depression evaluation* was carried out to identify depressions in the landscape that may also have to be removed as sinks.
- 5) The *Fill Sinks* tool was used to fill all sinks and depressions identified, resulting in a new DEM (*HydroDEM*)

After pre-processing, flow direction and accumulation grids, flowpaths and catchments were generated in order to derive the upstream areas of the morainic ridges with ArcHydro Tools. More information on the execution of these steps can be found in the ArcHydro v2.0 tutorial (ESRI, 2011).

- 1) From the Hydro DEM generated during preprocessing, a *Flow Direction* grid was made with the fieldwork area polygon as outer wall.
- 2) Flow Direction was adjusted in lakes using the lakes shapefile based on fieldwork and sentinel images.
- 3) From the Flow Direction Grid a Flow Accumulation grid was generated.
- 4) From the *Flow Accumulation* grid, a *Stream Network* was generated using an upstream cell threshold of 700 cells.
- 5) Stream Segmentation was performed to classify the stream network into unique segments (Stream Link).
- 6) Assign HydroIDs was performed to add Hydro IDs to the segments of the original stream feature class.
- 7) Stream Link and Sink Link (empty) grids were combined into a link grid.
- 8) For each stream segment, a *Catchment* was delineated using catchment delineation with Stream Link and Flow Direction grids as inputs.
- 9) The catchments were converted to polygons.
- 10) Within the polygon, *Drainage Line* features were created.
- 11) From the existing catchments, *Adjoint Catchments* were generated.

To create watershed for the morainic ridges, the "Create Watershed from Polygon" tool in ArcHydro Tools was used on the selected reconstructed moraine polygons. In some cases paleoglaciers had to be enlarged manually because later episodes of glaciation or mass movements had caused the catchment of a morainic ridge to become cut off from its initial source area.

Paleoglacier Delineation

Paleoglaciers were delineated as described in the original article by editing the watershed polygons using the *Editor Tool*. Paleoglacier geological cover percentages were calculated using the *Zonal Statistics Tool*.

ELA calculation

The ELA was calculated as the 25th percentile of elevation values of all raster cells within the paleoglacier polygon. A python script using ArcPy is available for this operation below. The contour line representing this altitude was selected and saved as ELA. Using the *Buffer Tool*, a zone around the ELA was generated, which was trimmed back to the paleoglacier extent using the *Clipping Tool*. Geological cover percentages under the ELA were calculated using the *Zonal Statistics Tool*.

ArcPy Script

.....

```
My adaptation of a script from geonet.esri.com to calculate percentiles of a raster within in a polygonal (like zonal statistics). The percentiles are calculated to provide an estimate of the ELA of paleoglaciers. Paleoglaciers are used as polygon input and a DTM as raster input. The ELA is calculated using the AAR method, where the percentile calculated by the script is 100% - AAR. Original script: https://geonet.esri.com/thread/95403 Runa Magnusson, 2016
```

```
import os
import sys
import arcpy
def main():
  # settings
  ras = r"E:\RUNA\_Peru\GISDatabase\PythonStuff\AsterDTM" \# input \ raster \ (esri \ grid)
  fc = r"E:\RUNA\_Peru\GISDatabase\PythonStuff\PaleoGlaciers.shp" # input polygons (.shp)
  lst_aar = [67, 75] # fill in the AAR values used for ELA calculation
  lst perc = [100 - x \text{ for } x \text{ in lst aar}]
  fld prefix = "ELA "
  start at = 0
  # set a workspace folder (usually the folder containing the inputs)
  arcpy.env.workspace = "E:\RUNA\Peru\GISDatabase\PythonStuff"
  arcpy.env.overwriteOutput = True
  # add fields if they do not exist in feature class. existing fields will be overwritten
  print "filling field list and adding fields"
  flds = []
  for aar in lst_aar:
     fld\_perc = "\{0\}\{1\}".format(fld\_prefix, aar)
     flds.append(fld_perc)
     if not FieldExist(fc, fld_perc):
       arcpy.AddField_management(fc, fld_perc, "LONG")
  print "flds={0}".format(flds)
  # enable spatial analyst
  arcpy.CheckOutExtension("Spatial")
  # loop through polygons
  print "loop through polygons"
  flds.append("SHAPE@")
  i = 0
  with arcpy.da.UpdateCursor(fc, flds) as curs:
     for row in curs:
       i += 1
       print "Processing polygon: {0}".format(i)
       if i \ge start_at:
          polygon = row[flds.index("SHAPE@")]
```

```
# Execute ExtractByMask
          print " - ExtractByMask"
          ras_pol = arcpy.sa.ExtractByMask(ras, polygon)
          del polygon
          outname = "ras{0}".format(i)
          ras_pol.save(outname)
          print " - saved raster as {0}".format(outname)
          # create dictionary with value vs count
          print " - fill dict with Value x Count"
          flds_ras = ("VALUE", "COUNT")
          dct = {row[0]:row[1] for row in arcpy.da.SearchCursor(outname, flds_ras)}
          # del ras pol
          # calculate number of pixels in raster
          print " - determine sum"
          cnt sum = sum(dct.values())
          print " - sum={0}".format(cnt_sum)
          # loop through dictionary and create new dictionary with val vs percentile
          print " - create percentile dict"
          dct_per = \{\}
          cnt_i = 0
          for val in sorted(dct.keys()):
            cnt_i += dct[val]
            dct_per[val] = float(cnt_i) / float(cnt_sum)
          del dct
          # loop through list of percentiles
          print " - iterate percentiles"
          for perc in lst_perc:
            # use dct_per to determine percentiles
            perc\_dec = float(perc) / 100
            print " - Perc_dec is {0}".format(perc_dec)
            pixval = GetPixelValueForPercentile(dct_per, perc_dec)
            print " - Perc for {0}% is {1}".format(perc, pixval)
            # write pixel value to percentile field
            print " - Store value"
            fld_perc = "{0}{1}".format(fld_prefix, (100 - perc))
            row[flds.index(fld_perc)] = pixval
          del dct_per
          # update row
          print " - update row"
          curs.updateRow(row)
  # return SA license
  arcpy.CheckInExtension("Spatial")
def GetPixelValueForPercentile(dctper, percentile):
  """will return last pixel value
   where percentile LE searched percentile."""
  pix_val = -1
  try:
     pix_val = sorted(dctper.keys())[0] # initially assign lowest pixel value
     for k in sorted(dctper.keys()):
       perc = dctper[k]
       if perc <= percentile:
          pix_val = k
```

```
else:
    break
except Exception as e:
    pass
return pix_val

def FieldExist(featureclass, fieldname):
"""Check if field exists"""
fieldList = arcpy.ListFields(featureclass, fieldname)
return len(fieldList) == 1

if __name__ == '__main__':
    main()
```

D2. LAB PROTOCOLS

1 Particle Size Analysis

For Particle Size Analysis, the <2mm fraction of soil samples is used. This fraction should be oven dried for at least 24 hrs at 70 degrees C. Depending on the nature of the samples, organic matter (OM), carbonates and iron oxides (Fe-oxides) should be removed, since these substances can co-agulate soils. In addition soluble salts should be removed to prevent them from co-flocculating the sample. The methodology described below was developed for glacial tills, containing little organic matter and carbonates but high amounts of iron oxides. It consists of extensive removal of OM and Fe-oxides, manual sieving and sedigraph analysis. It uses a Micrometrics Sedigraph III Plus with Micrometrics MasterTech S2 Autosampler. The methodology may need to be adapted for samples of a different nature and composition and for different sedigraph types.

Preparations:

750 mL Philips flasksTwo-decimal scale

- Four-decimal scale

- Oven Tins

Exsiccator

- 1) Weigh approximately 20 grams of oven dry soil material on a two-decimal scale into the Philips flasks and note the weight
- 2) On the same day, weight approximately 1 gram of the same soil material on a four-decimal scale into an oven tin of known weight.
- 3) Put the oven tin into the oven at 105 degrees Celsius for 24 hours. Place in exsiccator for 15 minutes and weigh back to obtain the moisture content of the soil at 70 degrees Celsius.

OM removal:

- Hydrogen peroxide

- Fume-hood

- Steam bath

- Ethanol

- Sodium Chloride

- 250 mL glass centrifuge tubes

- 4) To the Philips flasks, add 35 mL of demi-water and 15 mL of 33% hydrogen peroxide and leave under the fume hood for 24 hours. Afterwards, place the flasks on a steam bath to aid the oxidation of organic matter.
- 5) In case the flasks go dry, add demi water. In case all peroxide has reacted and no more small bubbles appear, add hydrogen peroxide in volumes of 15 25 mL at a time. Note the amount of peroxide added to each flask. In case oxidation reactions are too severe and a flask is about to overflow, add some drops of ethanol.
- 6) The organic matter has oxidized once no more large, persistent bubbles appear. Remove the flasks from the steam bath once this is the case.
- 7) Add 200 mL of demi-water to the flasks and leave to settle overnight. Add a tablespoon of NaCl if necessary to aid settling.
- 8) If samples have settled and the supernatant is absolutely clear, suck of the major part of the supernatant and take care not to disturb the soil particles.
- 9) Rinse the sample out of the Philips flasks using demi-water and collect in 250 mL glass centrifuge tubes.
- 10) Centrifuge the samples for 15 minutes at 1250 RPM. Increase the rotation speed if necessary, but not higher than 2000 RPM as centrifuge tubes may break. If samples do not settle, again add a tablespoon of NaCl.
- 11) If samples have settled and the supernatant is absolutely clear, suck of the major part of the supernatant and take care not to disturb the soil particles.

Fe-oxide Removal:

Sodium Citrate

- Sodium Bicarbonate

- ELGA water

- Magnetic stirrers

- Sodium Dithionite

- Fume-hood

- Steam bath

- Stirrers

- 12) Prepare a citrate-bicarbonate buffer to maintain a slightly alkaline pH (7.3; Mehra & Jackson, 1960) by adding 21g of sodium bicarbonate to 250 mL of ELGA water and adding 176.8g of sodium citrate to 2L of ELGA water. These solutions are dissolved using an magnetic stirrer and combined to yield a buffer consisting of a 8:1 parts mixture of 0.3M sodium citrate and 1M sodium bicarbonate solutions.
- 13) Add 150 mL of the buffer to the sediments along with 3.0 grams of sodium dithionite. Do this under a fume-hood.
- 14) After leaving the samples under the fume-hood overnight, place them on the steam bath. If the centrifuge tubes cannot stand upright on the steam bath, fill the Philips flasks with water and put the centrifuge tubes in the Philips flasks with a small item underneath to keep them from sinking. Wait until the water in the Philips flasks is at at least 70 degrees Celsius (preferably 80) and then leave them for 20 minutes, stirring every 5 minutes.
- 15) Once a has turned a perfect gleyic grey, all iron oxides have been removed. The centrifuge tubes can be taken off the steam bath and left to settle overnight.
- 16) If samples do not settle by themselves, they can be centrifuged for 15 minutes again, aided by addition of a tablespoon of NaCl if necessary.
- 17) If samples have settled and the supernatant is absolutely clear, suck of the major part of the supernatant and take care not to disturb the soil particles.
- 18) Samples that are not yet completely gleyic of colour should be processed from step 13 onwards again. Other samples receive 200 mL of demiwater and are centrifuged again. Again, once the supernatant is clear it is sucked off carefully.

Wet-sieving:

- 63 µm sieve

- Brushes

- Tin bowl

- Small aluminum oven tins

- 600 mL glass beakers

- 19) Samples are rinsed out of the centrifuge tubes using demiwater and collected on a 63 µm sieve placed in
- 20) Wet-sieve the sample by holding the sieve just under the water level in the tin bowl and gently stroking the sediment through the sieve with a brush for at least 10 minutes.
- 21) Once the addition of fresh demi-water on top of the sieve yields a clear fluid dripping through the sieve, the wet-sieving is finished.
- 22) Rinse the bottom and sides of the sieve and collect the fluid in the tin bowl. Rinse the $> 63 \mu m$ fraction out of the sieve into small aluminum oven bowls.
- 23) Rinse the contents of the tin bowl into a 600 mL glass beaker. Repeat steps 19 to 23 for each sample.

Fraction >63 um:

- 1mm, 500 μm, 250um, 1250um and 63um sieves + lid and bottom container

Shaking plate

Large funnel

- Brushes

- Aluminum tins

- Two-decimal scale

- 24) Place the aluminum bowls containing the $>63 \mu m$ fraction on the steam bath until almost all liquid has evaporated. Afterwards, place in the oven at 70 degrees overnight, with tin foil with holes covering the tin
- 25) Build a sieve tower of the 1mm, $500 \, \mu m$, $250 \, \mu m$, $125 \, \mu m$, $63 \, \mu m$ and bottom. Add a dry $>63 \, \mu m$ sample on top and place on a shaking plate for 10 minutes with amplitude set at 30. Afterwards, collect the contents of each sieve using a funnel and brush and weigh in a new tin of known weight using an at least two-decimal scale. Keep the residue in the bottom container ($< 63 \, u m$) after weighing it to be added to the $<63 \, u m$ sample material. Repeat for each sample.

Fraction <63 um:

- Steam Bath

- Freeze-dryer bottles

- Alcohol Bath

- Freezer

- Freeze-dryer

Metal spoon

- Brushes

- Two-decimal scales

- 26) Place the 600 ml glass beakers containing the dissolved <63 μ m fraction on the steam bath until at most 100 mL but preferably 50 mL is left.
- 27) Rinse samples out of beakers using demi-water into freeze-dryer bottles. Note the number and weight of each freeze-dryer bottle and corresponding sample ID.
- 28) Hang the freeze-dryer bottles in an alcohol bath at approximately -36 degrees for one hour and make sure all material is frozen.
- 29) Either store the frozen bottles in the freezer until further analysis or directly hang them onto a freezedryer unit. Only add new bottles once the chamber pressure has dropped to <100 mTorr. The temperature should remain around –30 to 50 degrees Celsius and chamber pressure should remain at < 100 mTorr.
- 30) Once freeze-dryer bottles feel warm to the touch, they can be removed from the freeze-dryer and weighed immediately.
- 31) Using brushes and a metal spoon, gently scrape all sediment out of the freeze-dryer bottles and collect in a labeled plastic tube using a funnel. Add the material of $<63 \mu m$ from the sieve-tower procedure.

Sedigraph Analysis:

- Calgon solution

- Measuring cylinder

- Pipette

- Sedigraph + carousel + beakers

- 32) Weigh 3.5g of this material on an at least one-decimal scale into a sedigraph glass beaker. Add approximately 70 mL of demi-water using a measuring cylinder and 500 μ L of calgon solution using a pipette.
- 33) Place these beakers on the sedigraph carousel and set the sedigraph to stir the samples for 60 seconds at high stirring speed and sonicate them for 10 seconds prior to injecting the suspension into the sedigraph.

The measurements of the $2mm-125~\mu m$ fraction using the sieve tower and the output of the sedigraph may be combined into a total overview of weight or weight-% per particle size class ranging from 2mm to $1~\mu m$. The original weight is compared to the sum of all fractions to obtain an idea of sieving losses or remaining particles of sodium chloride or dithionite. The original weight is corrected to dry weight using the gravimetric moisture content found by drying 1 gram of soil at 105 degrees C. The PSA may be complemented by measurements of larger fragments carried out prior to isolating the <2mm fraction. Software such as GRADISTAT (Blott & Pye, 2001) can be used to generate statistics of particle size distribution and textural classes.

2 CNS Analysis

CNS analysis can be used to obtain concentration of Carbon, Nitrogen and Sulphur per unit weight of soil. From the Carbon concentration, total OM per unit weight of soil can be obtained using the widely adopted assumption that 58% of OM in soil samples consists is carbon (Nelson & Sommers, 1988). CNS is performed on oven-dried, milled samples of the <2mm fraction, often in duplo.

Materials:

- Tins for oven-drying
- Glass vials
- Pulveriser with containers and milling marbles
- Tin foil packets

- Spatulas
- 4-decimal scale with milligram range setting
- Standard of known C, N & S content (sulphanilic acid)

Methods:

- 1) Weigh approximately 10 grams of soil on an at least 2-decimal scale, place in tin of known weight.
- 2) Place in oven at 70 degrees C for at least 24 hours.
- 3) Place in exsiccator for 15 minutes and weigh back the tin to obtain dry weight of the sample.
- 4) Transfer material to the pulveriser containers using three milling marbles.
- 5) Pulverise for 5 minutes at 400 RPM.
- 6) Transfer milled material to glass vials and clean the pulveriser containers and marbles before milling the next set of samples.
- 7) Prepare 12 CNS-standards by weighing tin foil rectangular packets and taring. Put a tin foil packet on a mirror (handle packets using a spatula).
- 8) Add 5 to 10 milligrams (note weight) of standard substance of known C, N and S content (sulphanilic acid) to the package and fold tightly. Check whether it is sealed properly by dropping it on the mirror.
- 9) Store packages in a pillbox with labelled rows and columns, not the weights and sample IDs for each pillbox location.
- 10) Fold sample material into tin foil packets in a similar way, adding 40 to 60 milligrams of sample.
- 11) Place samples in the Elementar CNS carrousel as follows: 8 standards, followed by 2 vacant spaces (blank), followed by sequences of 10 samples + 1 blank. At the end, add 4 standards.

The Elementar CNS returns weight-% of C, N and S. The C-content can be used to infer the amount of OM by multiplying the mass of carbon in grams by 1.72.

3 XRF Analysis

XRF analysis is performed on soil samples that have been sieved and homogenized as much as possible (for instance soil material sieved to < 2mm and milled as described in Appendix D2.2). Samples should be dried at at least 60 degrees Celsius. XRF analysis employs X-rays to excite elements within sample material. The resulting emission spectra of the material are used to infer the content of various elements in mg/kg (ppm). This protocol is written for soil sample analysis using a ThermoFischer Niton XL3 series handheld XRF analyser with a statif. Depending on which elements need to be analysed, one or more standards need to be selected that contain known quantities of the elements that are to be analysed.

Materials:

- Plastic cups + plastic foil that came with the XRF
- Pressurized air for cleaning
- Set of selected standards

Methods:

- 1) Make sure the measurement software is initialized properly (consult technician).
- 2) Put plastic foil over the plastic rings belonging with the XRF and seal them off with a small plastic lid. Create three of these cups. They should resemble the standards delivered with the XRF. Add about 1-2 cm of soil of the first three samples to the plastic cups.
- 3) Start by checking the data variability within a sample by measuring the sample 3 times, shifting the plastic cup over the X-ray window a little bit so that different parts of the soil sample are exposed. Analyse the variability of these measurements of the selected elements and determine the amount of measurements needed for each sample. For non-milled samples the measurements may vary more than the measurement error in which case about 3 measurements per sample will be needed. In other cases 2 or even only 1 measurement per sample will be enough.
- 4) Start the measurement series by measuring the standard(s).
- 5) Afterwards, the first 3 samples can be measured (as many times as deemed necessary).
- 6) After each batch of three samples, the standard(s) should be measure again. In the meantime the plastic cups should be cleaned out with pressurized air and loaded with new sample material.
- 7) End the sequence with a standard(s) measurement.

The output data will contain sequence number, measuring time, concentration and error for each element selected. These measurements have to be standardized using the standard measurements. This incorporates a correction for the measured standard concentrations and the actual standard concentration. For each measurement of each element, the correct reading can be inferred using the following formula:

Actual Value =

$$Meas_{samp} + \frac{(Meas_{NextStandard} - Actual_{Standard}) - (Meas_{PrevStandard} - Actual_{Standard})}{Time_{NextStandard} - Time_{PrevStandard}} * (Time_{Sample} - Time_{PrevStandard})$$
Eq. E1

Then, the multiple measurements per sample and their respective errors can be averaged.

4 Microwave extraction

Samples for which content of metals could not be determined using XRF, either due to limitations of XRF technology itself or lack of suitable standard materials, Microwave extraction and ICP-OES were used to quantify metal content. Microwave extraction was carried out on samples that received the same pre-treatment as XRF (<2mm, milled and dried).

Materials:

- Teflon microwave tubes
- HNO₃, 65%
- HCl, 37%
- 4-decimal scale
- ICP standard solutions
- ELGA water
- 50 mL flasks

Method:

- 1) Rinse all glassware with 4M nitric acid heated up to 60°C
- 2) Weigh in 250 mg of soil sample into the Teflon microwave tubes and add 2 blanks per series
- 3) Add 2 mL HCl and 4 mL HNO₃ to each sample. Leave for 60 minutes while swerving regularly.
- 4) Add 1 mL of ELGA water and close the Teflon tube
- 5) Place in the microwave for 55 minutes at xxxxW.
- 6) Transfer the content of the Teflon tubes to 50 mL flasks and fill up with ELGA water, homogenize the solution
- 7) Centrifuge the solution at 2000 RPM and transfer the required amount of supernatant for ICP-OES analysis.
- 8) Standard samples of 10 mL are produced from varying quantities of stock solutions to represent an appropriate range of the metals of interest, each complemented with 1ppm Yttrium, 500 μ L of the aqua regia solution (2:1 HNO₃ and HCl) and ELGA water

5 Mineralogical Analysis

This methodology was developed for the mineralogical analysis of rock fragments between 8 and 16 mm in diameter, sieved from glacial till sediments using sieves with round apertures.

Initially, rinse rock fragments thoroughly with soap and water. If properly cleaned, rocks may be analysed for mineralogical composition directly. If not, several steps may be required to clean them of remaining clay and iron oxide coatings. To rinse stones of clay coatings, an EDTA-solution of 0.1M may be prepared to disperse the clays. To remove iron oxide coatings, the EDTA solution may also prove sufficient. If not, an oxalic acid solution can be prepared.

Materials:

- EDTA
- Oxalic Acid Dihydrate
- ELGA water
- 200 mL glass beakers

- Magnetic stirrer

Methods:

- 1) Prepare an EDTA solution by dissolving 18.6g of EDTA in 500 mL ELGA-water and dissolve using a magnetic stirrer. Prepare more as needed.
- 2) Put approximately 50 rock fragments in a glass 200 mL beaker and add 150 mL of the EDTA solution.
- 3) Put in an ultrasonic bath for 10 minutes.
- 4) Repeat as desired with fresh EDTA solution.

If iron coatings are still present and mineralogical assessment is not possible, prepare and oxalic acid solution to dissolve further coatings. As a rule of thumb, if three rinsing sessions with EDTA solution do not yield the desired result, it is better to use an oxalic acid solution.

- 1) Dissolve 6.3g of oxalic acid dihydrate in 500 mL ELGA water and dissolve using a magnetic stirrer.
- 2) Use in the same way as described above for the EDTA solution.

Afterwards, rocks can be analysed mineralogically using the Streckeisen (1974) QAPF-diagram.

D3: DATA PROCESSING

1. EC Data Detrending

The detrending procedure makes use of a continuous dataset of measurements of EC on a fixed location in the Rio Buin (9°12′54.11″S, 77°37′0.56″W). The diurnal variation in EC is assumed to reflect varying contributions of glacial melt depending on diurnal temperature variations (Burns et al, 2011). As glacial melt discharge increases, specific conductance of water decreases since glacial meltwater generally has a lower conductance than surface water from other sources (Tranter et al., 2005). No significant precipitation was recorded during this monitoring period to affect diurnal dynamics.

To account for diurnal variations, the continuous dataset was detrended using the following protocol:

- 1. Calibration location data were standardized to relative values compared to maximum observed EC per location (ECmeasured/ECmax)
- 2. A trendline was fitted to this dataset by connecting all measurements at 16:00 at the calibration location and smoothing this trendline with a moving average of 11 measurement points to obtain a smooth trendline for day to day variance scaled to fraction of ECmax
- 3. This day-to-day trendline was subtracted from the data
- 4. Sine waves were fitted to describe diurnal variation in EC measurement for each of the monitoring locations separately
 - a. Phase of the sine wave is expected to vary with distance from the meltwater source. The amplitude of the sine wave is expected to be inversely related with distance to glacier due to increased mixing of water of various sources.
 - b. Measurement from active glacier source for each meltwater stream sampling location was measured in ArcMap using the *Distance Tool*
 - c. An empirical relation was set up of distance to glacier and phase and amplitude of the diurnal sine waves, using data from additional monitoring datasets from van Diemen et al., 2016.
 - d. For each meltwater stream measurement an empirical sine wave was set up.
- 5. For each meltwater stream measurement point the day-to-day trendline and specific sine wave were summed into one function.
- 6. The maximum EC from this function was used as detrended ECmax.

2. Ion Balance

Using the cation concentrations from ICP-OES analysis, anion concentrations from Auto Analyser data, field measured pH and TOC data from the TOC/TN analysis, a total ion balance can be generated to assess data quality.

1. Calculate the negative charge associated with dissolved organic matter using empirical relations from Olivier et al. (1983).

pK =
$$0.96 + 0.90$$
 pH - 0.039 (pH)² [-] eq. E2
K = 10^{-pK} [-] eq. E3
[RCOO-] = K*[$10*DOC$]/ (K + [H⁺]) [$\mu eq/L$] eq. E4

2. For all cation and anion data, multiply concentrations in µmol/L with the charge equivalents of the ion to calculate total positive and negative charge in micro-equivalents per liter.

Sum anions* =
$$[NO_x] + 3*[PO_4^{3-}] + 2*[SO_4^{2-}] + 2*[CO_3^{2-}] + [HCO_3^-] + [Cl^-] + [RCOO^-]$$
 [$\mu eq/L$] eq. E5
Sum cations* = $[H^+] + [NH_4^+] + [Al] + 2*[Ca] + 2*[Fe] + [K] + [Li] + 2*[Mg] + 2*[Mn] + [Na] + [Sr] + 2*[Ba]$ [$\mu eq/L$] eq. E6